UNIVERSITY
OF MICHIGAN
JAN 31 1957
ENGINEERING
LIBRARY

Engin
QC
151
J86
v.1
no.5

JOURNAL OF FLUID MECHANICS

VOLUME 1 PART 5

NOVEMBER 1956

Printed and Published by

TAYLOR & FRANCIS LTD

RED LION COURT, FLEET STREET, LONDON, E.C.4

The JOURNAL OF FLUID MECHANICS exists for the publication of theoretical and experimental investigations of all aspects of the mechanics of fluids, and is issued in six parts per volume.

Editor:

Dr. G. K. BATCHELOR, Cavendish Laboratory, University of Cambridge, Cambridge, England.

Assistant Editors:

Dr. T. B. BENJAMIN, Dr. I. PROUDMAN.

Associate Editors:

Prof. G. F. CARRIER, Pierce Hall, Harvard University, Cambridge 38, Massachusetts, U.S.A.

Prof. W. C. GRIFFITH, Palmer Physical Laboratory, Princeton University, Princeton, New Jersey, U.S.A.

Prof. M. J. LIGHTHILL, Department of Mathematics, The University, Manchester, England.

Authors wishing to have papers published in the JOURNAL should communicate them to any one of the persons named above, choosing one in their own country where possible.

Authors are urged to ensure that their papers are written clearly and attractively, in order that their work will be readily accessible to readers.

Manuscripts should be typed in double spacing on one side of the paper only, with references listed at the end in alphabetical order of authors. Drawings should be done on a large scale in Indian ink on tracing cloth or drawing paper, captions being typed on a separate sheet. Proofs of papers from overseas will usually be despatched to authors by airmail. Authors are entitled to receive 50 offprints of a paper in the JOURNAL free of charge, and additional offprints can be purchased from the publisher.

PRICE £1 ($3.00) per part

Subscription, £5 10s. 0d. per volume of six parts, post free ($16.50 in U.S.A. and Canada)

Agents for U.S.A. and Canada:

Academic Press Inc., 111 Fifth Avenue, New York 3, N.Y., U.S.A.

JOURNAL OF FLUID MECHANICS
Volume 1, Part 5 November 1956

CONTENTS

The refraction of shock waves at a gaseous interface
by ROBERT G. JAHN 457

Supersonic flow past a bluff body with a detached shock Part II Axisymmetrical body
by W. CHESTER 490

An inequality concerning the production of vorticity in isotropic turbulence
by R. BETCHOV 497

The almost-rigid rotation of viscous fluid between concentric spheres
by IAN PROUDMAN 505

The speed of drifting bodies in a stream
by J. R. D. FRANCIS 517

Outline of a theory of turbulent shear flow
by W. V. R. MALKUS 521

On the motion of small spheroidal particles in a viscous liquid
by P. G. SAFFMAN 540

Reviews 554

JOURNAL OF FLUID MECHANICS

—o—

Orders originating

in

UNITED STATES OF AMERICA

and

CANADA

should be sent to the sole agents

ACADEMIC PRESS INC.

111 Fifth Avenue,

New York, 3,

N.Y., U.S.A.

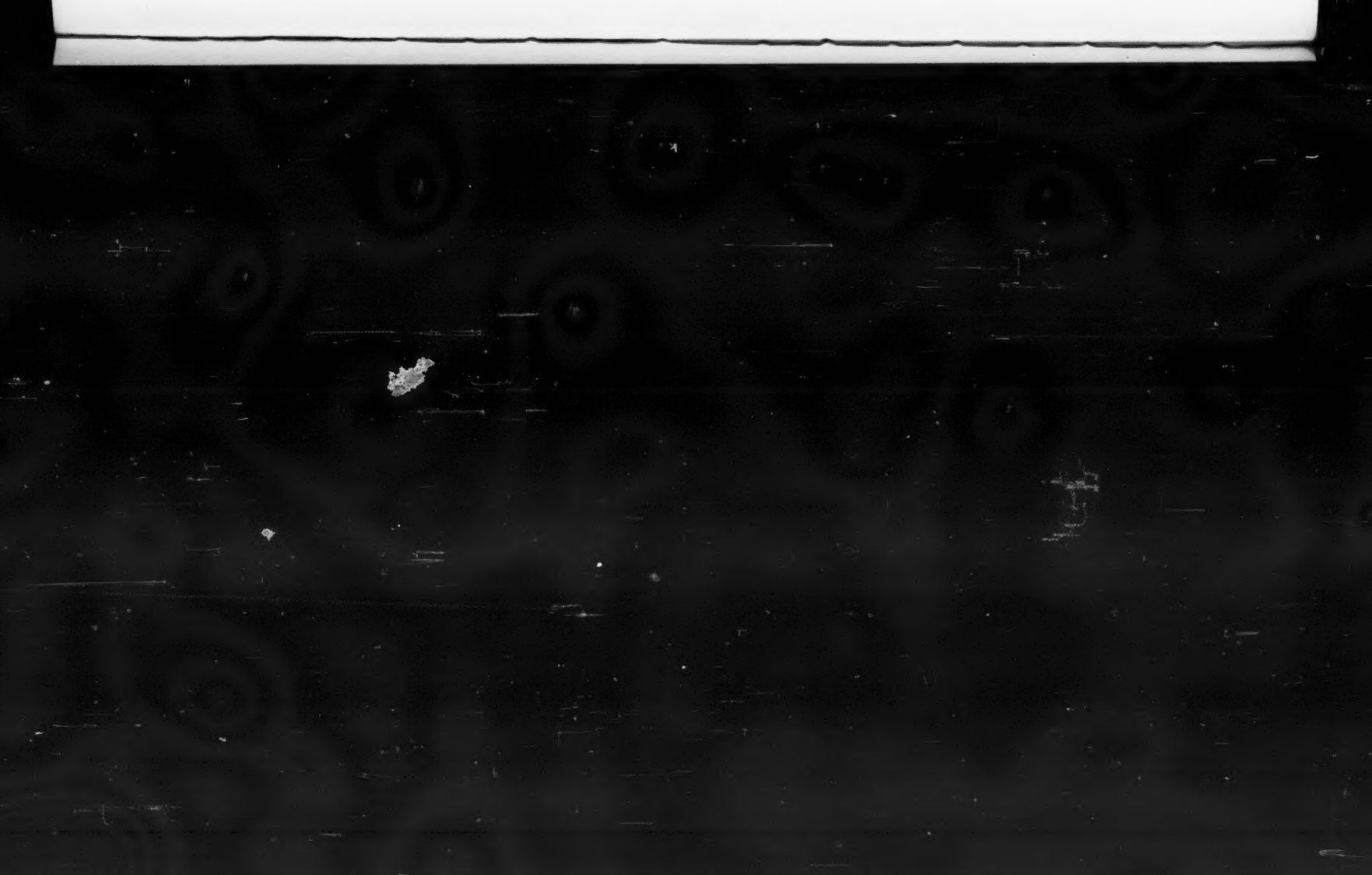

The refraction of shock waves at a gaseous interface

By ROBERT G. JAHN
Department of Physics, Lehigh University, Bethlehem, Pennsylvania

(*Received* 24 *April* 1956)

SUMMARY

A programme of shock tube experiments has been conducted to study the refraction of plane shock waves at interfaces between two gases. Shocks of strength $\xi = 0{\cdot}85$ (weak) and $\xi = 0{\cdot}30$ (fairly strong) were allowed to impinge, at various angles of incidence, on interfaces between air/CO_2 and air/CH_4, and the resulting configurations were photographed through a Mach–Zehnder interferometer. From the interferograms, measurements were made of the strengths of the reflected waves, and of the angles of refraction, and the values were compared with the theoretical calculations of Polachek & Seeger (1951). Within the range of parameters for which the refraction model assumed by the theory is applicable—the so-called 'regular refraction' region—the observations were in excellent agreement with the theoretical predictions.

When the study was extended to ranges of the parameters for which the theory is clearly inadequate, a succession of rather complex 'irregular refraction' patterns was observed. Although these configurations were highly interesting qualitatively, each of them involved curved shocks, non-uniform regions of flow, and other less simple processes which discouraged any formal theoretical analysis. On a less rigorous basis, however, it could be shown that these patterns were internally consistent, and that each represented a distortion of a regular refraction process which was reasonable under the prevailing aerodynamic conditions.

Certain observations in these refraction experiments appear to be of some significance outside the specific problem. (i) The sensitivity of strong shock refractions to the values of the specific heat ratio γ for the two gases suggests a possible technique for the measurement of γ and its temperature dependence. (ii) Two of the irregular refraction patterns display a transition process which would be equally appropriate to the onset of the Mach configuration in the shock reflection problem. (iii) Some irregular refractions can be considered as special cases in the problem of the interaction of a shock and a boundary layer.

I. INTRODUCTION

Of the many non-linear phenomena available for physical study, the behaviour of shock waves in gases is one of the neatest and least complex.

Even so, shock wave problems are difficult to treat theoretically, and computations on even the most fundamental shock interactions tend to become involved and somewhat ambiguous. Normally it must fali to direct experiment to clarify the theoretical predictions, and to extend the understanding into regions too complex for mathematical solution. This paper discusses a programme of shock tube experiments which is intended to clarify and supplement the existing theoretical information on one of the most basic shock interactions—the refraction of plane shock waves at an interface between two gases. It is a condensation of a doctoral thesis submitted by the author to the Department of Physics, Palmer Physical Laboratory, Princeton University. Throughout the paper, a dagger (†) is used to indicate specific points discussed in greater detail in the original work, which is available on request from the Princeton University Library.

II. Theory

Theoretical description of this problem has been formulated independently by Taub (1951) and Polachek & Seeger (1951). They assume the same, somewhat idealized model for the refraction process, which is outlined briefly here to introduce the notation and terminology in this paper (see figure 1).

A plane, flat-topped shock I of strength ξ (ξ = pressure ahead/pressure behind) travelling in an ideal (inviscid, with constant specific heat and zero thermal conductivity) gas (1) is incident at some angle α on a plane interface O of another ideal gas (5). Assume that a plane, flat-topped shock T of strength ξ'' is transmitted at an angle α'', and a similar shock RS of strength ξ' is reflected at an angle α'. Assume also that the gas interface passed over by the intersection X is deflected through an angle Δ, and that each of the five angular regions (1) to (5) formed by this configuration is uniform in all its pertinent properties: pressure p, density ρ, temperature T, velocity of sound a, entropy s, and gas flow velocity $\boldsymbol{u}$. Such a process will be called a 'regular refraction'.

The problem is formulated from the point of view of an observer travelling with the intersection point X. Such an observer sees a certain gas inflow velocity in regions (1) and (5), $\boldsymbol{u}_1 = \boldsymbol{u}_5$. The gas flow $\boldsymbol{u}_1$ is decelerated and deflected through an angle δ by I, and again decelerated and deflected through δ' by RS. The flow $\boldsymbol{u}_5$ is deflected through δ'' and decelerated by T. The problem is solved by appplying the Rankine–Hugoniot shock equations, in the form relating change in flow velocity to shock strength, across I, RS, and T, under the boundary requirements that the outflow velocities $\boldsymbol{u}_3$ and $\boldsymbol{u}_4$ be parallel (though not necessarily equal), and the exit pressures be the same, that is, under the requirements $\delta + \delta' = \delta'' = \Delta$, and $p_3 = p_4$.

Polachek & Seeger (1951) increased the range of applicability of their refraction model by admitting the possibility that, instead of a shock, the reflection could be a Prandtl–Meyer angular rarefaction wave, centred at X. Such a reflection (hereafter denoted by RR) would accelerate the flow $\boldsymbol{u}_2$

and deflect it toward, rather than away from the interface. Furthermore, they recognized that any particular gas combination was not necessarily restricted to just one or the other type of reflection, but that reflected shocks might occur for small angles of incidence, and reflected rarefactions for more glancing angles, or vice versa. (The angle of incidence at which such a change takes place we call α_t—the transition angle.)

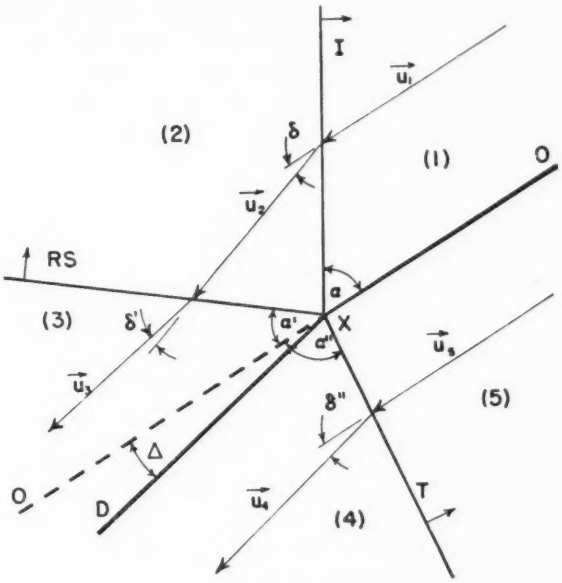

Figure 1. Assumed configuration for the shock refraction process. I = incident shock; RS = reflected shock; T = transmitted shock; α, α', α'' = angles of incidence, reflection, refraction; X = point of intersection of I, RS, and T with interface; OXO = original interface; XD = deflected interface; Δ = angle of deflection of interface; $\boldsymbol{u}$ = gas flow velocity; δ, δ', δ'' = angles of deflection of flow by shocks I, R, T, respectively. Numeral subscripts refer to the 5 angular sectors of the pattern.

Both Taub (1947) and Polachek & Seeger (1951) have carried out extensive numerical calculations, based on their own formulations, of the reflected and refracted wave strengths and angles for various gas combinations, shock strengths, and angles of incidence. In both cases, the automatic calculators can solve the problems only incompletely. For some values of the pertinent parameters they return several solutions; for others, none at all. In the former cases it is necessary to choose one branch of the solutions on the basis of some boundary value criteria, such as the known behaviours in the limits $\xi \to 1$ (acoustic case) and $\alpha \to 0$ (normal incidence). In the latter situations it is presumed that this

idealized model for the refraction process is inadequate to satisfy simultaneously all of the aerodynamic requirements, and that some other, more complex processes must occur physically.

III. Design of the experiments

The theoretical approach outlined above was given encouragement by some early experimental work of Stoner, Woodbridge & Davies (1952), Bitondo (1950), and the Princeton laboratory, which indicated that a process quite similar to that assumed by the theory did occur physically. This process was observed to occur for each gas combination and shock strength tested, over a range of angles of incidence from normal up to a certain limiting angle, which depended on ξ and the gas combination. In the range of α beyond this limiting angle, other more complex interactions, called 'irregular refractions', were observed, which were clearly incompatible with the simple process assumed by the theory. However, this early work was largely qualitative, involving shadow photographs and streak photographs, from which it was possible to measure wave angles, but not shock strengths or pressure fields directly. It was felt that an experiment which provided direct measurements of the wave strengths and pressure distributions throughout the entire refraction field was necessary if the assumptions and solutions of the theory were to be checked thoroughly and the complex irregular patterns were to be understood at all.

Of the two sets of calculations that were available, those of Polachek & Seeger (1951), which included the cases both of reflected shocks and reflected rarefactions, seemed more appropriate for experimental comparison. (Henceforth we refer to these exclusively.) The results of those computations were presented in the form of graphs of $1/\xi'$ *vs* α and α'' *vs* α for seven shock strengths and twenty-four gas combinations. These graphs, largely unpublished, were made available from the Naval Ordnance Laboratory, by the kind cooperation of Mr L. D. Krider. The experimental work described below was first directed toward a quantitative appraisal of these regular refraction solutions, and then extended to explore, qualitatively, the theoretically opaque regions of irregular refraction.

The Princeton laboratory is fortunate to possess a 5-inch Mach–Zehnder interferometer, with which the gas density in the entire interaction field can be evaluated. With this equipment available, the experimental problem resolved itself into the creation of a suitable shock wave refraction process in the test section of the shock tube. This, in turn, depended primarily on the accomplishment of a nearly ideal separation of two gases to form a plane refracting interface there. To date, the only successful means of gas separation we have found for this experiment has been by some type of film or membrane. Such a film must be sufficiently strong to withstand the hydrostatic pressure of the heavier gas, and must be impermeable to both gases. On the other hand, it must have a sufficiently small mass for its acceleration by the incident shock not to interfere appreciably with the refraction process.

Finding a film that satisfies these requirements is the key to the entire experiment. A natural first attempt was to try soap films, which have conventionally been used for similar purposes (cf. especially Stoner's use of soap films for refraction experiments). It quickly appeared, however, that soap films had several inherent disadvantages in this application. (i) They must be drawn in place at the time that they are to be used. (ii) They evaporate, thereby contaminating with water vapour the gases they are separating. With some gases (for example, CO_2) they react chemically. (iii) If used in any position other than horizontal, they drain toward the lower edge and become non-uniform in thickness. (iv) They stretch comparatively easily, and hence tend to bow out under the hydrostatic pressure of the heavier gas, thereby establishing a curved interface. (v) When broken accidentally, or by the incident shock, they splatter the optical flats with soap solution.

After considerable investigation of this film problem, a more suitable gas separation technique was developed using a commercial lacquer film ('Zapon–Aquanite A', a product of the Atlas Powder Company, Wilmington, Delaware). Briefly†, the films are cast on a surface of distilled water, lifted off on stainless steel frames, and allowed to dry. They weigh, when dry, approximately 5 micrograms/cm^2, and in thickness are a small fraction of one wavelength of visible light. These Zapon films overcome the above disadvantages of the soap films, yet are simpler and more convenient to prepare. They can be made lighter, in total mass, than the soap films that would be needed to hold the same gases over the same size span. It is no exaggeration to say that it was the neatness and manageability of these thin films which made possible an accurate quantitative refraction experiment.

The bulk of the apparatus had to be designed around these all-important films. For example, it was necessary to reduce the effective width of the shock tube test section from 4 in. to 1 in., even though this decreased the optical sensitivity of the experiment, since thereby we could gain a factor of about sixteen in the strength of a film of given thickness. Also, it was necessary to grind narrow slots in the glass windows of the observation section, in order that the edges of the stainless steel frames that held the films could be recessed therein and not obstruct the gas flow in the region of interest.

The apparatus and technique of the experiment can best be visualized by reference to the diagram and photograph shown in figures 2 and 3 (plate 1). The principal piece of special equipment is a shock tube test section *H*, made of 1-in. dural plate and having internal dimensions 35 in. × 17$\frac{1}{4}$ in. × 1 in. Through the walls of this test section is mounted a cylindrical refraction cell *K*, which contains the two slotted observation windows *R*, and suitable valves and seals for introducing and holding the refracting gas. This cell rotates, and with it the interface-forming film *J*, to permit incidence of the shock wave from any angle from normal to glancing. The lower part of the test section contains a system of gears and shafts which permits a two-directional adjustment of an 18-in. leading plate *P*. The purpose of this

plate, and a similar but shorter back plate Q, is to present the incident shock to the gas interface in as neat and uncomplicated a manner as possible.

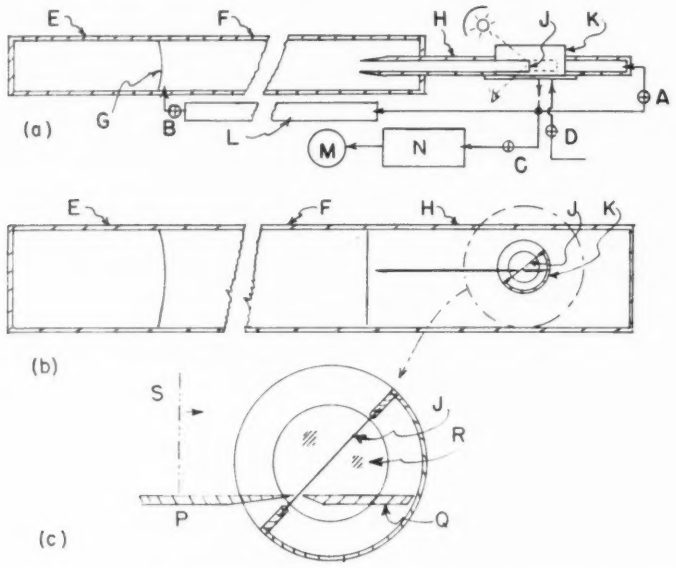

Figure 2. Schematic diagram of shock tube and auxiliary equipment for refraction experiments : (a) top view; (b) side view; (c) enlargement of test cell. A, B, C, and D are valves controlling the flow of gases to and from the rear half of the refraction cell; E = shock tube chamber; F = shock tube channel; G = plastic diaphragm; H = test section; J = interface-forming film; K = refraction cell; L = exhaust tank; M = mechanical pump; N = low-pressure reservoir; P = leading plate; Q = back plate; R = slotted glass windows; S = shock front advancing on refraction cell.

The technique actually followed in these experiments might best be illustrated in the form of a step by step recipe.

(i) The films are cast on their frames and allowed to dry.

(ii) The entire shock tube is completely evacuated, and the appropriate pressure is set in the high pressure chamber E. The channel F and test section H are then returned to atmospheric pressure.

(iii) The Zapon film, held on the stainless steel frame on which it was cast, is set into place between the slotted windows J. The refraction cell K is inserted into the test section at the desired angle and sealed to it. (Note that it is necessary to carry out steps (ii) and (iii) in this order. The thin Zapon films are so delicate that, if they were present inside the shock tube while the high pressure was being set in the chamber, they would be broken by the minute pressure pulses emitted by the plastic diaphragm G as it stretches into position.)

(iv) The leading plate P and back plate Q are adjusted until they nearly touch the film interface at its most forward point.

(v) With valves A and B open, the shock tube channel and test section are evacuated again, quite slowly, until p_1 and p_5 are equal to the desired downstream pressure. (The connection through valve A equalizes the pressures on either side of the film during the pumping process more readily than the longer connection *via* valve B.)

(vi) With valve A closed and B open, the refracting gas is now introduced very slowly into the rear of the cell *via* needle valve D, replacing the air there which exhausts into a large tank L mounted by the side of the shock tube. The other end of this exhaust tank is directly connected to the shock tube channel, thereby automatically maintaining $p_1 = p_5$. The tank is sufficiently large, and contains baffles so arranged that practically none of the exhaust gas ever drifts into the shock tube. Since the flow path of this arrangement is long compared with the size of the various orifices involved in the plumbing, p_5 tends to remain slightly higher than p_1 for any reasonable rate of flow. To compensate for this, needle valve C, connecting an evacuated reservoir (N) with the exhaust line, provides a further fine adjustment on p_5.

An external indicator of the pressure difference across the film, of the extreme delicacy needed to protect the films throughout the above process, might be difficult to arrange. But fortunately, since the interior of the refraction cell is visible through the windows, the films themselves can serve as pressure indicators. Normally, they respond to a pressure difference by a slight elastic bowing into the lower pressure region before they break. By careful observation of such distortions it is usually possible to control the gas flows sufficiently accurately to avoid a rupture. In practice, the operator, holding needle valve D in one hand and C in the other, watches the oblique reflection of a circular light source from the front face of the film. As the film bows slightly in or out under an incipient pressure difference, the reflected image becomes elliptical in one direction or the other. Keeping this reflected image as nearly circular as possible, the operator gradually opens the two valves until a reasonable flow of gas is established.

(vii) After the gas has been flowing thus through the rear half of the cell for five or ten minutes, the shock tube is fired, sending a plane, flat-topped shock wave down the tube toward the test section. Two sharp plates extending up the tube from the test section literally slice out of this shock front a 1-in. strip, which then travels over the leading plate and is presented to the 5 in. $\times$ 1 in. gas interface in the refraction cell.

Spark photographs of parallel fringe interferograms of the resulting refraction process are taken through the Mach–Zehnder interferometer. These interferograms are analysed by the standard superposition method (see Bleakney & Griffith 1954) to determine the density field, from which the shock strengths and pressure distributions can be computed.

Measurements of the wave angles can also be taken directly from the interferograms.

White light interferograms are obtained simultaneously, which aid in determining the integral fringe shift across the various density discontinuities. Two light screens record the velocity of the incident shock wave as it travels down the tube and thereby offer a double check on its strength.

There are three significant restrictions on the ideality of this experiment: the effect of the finite mass of the film, which will be discussed later; the inability to obtain completely pure gas in the refracting cell, which must be considered in the evaluation of the data†; and one other, which arises as an unavoidable consequence of the physical boundaries at which the observed refraction process begins. Nowhere in the theoretical treatment is there considered the practical limiting condition that the outflow from the reflected and transmitted waves must be supersonic in their respective gases with respect to the intersection point if regions (3) and (4) are to retain portions undisturbed by foreign signals. That is, regardless of the apparatus, the 'corner' at which the refraction process starts will radiate signals which travel out into the flow with the local sound velocity. For sufficiently glancing angles, such corner signals can 'catch' the intersection point, distort the reflected or transmitted waves, or both, and destroy the uniformity of all of regions (3) and (4), thereby violating the theoretical assumptions. This effect imposes on the regular refraction process two limiting angles†, α_{sr} and α_{st}, beyond which the observations cannot be expected to agree with the theoretical predictions. Fortunately these angles usually occur near the end of the theoretical regular refraction region, and therefore this situation does not require serious consideration until one wishes to study the irregular refraction configurations (see § VI).

Five dependent quantities are available for measurement from the interferograms obtained by the technique outlined above: ξ', ξ'', α', α'', and Δ. Of these, ξ' and α'' are the most significant to study. ξ', the strength of the reflected wave, is the most sensitive index to the refraction process, changing by large fractions of itself for comparatively small changes in the experimental conditions; and although the reflected waves are always quite weak, and the fringe shifts across them correspondingly small, the interferometric technique permits sufficiently accurate measurement of ξ' to make it an ideal quantity to study. The angle of refraction α'', though less sensitive to the parameters, is always sharply defined on the interferograms.

The remaining three quantities cannot be obtained with comparable accuracy. The evaluation of the refracted shock strength ξ'' is rather sensitive to the optical properties, and hence to the purity of the refracting gas, which varies appreciably from shot to shot. The reflected wave is so weak that the angle α' it makes with the interface is not measurable with adequate precision. (This measurement is particularly difficult when the reflection is a rarefaction fan.) Finally, the measurement of the deflection angle Δ is inaccurate because the deflected interface is rather broad and indistinctly defined on the interferograms, and because this region of the

pattern is complicated by spurious signals from the corner. Fortunately, it is also true that the angles α' and Δ are less sensitive indices to the refraction pattern than the other variables†.

Therefore, in these experiments we concentrated on the measurement of ξ' and α''. Since one of these pertains to the reflection and one to the refraction, accurate evaluation of these two can check the entire regular refraction solution. In the analysis presented in the following sections, our approach is to superimpose experimental data of ξ' and α corrected for conditional variations, on the theoretical curves of $1/\xi'$ *vs* α for the appropriate shock strength and gases. We also compare theoretical curves of α'' *vs* α with the experimental values and show that these are less sensitive to the conditions of the problem. In a few cases, we include a few spot checks on α', ξ'', and Δ to preclude any major deviation from the assumed configuration from passing unnoticed.

Once the feasibility of the technique outlined above was established by a few preliminary tests, it became necessary to select the range of initial conditions that a systematic set of experiments should cover. In this experiment, as in almost any practical refraction situation, the five independent variables of the theory (ξ, α, γ_1, γ_5, a_1/a_5) are embodied in three physical conditions, ξ, α, and the gas combination. Of the many combinations of these conditions which could be investigated in the shock tube, it was desirable to select those cases that could be handled most simply, yet still provide a truly representative check of the idealized theory. In the experiments described below, study was made of the refraction of shocks of strength $\xi = 0{\cdot}85$ and $\xi = 0{\cdot}30$ incident at angles from $\alpha = 0$ to glancing, on interfaces between air and carbon dioxide, and air and methane (hereafter denoted by air/CO_2 and air/CH_4). The reasoning behind these choices can only be outlined briefly here†.

The theory predicts two distinct classes of solutions, those which involve a reflected shock at $\alpha = 0$, and those which involve a reflected rarefaction at $\alpha = 0$, depending on the condition

$$\frac{\Gamma_5}{\Gamma_1} = \left\{\frac{\gamma_5[(\gamma_5+1)+(\gamma_5-1)\xi]}{\gamma_1[(\gamma_1+1)+(\gamma_1-1)\xi]}\right\}^{1/2}\frac{a_1}{a_5} \gtrless 1.$$

More detailed study of the way in which the gas properties enter into the problem, and of the results of the computations for many varied gas combinations, indicates that, beyond this broad distinction, there is no further significant subdivision of the solution types with respect to gas combinations.

In other words, we can reasonably expect that one representative gas combination from each of the two major classes will adequately simulate the effect of any possible arrangement of the conditions ξ, α, a_1/a_5.

An obvious simplification in the experiment is gained if we choose the gas (1), which in our arrangement must fill the entire shock tube channel, to be air. For the refracting gases (5), other than the requirement that one be 'faster' and one 'slower' than air, the only obvious properties to consider

are their manageability, index of refraction, and the ratio of their sound speed to that of air. In preliminary experiments, refracting gases which were considerably different from air, such as helium and freon, were tried on the theory that the magnitude of the refraction effects would be largest for the most dissimilar combinations. However, the large density differences involved required rather heavy films to withstand the hydrostatic pressures. Also, the large differences in index of refraction made it impossible to obtain good optical fringes over the entire field of both gases. In the long run, it was found best to study two less severe gas combinations, air/CH_4 and air/CO_2. Although the refraction effects are somewhat less pronounced for these cases, the increased precision with which the experiment can be performed more than compensates for this, and a more accurate check on the theory can be made.

The shock strengths $\xi = 0{\cdot}85$ and $0{\cdot}30$ were chosen, under considerations of operating convenience and pressure limitations of the shock tube, to provide the most reasonable check on the ξ-dependence of the refraction theory†.

The specific details of these experiments and the results obtained from them are described in the remaining three sections of the paper. § IV covers the weak shock experiments, and their results in the regular refraction regions. § V presents the strong shock, regular refraction experiments. In § VI we conclude with a description and brief analysis of the many curious patterns observed in the irregular refraction regions at both shock strengths and for both gas combinations.

IV. Experiment 1: the regular refraction of weak shocks

The first experiment studied the refraction of shocks of strength $\xi = 0{\cdot}85$ at interfaces between air/CO_2 and air/CH_4 for the dual purpose of testing the technique and apparatus outlined above, and of checking the regular refraction solutions at this shock strength. To accomplish this, refraction interferograms, samples of which are shown in figure 4 (plate 2), were taken in the manner described in § III. From these, measurements were made of reflected wave strengths, angles of refraction, and pressure distributions throughout the interaction field in sufficient quantitative detail to permit reasonable comparison with the appropriate theoretical computations.

Unfortunately, the numerical solutions computed by Polachek & Seeger (1951) involve approximate values for the pertinent gas constants. Specifically, they have assumed that the ratio of specific heats, γ, for both CH_4 and CO_2 is exactly $\frac{4}{3}$, and have rounded off the air/CH_4 and air/CO_2 sound speed ratios to convenient decimals. Before attempting any experimental comparison with their results, therefore, it was necessary to adjust their solutions by using more realistic values for the gas properties. Since these are rather small adjustments, it is adequate to evaluate them by approximate methods. For example, we chose to find the corrections at a few convenient special angles, such as $\alpha = 0$, α_t, α_e, where the computations are simpler, and then to interpolate the remainder of the solutions graphically†.

The conditions of the experiments could not be held sufficiently close even to these more realistic theoretical assumptions to permit immediate comparison of the results. Each observation had first to be adjusted for the experimental deviations from ideality mentioned in § III.

(i) The theoretical curve is based on $\xi = 0{\cdot}85$. The shock strengths actually used differ by as much as 0·025 from this value. The normalization was handled by cross-plotting graphs of $1/\xi'$ *vs* ξ for various values of α from the theoretical graphs of $1/\xi'$ *vs* α for various values of ξ. Taking the slope of the former at the point $\xi = 0{\cdot}85$ yields a function of α which, when multiplied by the deviation of the experimental value of ξ from 0·85, is just the correction desired.

(ii) Any incompleteness in the gas replacement process resulted in an impurity of the refracting gas and a consequent discrepancy from the values of γ_5 and a_1/a_5 assumed by the theory. The degree of this impurity was measured from a 'blank' interferogram, taken just before the shock tube was fired. The fringe difference across the boundary could be computed from the known index of refraction for the pure gas, and any discrepancy between this difference and that measured on the 'blank' could be used to determine the relative impurity. With this measure of the efficiency of the replacement process, and knowing the composition of the bottled gas, it was then possible to calculate a new γ_5 and a_5 for the impure refracting gas; and from these, corrections to the experimental observations could be made†.

(iii) The effect of the finite mass of the interface-forming film on the refraction configuration had to be checked experimentally. For this particular case, study was made of the density fields resulting from the normal incidence of shocks on films of various thicknesses, with air on both sides. The effect of films even five times more massive than those regularly separating the gases was found to be surprisingly small. Although sharp pulses were reflected from the films, their effective strength, that is, the ratio of the pressure before and after the pulse, was never larger than the 0·001 uncertainty with which the pressure ratio could be measured.

It is conceivable that some other complications could arise from this cause for gas combinations other than air/air and at angles other than $\alpha = 0$. Isolated tests were made at other such conditions, the net result of which was to support the assumption that in neglecting the mass of the film the error introduced was not greater than the uncertainty in the interferometric measurement of $1/\xi'$†. Actually, in the preparation of the data, account was taken of the almost trivial correction suggested by extrapolating the film test results to zero thickness.

In considering the results of this experiment, it is first to be emphasized that the qualitative nature of the interferograms taken in the regular refraction regions agrees closely with the assumptions of the theory. Namely, within the limits of the observation, each pattern is composed of an incident, reflected, and refracted wave, which are radially straight for a finite distance

from the point of intersection with the interface, and between which are regions of uniform pressure. In no case has any evidence been seen of other signals, either continuous or sharp (except, of course, the corner signals mentioned previously) or of any non-uniformity in the angular regions.

The quantitative results may best be seen in figures 5 and 6. In figure 5 are plotted the observed values of $1/\xi'$ and α. The dotted curves of $1/\xi'$ *vs* α represent the original solutions of Polachek & Seeger (1951). The solid curves are those same solutions, corrected by the use of more realistic gas

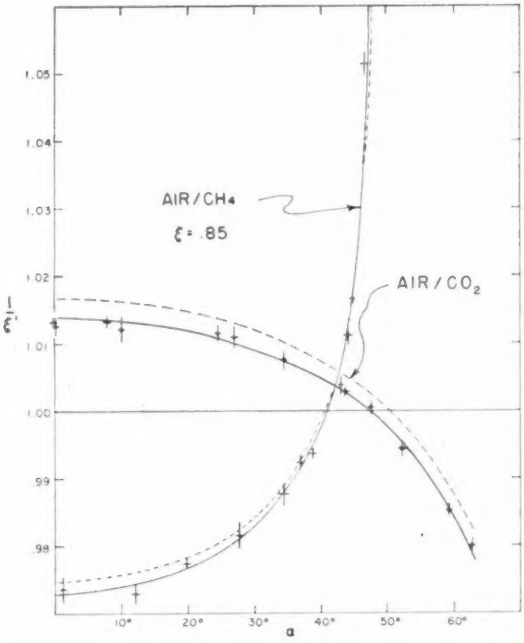

Figure 5. Experimental values of reflected wave strength ξ' superimposed on theoretical predictions, for air/CO_2 and air/CH_4 with $\xi = 0{\cdot}85$. Dotted curves represent original Polachek & Seeger (1951) solutions. Solid curves represent the same solutions, adjusted for realistic gases.

constants. The experimental points themselves have been individually corrected for variation in incident shock strength, gas purity, and film mass, wherever appropriate. The error boxes reflect the ability to evaluate $1/\xi'$ from the interferograms with an accuracy of from $\pm 0{\cdot}0005$ to $\pm 0{\cdot}0020$, dependent on the particular interferogram.

Also available for comparison with the theory are the experimental values of α'' and α. In figure 6 the dotted lines of α'' *vs* α represent the original calculated solutions at $\xi = 0{\cdot}85$; the solid lines are those solutions

corrected as above. The experimental points that are superimposed on them (error boxes are $\pm 0{\cdot}5°$) have again been corrected for gas impurity, but not for their variations in incident shock strength, since small changes in ξ caused no observable differences in α''. As evidence of this insensitivity, these graphs also show (dashed lines) the computed solutions for a much stronger shock, $\xi = 0{\cdot}30$. The curve for $\xi = 1{\cdot}00$, when plotted, could barely be distinguished from that for $\xi = 0{\cdot}85$.

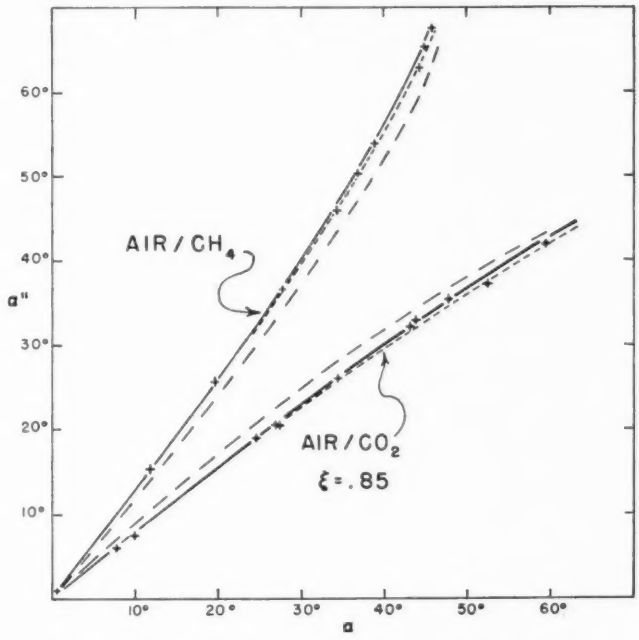

Figure 6. Experimental values of α'' superimposed on theoretical predictions, for air/CO_2 and air/CH_4 with $\xi = 0{\cdot}85$. For explanation of dotted and solid curves, see figure 5. Dashed curves represent theoretical solutions for $\xi = 0{\cdot}30$.

A few spot checks were made on the other three measurable quantities, ξ'', α', and Δ. These quantities were not studied so thoroughly as ξ' and α'', and in no case was any attempt made to correct the data for variations in the experimental conditions, or to adjust the computations for more realistic gas combinations. Rather, these measurements, a few samples of which are shown in tables 1 and 2, served merely as a reassurance that no major deviations from the theory were being overlooked by restricting the study of these quantities.

α deg.	α' theo. deg.	α' exp. deg.	Δ theo. deg.	Δ exp. deg
	Air/CO_2			
0	0	0	0	0
10	8·5	8·3	1·1	1·1
30	26·7	27·6	2·7	2·9
50	48·0	47·2	—	—
	Air/CH_4			
0	0	0	0	0
10	8 5	8·8	1·1	1·2
30	27·7	26·8	2·7	3·0
50	48·0	48·9	—	—

Table 1. Rough spot checks of α' and Δ.

α deg.	ξ'' theo. ($= \xi\xi'$)	ξ'' exp.
	Air/CO_2	
34·5	0·854	0·851
52·5	0·858	0·859
	Air/CH_4	
12·0	0·876	0·878
46·5	0·850	0·851

Table 2. Rough spot checks of ξ''.

V. Experiment 2: the regular refraction of strong shocks

The interferograms obtained of the stronger shock refraction patterns, a few samples of which appear in figure 7 (plate 3), appear much the same as those taken of the weaker shock case. There have been, of course, certain quantitative changes in the various parameters, notably the increase in strength of each of the three signals, and the change in relative sizes of the angles of the configuration. The deflection of the interface, Δ, for example,

is uniformly larger, in accordance with the higher flow velocity set up by the stronger incident shock. Similarly, the compounding of this higher flow velocity with the relative velocity of the reflected wave has tended to increase α' for those cases where $\alpha+\alpha' > 90°$ and to decrease α' for those cases where $\alpha+\alpha' < 90°$ (i.e. the flow 'blows back' the reflected wave). Also, the angle of refraction α'' now assumes a value closer to α for both the 'slow/fast' and 'fast/slow' cases, for all $\alpha < \alpha_t$†.

An interesting feature is exhibited in the white light interferograms, figures 7 c and 7 d (plate 3). The reflected shock from the air/CO_2 interface at $\alpha = 0$ (figure 7 c) is quite sharp and flat-topped. However, the reflected rarefaction from the air/CH_4 interface (figure 7 d) has already spread out considerably. Its trailing edge is actually behind the original interface position. Also note that the leading edge of this rarefaction is preceded by a slight compression bump, due presumably to the finite mass of the film.

All of the interferograms obtained in the regular region at this shock strength exhibit excellent radial straightness of the signals, and uniformity of density and pressure within each of the five angular segments, thereby displaying again a close correspondence between the experiment and the theoretical problem.

Air/CO_2	α'' deg.	ξ	$1/\xi'$
Measured value	$39{\cdot}0 \pm 1{\cdot}0$	0·305	1·0769
Correction for 9% impurity of CO_2	+0·4	—	+0·0078
Correction to make results relate to $\xi = 0{\cdot}300$	—	−0·005	+0·0016
Corrected value	39·4	0·300	1·0863

Table 3. Typical sample of corrections applied to measured values of $1/\xi'$ and α''.

Measurements of $1/\xi'$ and α'' were extracted from the interferograms just as before. Again, certain corrections needed to be made before the observed values could be compared with the theoretical calculations. The adjustment of the Polachek & Seeger (1951) solutions for the realistic gas constants was repeated as above. The corrections of the experimental values for the mass effect, the purity of the refracting gas and variation in incident shock strength also proceeded as described for the weak shock case†. As an illustration of the relative importance of the various corrections for a strong shock experiment, table 3 shows a breakdown of the computations for one typical pattern.

In evaluating the results of these experiments it is well to bear in mind that the optical sensitivity of the measurements was considerably reduced

by the necessary use of a low p_1. Assuming that it is possible to measure an interferogram to $\pm 0{\cdot}03$ fringes, $1/\xi$ could be determined to $\pm 0{\cdot}015$ and $1/\xi'$ to $\pm 0{\cdot}006$. Considering the other uncertainties of the experiment, the error limits for $1/\xi'$ range from $\pm 0{\cdot}006$ to $\pm 0{\cdot}009$. The angle α'' could normally be determined to $\pm 1{\cdot}0°$, except in a few cases where the corrections were sufficiently large or uncertain to warrant $\pm 2{\cdot}0°$ limits.

Despite this decrease in precision, the results, plotted in figures 8, 9, and 10, show that the experiment is still sufficiently sensitive to trace out a curve of agreement with the corrected Polachek & Seeger computations.

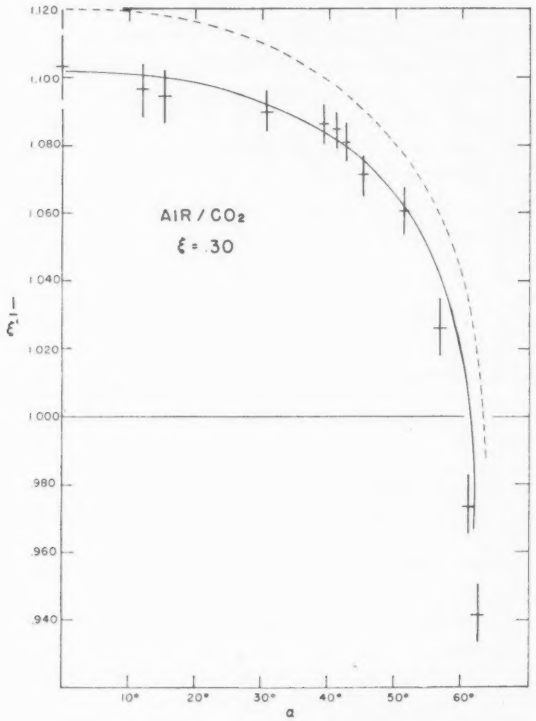

Figure 8. Experimental values of $1/\xi'$ superimposed on theoretical predictions, for air/CO_2 with $\xi = 0{\cdot}30$. For explanation of dotted and solid curves, see figure 5.

In particular it is interesting to note that the experiment is again capable of choosing between the theoretical curves for the realistic and idealized gases, even though the values of γ and the sound speeds were changed only by 2% or 3%. Consideration of the sensitivity of the experiment to changes in γ suggests the possibility of designing a more appropriate version of the

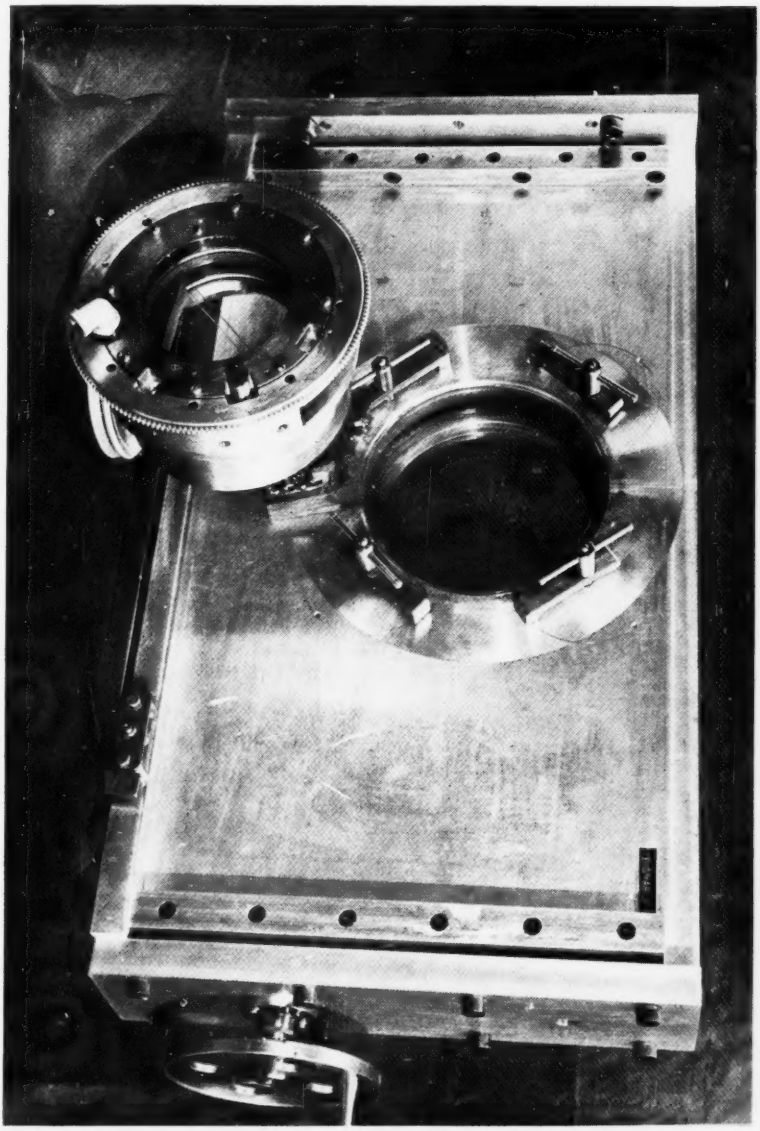

Figure 3. Refraction test section, with rotatable cell removed.

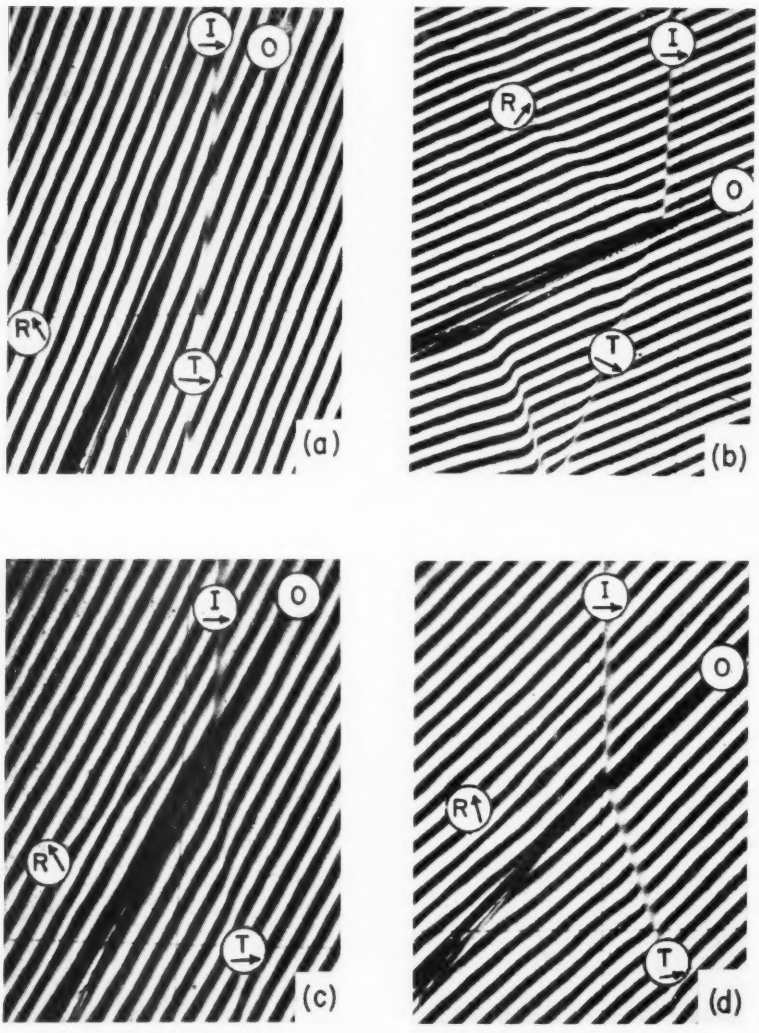

Figure 4. Refraction interferograms for shock strength $\xi = 0{\cdot}85$: (a) air/CO_2, $\alpha = 25°$ (reflected shock); (b) air/CO_2, $\alpha = 63°$ (reflected rarefaction); (c) air/CH_4, $\alpha = 27°$ (reflected rarefaction); (d) air/CH_4, $\alpha = 45°$ (reflected shock). I, R, T = incident, reflected, and transmitted waves; O = original interface; arrows indicate directions in which I, R, and T are travelling. Fringes shift toward lower right for increase in pressure.

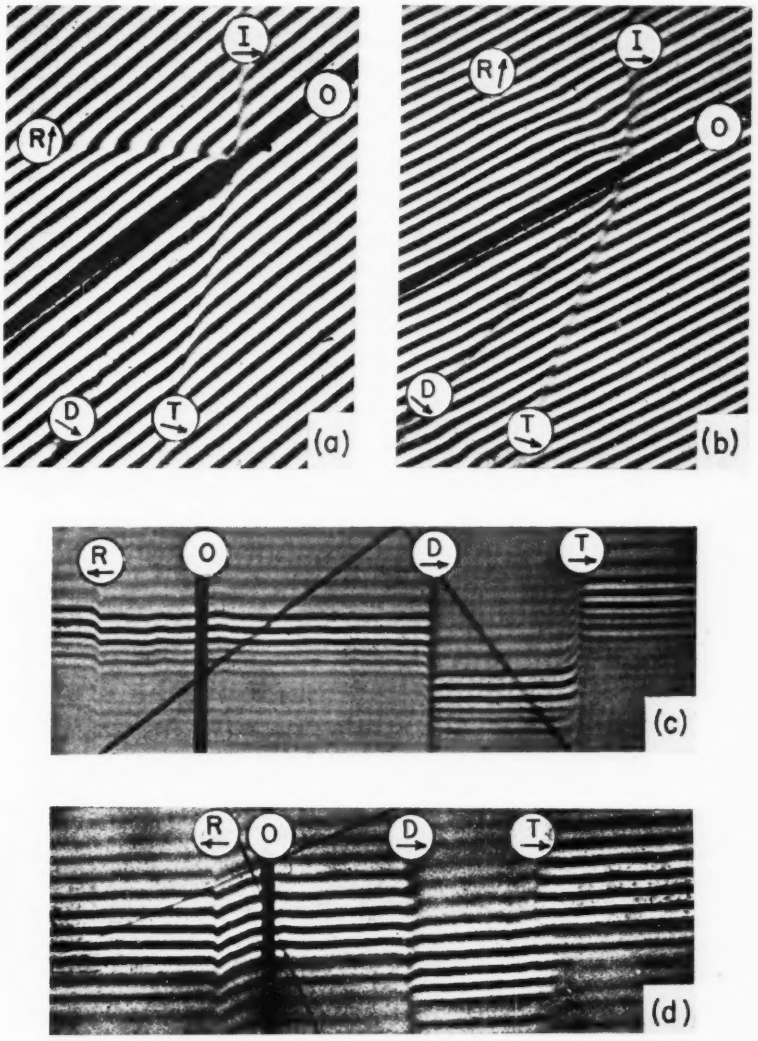

Figure 7. Refraction interferograms for $\xi = 0{\cdot}30$: (a) air/CO_2, $\alpha = 53°$ (reflected shock); (b) air/CO_2, $\alpha = 63°$ (reflected rarefaction); (c) air/CO_2, $\alpha = 0°$ (reflected shock); (d) air/CH_4, $\alpha = 0°$ (reflected rarefaction). I, R, T = incident, reflected, and transmitted waves; O = original interface; D = deflected interface; arrows indicate directions in which waves are travelling. Fringes shift down for increase in pressure.

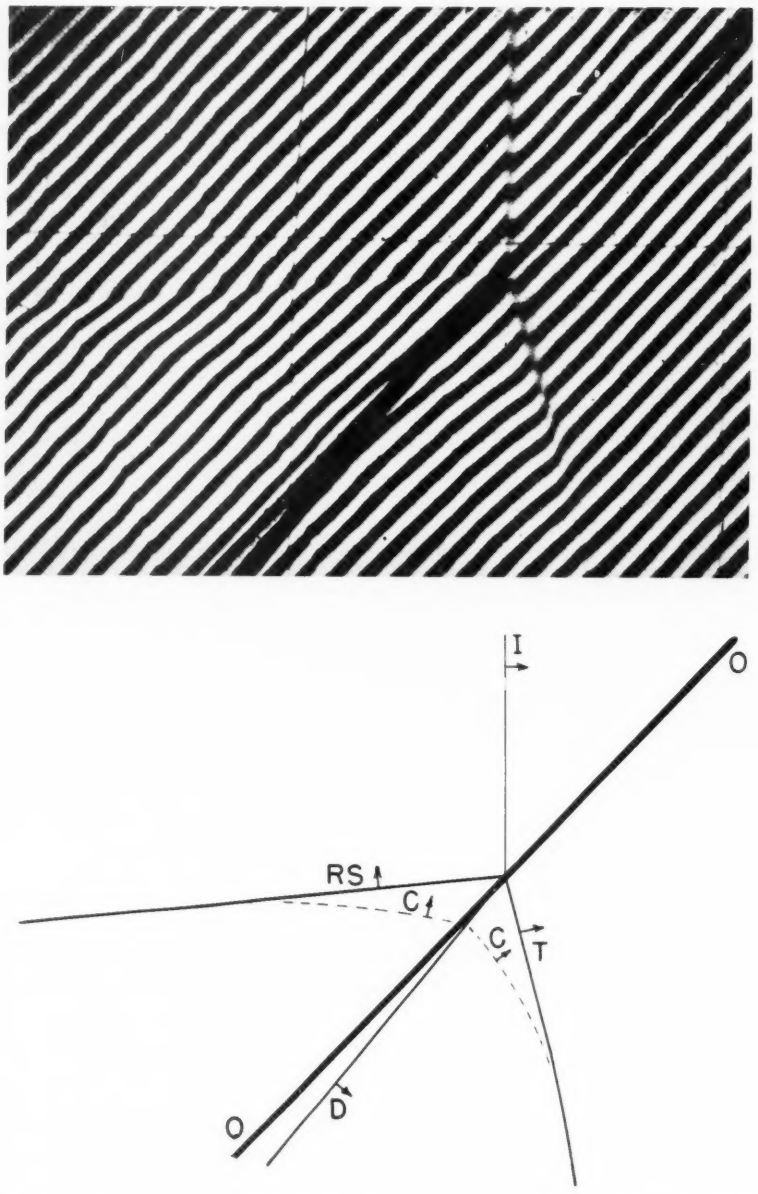

Figure 14 (a). Air/CH_4, regular refraction. (I, RS, T = incident, reflected, transmitted shocks; O, D = original, deflected interfaces; C = corner signal.)

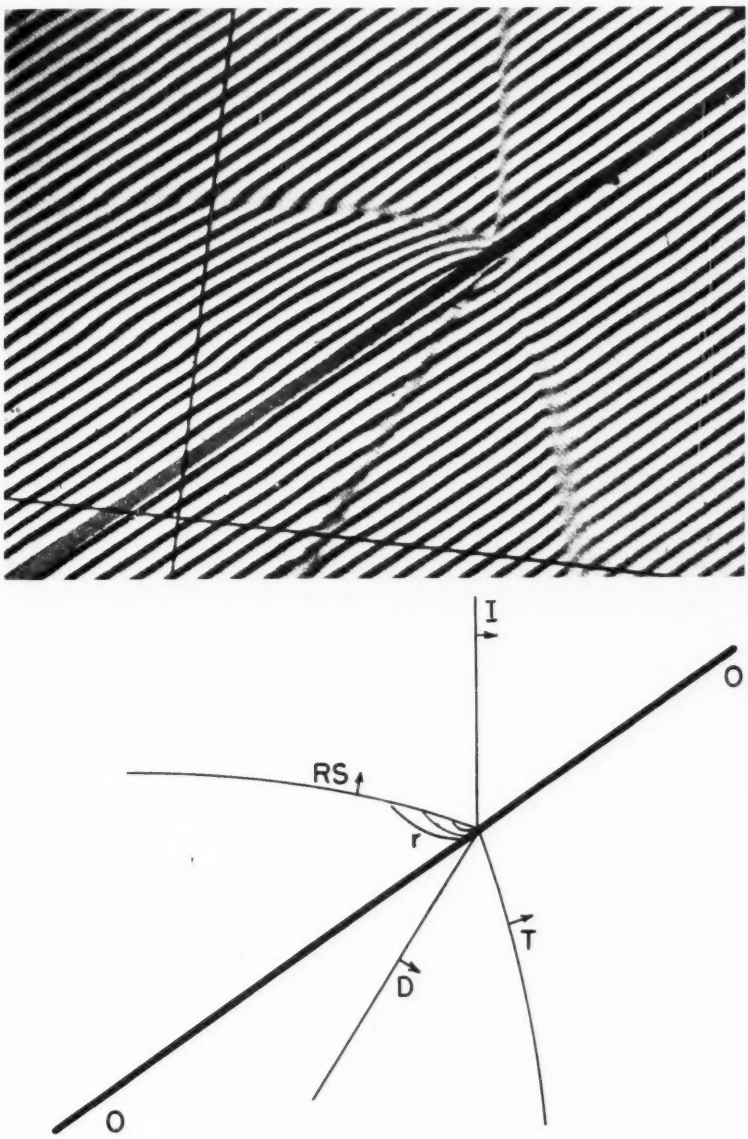

Figure 14 (b). Air/CH_4, irregular refraction, $a > \alpha_c$. (I, RS, T = incident, reflected, transmitted shocks ; O, D = original, deflected interfaces; r = sonic rarefaction front.)

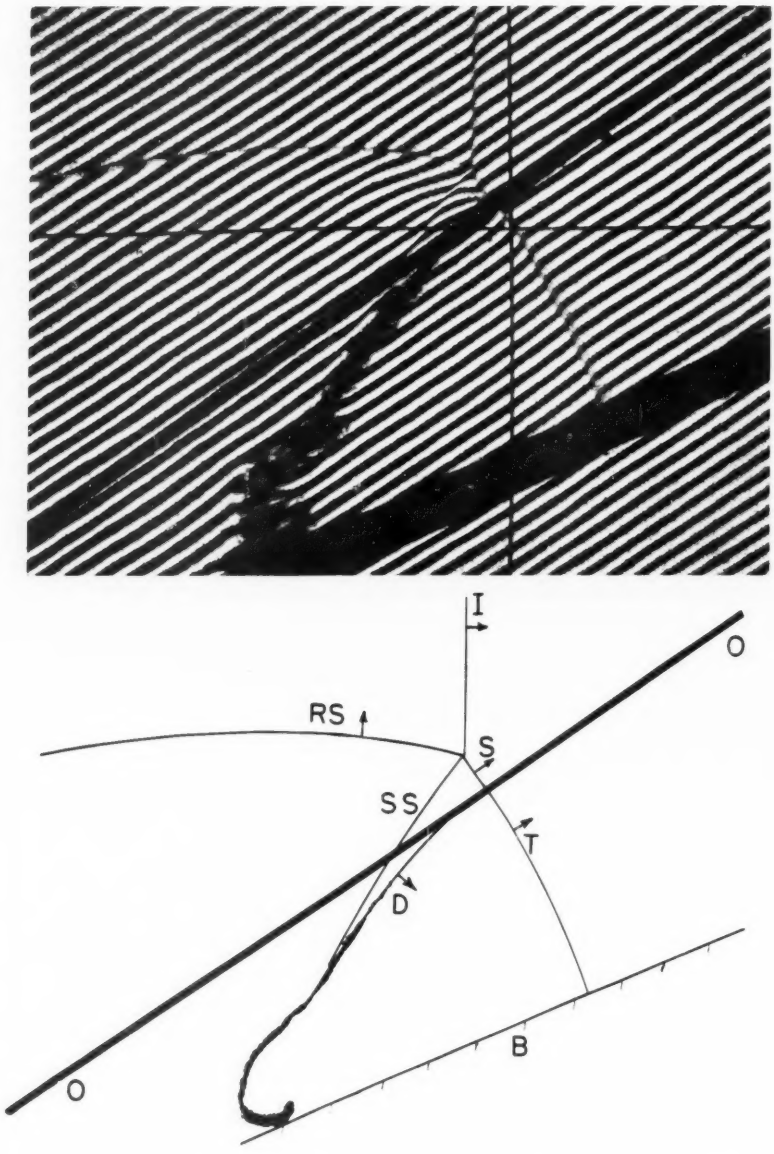

Figure 14 (c). Air/CH_4, irregular refraction, $\alpha > a_A$. (I, RS, T = incident, reflected, transmitted shocks; O, D = original, deflected interfaces; S = stem shock; SS = slipstream; B = back plate.)

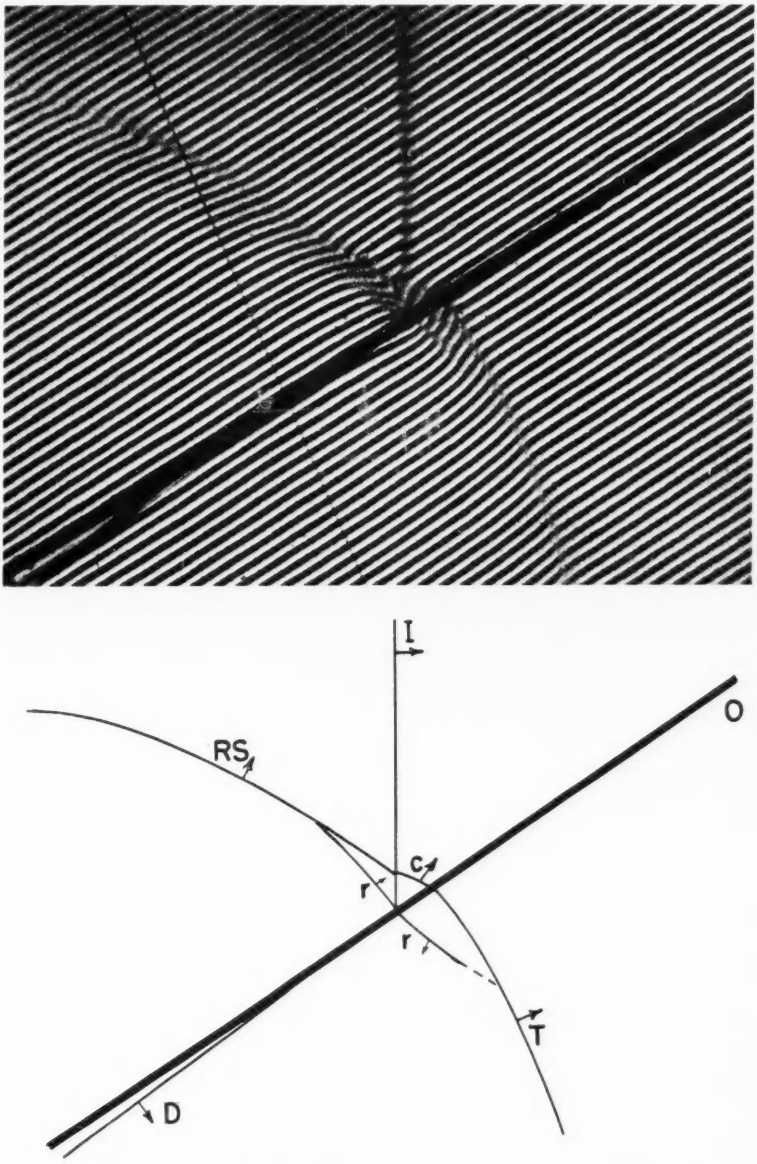

Figure 14 (d). Air/CH_4, irregular refraction, $\alpha > \alpha_i$. (I, RS, T = incident, reflected, transmitted shocks; O, D = original, deflected interfaces; c, r = sonic compression, rarefaction fronts.)

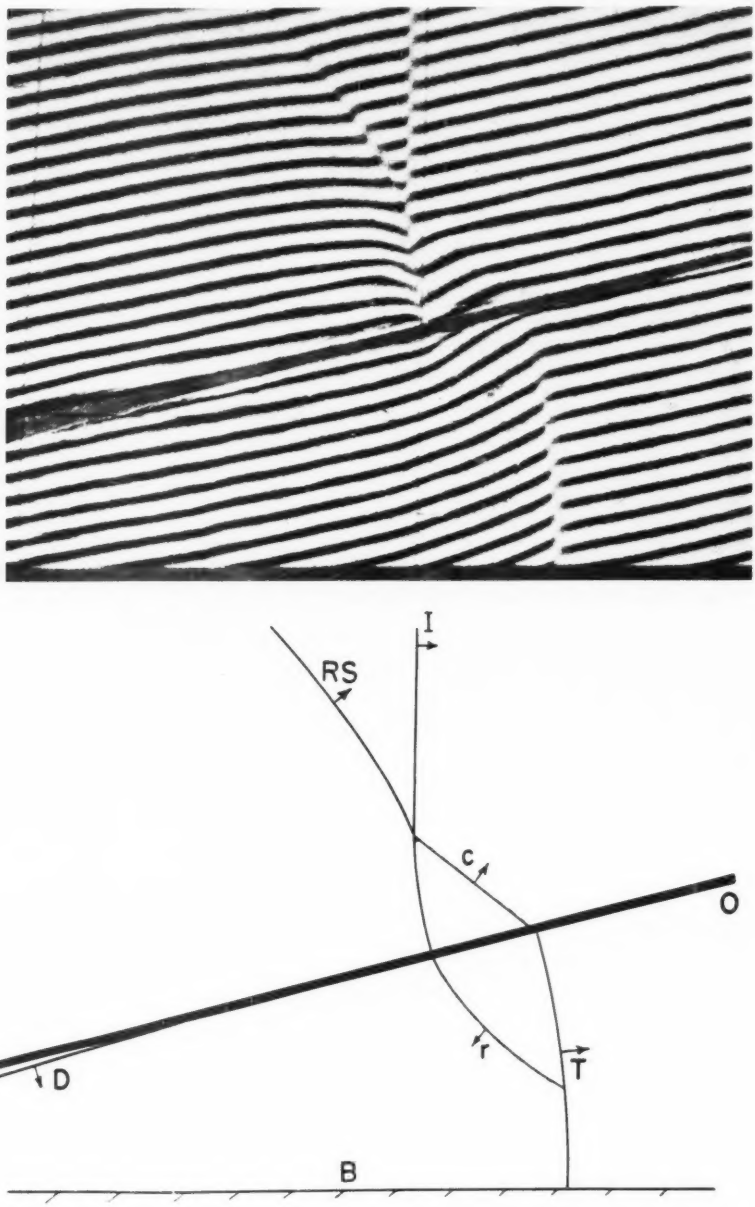

Figure 14 (e). Air/CH_4, irregular refraction, $\alpha > \alpha_j$. (I, RS, T = incident, reflected, transmitted shocks; O, D = original, deflected interfaces; B = back plate; c, r = sonic compression, rarefaction fronts.)

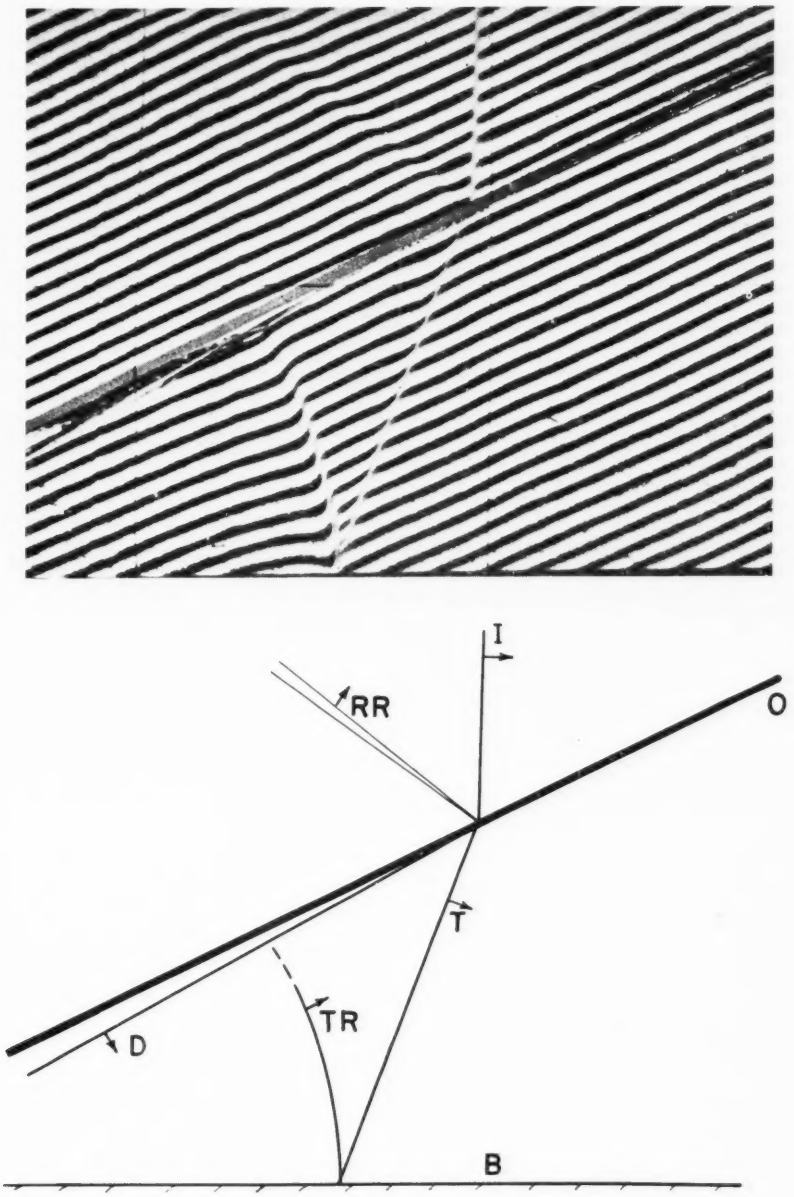

Figure 14 (f). Air CO_2, regular refraction (I, T = incident, transmitted shocks; RR = reflected rarefaction; O, D = original, deflected interfaces; B = back plate; TR = reflection of T from B.)

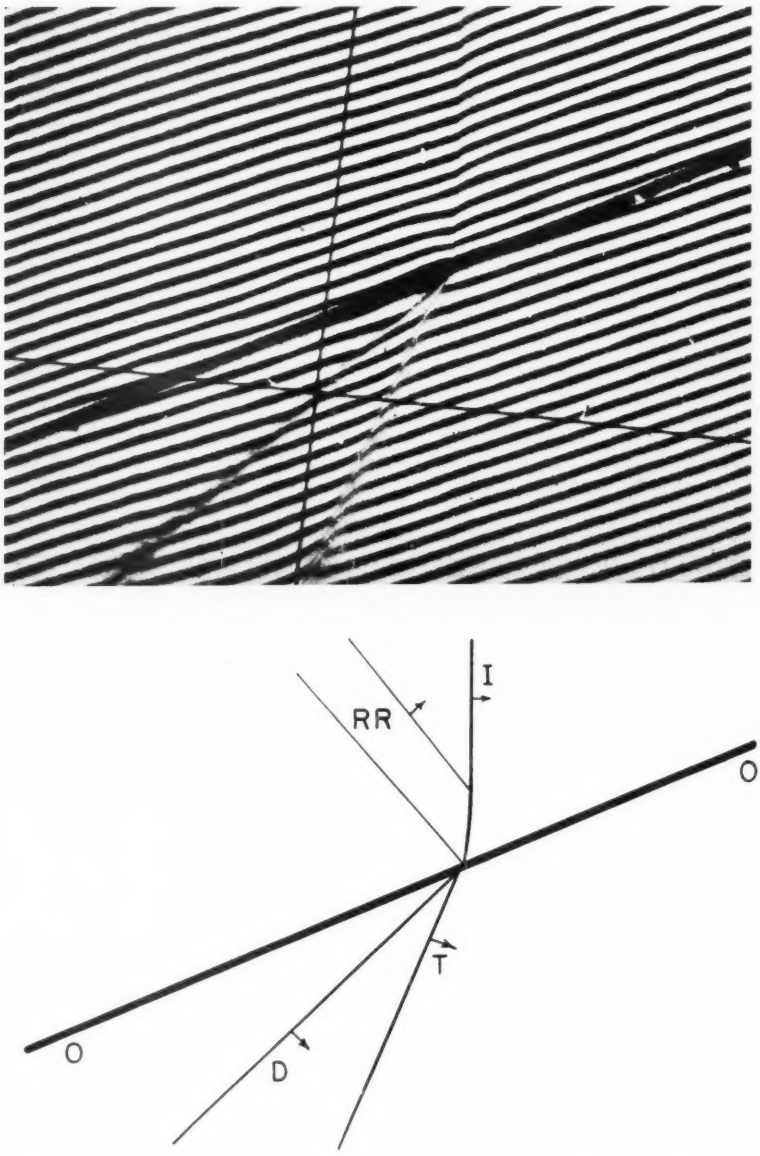

Figure 14 (g). Air/CO_2, irregular refraction, $\alpha > \alpha_{\mu}$. (I, T = incident, transmitted shocks; RR = reflected rarefaction; O, D = original, deflected interfaces.)

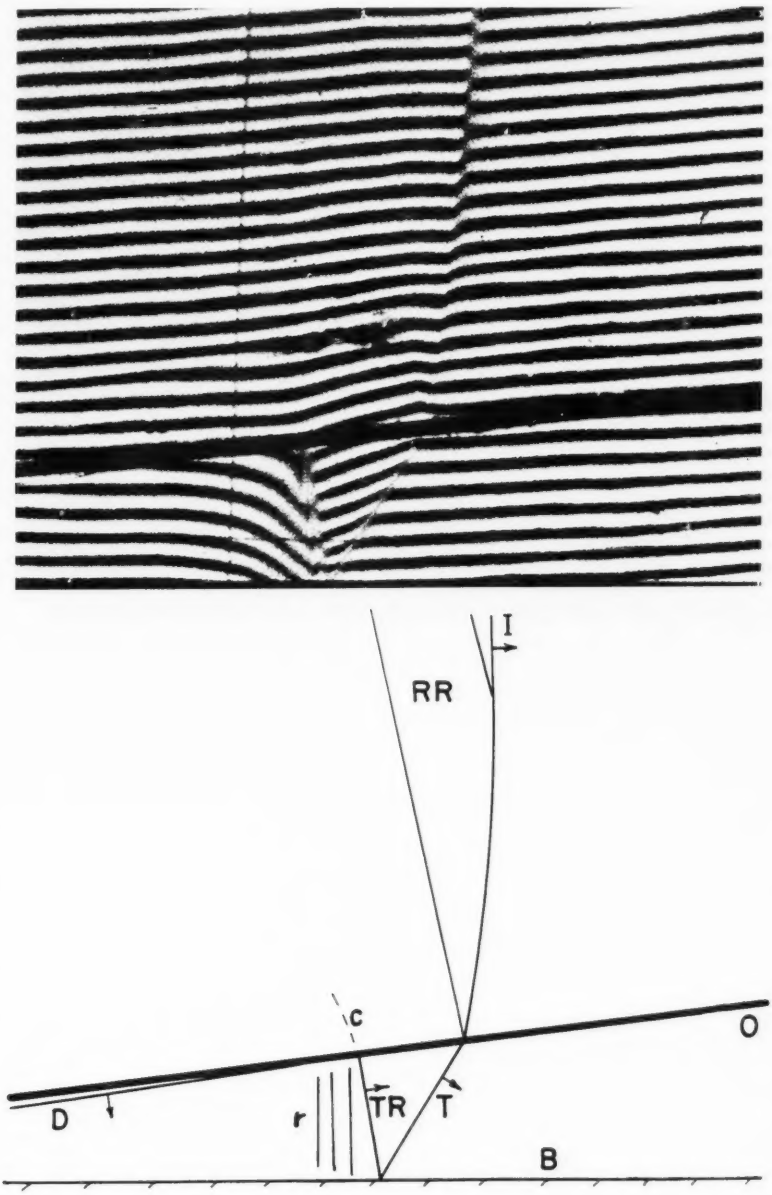

Figure 14 (h). Air CO_2, irregular refraction, $\alpha > \alpha_{cr}$. (I, T = incident, transmitted shocks; RR = reflected rarefaction; O, D = original, deflected interfaces; B = back plate; c, r = compression, rarefaction fronts; TR = reflection of T from B.)

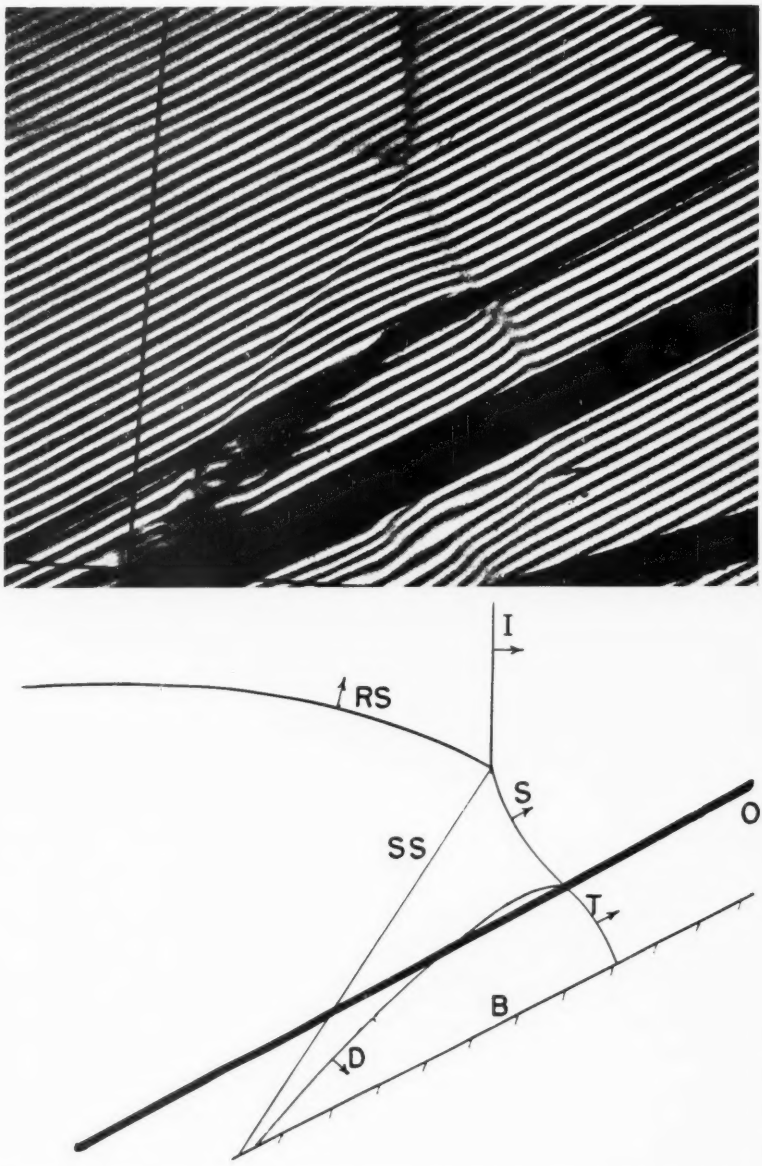

Figure 18. Irregular refraction interferogram for air CH_4 with $\xi = 0{\cdot}30$, $\alpha > \alpha_i$, and back plate B set parallel to the original interface O—a simulation of a thermal boundary layer.

normal refraction case, specifically to measure γ for either the refracting gas or air. For example, in going to progressively stronger incident shocks, it would be possible to study the dependence of γ on temperature. (These ideas were first suggested to the author by Professor W. Bleakney.)

The agreement between the theoretical and experimental values again permits endorsement of the Polachek & Seeger computations, and their choice of the physically realistic branch of the numerical solutions, for the

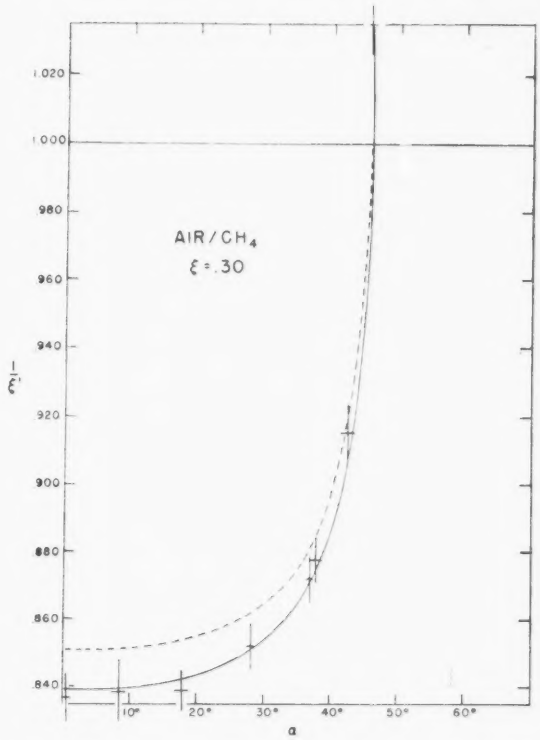

Figure 9. Experimental values of $1/\xi'$ superimposed on theoretical predictions, for air/CH_4 with $\xi = 0{\cdot}30$. For explanation of dotted and solid curves, see figure 5.

specific cases studied here. More generally, by the reasoning offered in § III, it can now be inferred that the theory of regular refraction from which these computations were made is valid for any shock strength from the acoustic limit, $\xi = 1{\cdot}00$, to $\xi = 0{\cdot}30$, and for any gas combination having constant values of γ_1, γ_5, and a_1/a_5 in this range of values of ξ.

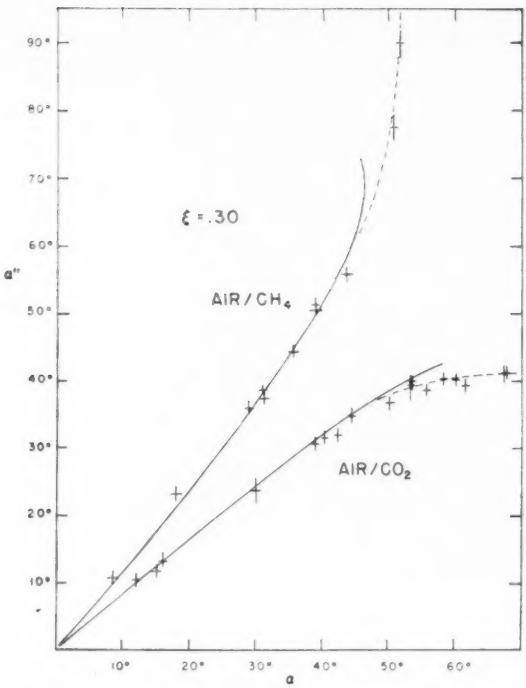

Figure 10. Experimental values of α'' superimposed on theoretical predictions, for air/CO_2 and air/CH_4 with $\xi = 0{\cdot}30$. Solid curves are adjusted Polachek & Seeger (1951) solutions. Dotted lines follow experimental points into irregular refraction regions.

VI. Experiment 3 : irregular refraction

In the mathematical formulation of the theory of shock wave refraction there arise certain upper limits on the angle of incidence α, beyond which no real solutions can be obtained for the assumed configuration. The region from $\alpha = 0$ to the smallest of these limiting angles for a particular refraction problem is defined as the region of regular refraction for that problem. So far our experiments have been concerned exclusively with this region and have indicated the validity of the refraction theory within it. We now consider the refraction problem for angles of incidence beyond the limiting angles, where the idealized theory becomes inadequate.

The failure of the theory to produce realistic solutions beyond the first limiting angle implies physically that the assumed regular refraction process has been replaced by some other type of interaction. Actually, we find experimentally that several different configurations occur in this region, each of them more complex than the regular refractions. These irregular interactions are a significant part of the overall refraction problem. In no

case do the regular refraction solutions persist through to $\alpha = 90°$; in fact, for many reasonable gas combinations, the first limiting angle is quite small, so that the irregular regions for these problems are larger than the regular ones. For this reason alone, some survey of the irregular phase is needed to complete the experimental refraction study. But even beyond their significance in the specific problem, irregular refractions are interesting phenomena in their own right.

In presenting the results of this group of experiments, the approach will be simply to display examples of the various types of configurations that were observed in the irregular refraction regions, and describe the principal features of each pattern. Then, in the absence of any quantitative theory with which to compare the observations, it is interesting to consider, at least qualitatively, the correspondence between the theoretical limiting conditions of regular refraction theory and the irregular patterns that result when those conditions are exceeded. For example, it is possible to show that the various patterns are related to each other in a continuous sequence, and that they may be considered to evolve from one to another, beginning with the regular pattern, under the influence of those aerodynamic requirements which bring about the limiting conditions. In order to appreciate this relation of the irregular patterns to the limiting conditions, it is best first to discuss the theoretical critical angles and the physical restrictions they represent.

Recalling the formulation of the regular refraction problem outlined in § II, it is possible to anticipate several situations which will make one or more of the assumptions of the idealized model untenable. These may be discussed most conveniently in terms of the smallest angles of incidence at which, for fixed values of the other parameters, the complicating effects first occur. These limiting angles are as follows.

(*i*) α_a *and* α_A

The theory assumes that the reflected wave will be either a radially straight shock, or a Prandtl–Meyer expansion fan, both centred on the point of intersection of the incident shock with the gas interface. For sufficiently large α, however, region (2) becomes subsonic with respect to the point X. Hence, the angle at which this situation begins is a limit on the assumed configuration. Note that this angle, denoted by α_a, depends only on the value of γ for gas (1) and on the incident shock strength. Actually, if the reflection is a shock, the limit α_a is not strictly appropriate. Rather than require the outflow from the incident shock to be just sonic with respect to the reflection, we should require the flow to be sufficiently supersonic to permit the existence of the finite shock demanded by the pressure and deflection conditions. For example, for $\xi = 0{\cdot}30$ in air, $\alpha_a = 61{\cdot}5°$; however, for air/CH_4, a reflected shock with $1/\xi' = 1{\cdot}20$ occurs at this angle. Such a shock requires the inflow Mach number to be approximately 1·09, and hence the true limit, which we denote by α_A, is some 4 or 5 degrees lower than α_a.

(*ii*) α_i *and* α_j

In those cases where $a_1 < a_5$ ('slow/fast'), α'' normally exceeds α, and thus reaches 90° at some $\alpha < 90°$. Expressed more rigorously, it is a consequence of the assumed pattern that $Ma_1/\sin\alpha = M''a_5/\sin\alpha''$, where M'', the Mach number of the transmitted shock, is fixed, independently of this relation, by the pressure and deflection requirements of the problem. Clearly, if the value of M'' computed from these requirements exceeds $Ma_1/a_5 \sin\alpha$, the value of α'' predicted for the assumed pattern becomes imaginary. Physically this must correspond to a limit on the regular refraction configuration. The angle of incidence at which this effect begins is denoted by α_i, and is given by

$$\sin^2\alpha_i = \left(\frac{Ma_1}{M''a_5}\right)^2 = \left(\frac{a_1}{a_5}\right)^2\left(\frac{\gamma_5}{\gamma_1}\right)\frac{[(\gamma_1+1)+(\gamma_1-1)\xi]}{[(\gamma_5+1)(1/\xi')+(\gamma_5-1)\xi]}.$$

(In calculating this angle for tabulation, Polachek & Seeger (1951) have introduced the approximation $1/\xi' = 1$. In some cases, particularly as $\xi \to 0$, this leads to sizeable error, and even to a misplacing of this limit with respect to the others.)

In one sense α_i corresponds to the angle of total internal reflection in optics, since, at this angle, the transmitted signal is travelling parallel to the interface. The analogy is incomplete, however, since in no case short of an infinite impedance ratio across the interface will the incident shock be totally reflected.

It is expedient to define another critical angle α_j which is related to, but always larger than, α_i by

$$\sin\alpha_j = \frac{Ma_1}{a_5}.$$

When $\alpha = \alpha_j$, the point of intersection of the incident shock, X, travels along the interface with a velocity just equal to a_5. For $\alpha > \alpha_j$, therefore, region (5) becomes subsonic with respect to this intersection point, and consequently the transmitted wave can no longer be a shock. Also, some of the region *ahead* of X, both in (5) and (1), can now be influenced by things happening at and behind X.

(*iii*) α_e

There exists one other limit, which is somewhat more intrinsic than the others, in that it concerns the extent of compatibility of the pressure and deflection requirements. Stated simply, as α becomes larger, an angle of incidence is reached beyond which it is no longer possible to satisfy both the pressure and deflection requirements by any arrangement of strengths and positions of the reflected and transmitted waves. The situation is sufficiently analogous to the extreme angle occurring in the theory of regular reflection to justify the same notation, α_e, for this regular refraction limit. Beyond this angle, the equations produce no real solutions. In most cases, the theoretical curves of $1/\xi'$ *vs* α double back to presumably unrealistic alternative values of ξ' at α_e.

The significance of α_e is increased by the fact that it invariably precedes α_i for any gaseous refraction. The proof of this can be stated very simply. At $\alpha = \alpha_i$, $\alpha'' = 90°$, hence δ'', the deflection of the flow by the lower path, is zero. Then, in order to have $\delta + \delta' = \delta''$, δ' must be equal to $-\delta$, and this is obviously impossible with ξ' an order of magnitude weaker than ξ. Therefore the α_e-condition must have occurred before $\alpha = \alpha_i$. In other words, a regular refraction pattern with $\alpha'' = 90°$ cannot be achieved.

Thus it must be α_e or α_a (or α_A, whichever is appropriate) that establishes the extent of the regular refraction regime and introduces the first irregular pattern. The order in which these limits occur depends on both the gas combination and the incident shock strength. For most combinations in which a_5 is substantially larger than a_1, the deflection condition becomes critical before region (2) becomes subsonic. In these cases, α_e occurs first. For most combinations in which $a_5 \doteq a_1$, or $a_5 < a_1$, however, the limiting angles α_e and α_a (or α_A) are quite close and the order of their occurrence depends on the incident shock strength†.

(At this point it might be argued that, for any given refraction problem, all limiting angles except the first have only academic significance, for they are derived as limits to a regular refraction process which terminates before they are reached. While it is true that the numerical values of these angles computed on this basis are not entirely realistic, the requirements on the refraction process that they represent are still pertinent, even for the irregular configurations, and the effects resulting from violating these requirements are observed experimentally at sufficiently large α. In fact, the effects associated with exceeding α_i and α_j, which can never be the first limiting angles, are the most pronounced of all the irregular interactions.)

(*iv*) α_{sr} *and* α_{st}

In any physically realistic refraction situation, it is also necessary to consider two other practical limits to the existence of a regular pattern. As mentioned in § III, the ideal regular configuration can be realized experimentally only so long as the outflow in regions (3) and (4) is fast enough to prevent signals from the 'corner' from overtaking the intersection point. Beyond some limiting angle of incidence, this condition cannot be met and various signals, associated with the physical corner at which the refraction process began, are able to overtake and contaminate the region of interest in the pattern. This complication is not, of course, peculiar to the refraction problem. Almost any two- or three-dimensional shock interaction experiment must reckon with this situation in one form or another (in particular the Mach reflection problem, cf. Fletcher, Taub & Bleakney 1951). The persistent occurrence of corner interference in such problems has often inspired philosophical discussion about the futility of considering them without complete specification of the physical corners at which the processes will begin. Rather than digress into that arena, however, we will merely state here the nature of the corner signals in the refraction problem, and indicate methods of treating this complication†.

In a refraction problem, the corner signal may be either a compression or a rarefaction front. Its phase and strength are determined by (i) the phase and strength of the reflected wave, (ii) the interaction of the transmitted shock with the back boundary, and (iii) the nature of the mechanical corner formed by the leading plate and back plate, around which the flow behind the transmitted shock must deflect (see figure 11). In a sense, each of

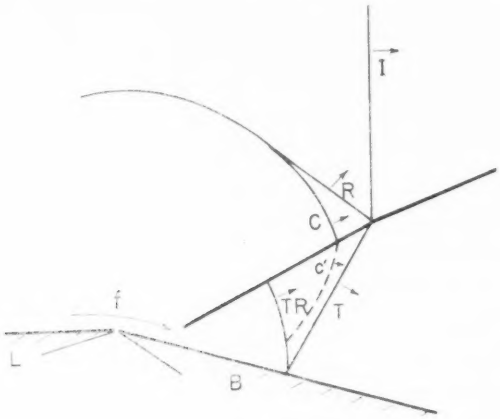

Figure 11. The corner signals in a refraction experiment. The reflection TR of the transmitted shock T, the deflection of the flow f around the corner formed by the leading plate L and the back plate B, and the finite length of the reflected wave R, each contribute to a composite corner signal C which radiates from the corner with the local speed of sound in the two gases. In general, these speeds differ, and hence a secondary signal c' is transmitted across the deflected interface from the faster to the slower medium, ahead of the original corner signal in that medium.

these three effects contributes a component to a composite corner signal which radiates from the point of origin of the process with the local velocity of sound, compounded vectorially with the flow velocity.

It is the 'catching up' of this composite signal with the intersection point in the incident and refracting media that constitutes the experimental limits α_{sr} and α_{si}. If this corner signal is a net rarefaction, the effect of its overtaking a shock will be to weaken the shock and curve it backward (making it less normal to the flow); if it is a net compression, it will tend to strengthen the shock, thereby curving it forward (more normal to the flow).

Note that the strength and phase of the first component is fixed automatically for a given refraction situation, but that the latter two are under the control of the experimenter who, by changing the angle of the back plate, can vary the strength of these components and hence the strength of the composite signal. In practice, use was made of this valuable feature *via* two complementary procedures which served to separate the effects associated entirely with the idealized irregular refraction process from those which are dependent on the corner situation.

(i) A given irregular refraction was performed with the back plate set to form a corner signal which was a net compression. The same refraction was performed with the back plate reset to form a net rarefaction corner signal. Those effects which appeared the same for both cases were assumed to result solely from the refraction process.

(ii) The back plate was adjusted so that the various contributions to the corner signal compounded to zero in the region of interest. This could be done by setting the back plate to some intermediate angle such that the net contribution from the mechanical corner and the transmitted wave interactions just balanced the uncontrollable component associated with the reflection process. In this way, the most interesting part of the refraction pattern could be observed, free from corner interference.

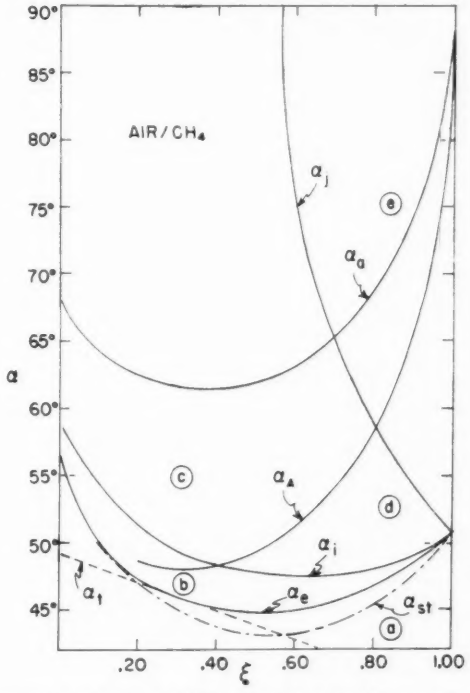

Figure 12. The critical angles for air/CH_4 *vs* incident shock strength. Circled letters refer to corresponding interferograms in figure 14 (plates 4 to 8).

The considerations outlined above suggest the following physical behaviour. As the angle at which the shock impinges on a specific gas/gas interface is made more and more glancing, an angle of incidence is reached—the first limiting angle for the case involved—beyond which the regular refraction pattern cannot occur, but is replaced by a new configuration. We expect that this new configuration will be related to the regular pattern it has replaced, in fact that it will be a distortion of it, and that this distortion

will be such that the flow requirements that brought about the demise of the regular pattern are now reconciled. As the angle of incidence is increased further, a limiting condition for this irregular pattern may be reached, at which point a new distortion of the configuration must occur to accommodate the second critical requirement. The pattern will continue to evolve in this way, adjusting itself to each new requirement by some distortion, until α reaches 90°.

In figure 14 (plates 4 to 11) are displayed samples of the super-critical patterns that were observed for the air/CO_2 and air/CH_4 gas combinations. Figures 14 a to 14 e show an essentially complete series of irregular configurations for air/CH_4, arranged in order of increasing angle of incidence. Figures 14 f to 14 h show a similar series for air/CO_2. Each interferogram is accompanied by a line diagram to clarify the position and nature of the various signals involved in the interaction.

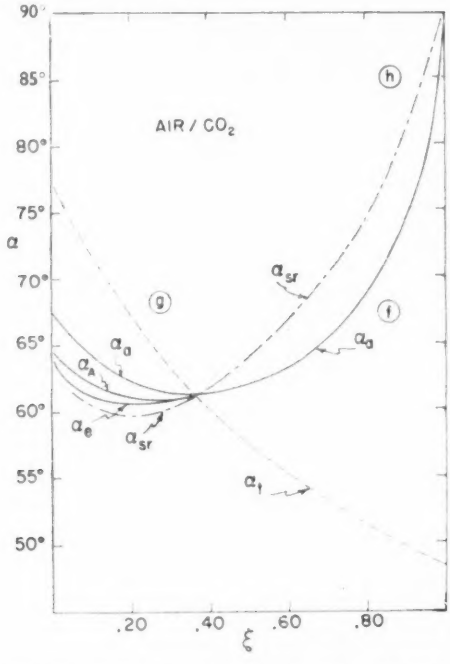

Figure 13. The critical angles for air/CO_2 *vs* incident shock strength. Circled letters refer to corresponding interferograms in figure 14 (plates 9 to 11).

The relation between a given configuration and the various critical angles may be visualized by reference to figures 12 and 13, in which are plotted the pertinent critical angles as functions of the shock strength for the two sets of gases. On these figures, the regions characterized by the subsequent interferograms are indicated by circled letters corresponding to

the appropriate patterns in figure 14. Note especially that the critical angles have substantially different values at the two shock strengths used, namely $\xi = 0{\cdot}85$ and $\xi = 0{\cdot}30$. This feature, and the previously mentioned extra degree of freedom available in the back boundary, were utilized extensively to separate the various irregular refraction effects from one another and from the corner effects†. In a few cases, two critical angles fall so closely together that it is not possible to separate out their two effects by a single picture taken between them, and less direct methods have had to be used to study that region. Nevertheless, it has been possible to construct, from interferograms such as these, a rather complete catalogue of the irregular refraction effects and their relation to specific critical conditions. This may best be illustrated by brief separate discussions of each of the patterns.

The air/CH_4 irregular refraction patterns

Figure 14a (plate 4) shows the regular refraction pattern that exists for the air/CH_4 combination just below the first critical angle. Note that all three shocks are straight, and that the angular regions between them are uniform in the neighbourhood of the intersection point. In the regions behind the reflected and transmitted waves, it is possible to observe a weak rarefaction front. This is the corner signal for this particular arrangement of the boundaries; at this angle of incidence it has not been able to overtake the region of interest.

As the angle of incidence is increased, the first limiting angle to be exceeded is α_e. Figure 14b (plate 5) shows the pattern that is observed for this situation at $\xi = 0{\cdot}30$. Since α_{st} has also been exceeded, it becomes necessary to investigate the extent to which the corner signal is contaminating the refraction pattern. In practice this was done by comparing many patterns taken in this same irregular region, at different shock strengths and with different settings of the back boundary, to separate out those effects which were boundary-dependent and hence not directly related to the exceeding of the α_e-condition†. This done, the following features of figure 14b remain attributable to the refraction process.

The reflected wave *RS* is curved all the way into the intersection, and its strength increases very rapidly near the intersection. In its region of greatest strength, *RS* is followed by a sharp expansion region, which has the effect of 'peaking' the reflected shock, the front of which is now comparable in strength to the incident shock! Curiously enough, none of the other regions or signals in the pattern are appreciably disturbed. Even the deflected interface, which is adjacent to the outflow from this anomalous reflection, is still radially straight from the intersection point.

It is best next to consider the effect of exceeding α_A, which is shown in figure 14c (plate 6) for $\xi = 0{\cdot}30$. When adequate compensation for the corner effects has been made, in a similar manner to that described above, the following features of the pattern remain pertinent to the refraction process for this case.

A configuration much like a Mach reflection exists on the air side of the interface, complete with a Mach stem, a curved, varying strength reflection, and a slipstream from the triple point. The reflected signal and the stem are both peaked near the triple point. The deflected interface is now curved along its entire length and approaches quite close to the slipstream as the two near the back plate. Thereafter they both exhibit an almost turbulent curling.

The effect of exceeding α_t is not very noticeable at the stronger shock strengths, and α_j is imaginary there, so to study these we returned to the case $\xi = 0{\cdot}85$. The onset of the process is shown in figure 14 d (plate 7). Note that several significant alterations have taken place. The transmitted shock has degenerated, near the interface, into a continuous compression, the leading edge of which is overrunning the intersection point of the incident shock slightly. A compression pulse has been retransmitted into region (1), ahead of the incident shock *I*. This, in turn, deforms *I* near the interface. The reflected shock and the sharp rarefaction region following it (cf. 14 c, plate 6) have been distorted into a complex pulse, the leading edge of which has advanced up the back of *I* to the point where *I* intersects the retransmitted compression.

As the angle of incidence increases still further, the effects just described become more distinct. For example, figure 14 e (plate 8) displays the situation for $\alpha \doteq \alpha_j$. In this case, the inflow in region (5) on the transmitted wave would not be even sonic if *T* did not run out ahead. Two differences may be noted between this pattern and that for $\alpha > \alpha_i$. The transmitted shock has now degenerated completely into a compression front at the interface. Also, the reflection is a cleaner shock, and the rarefaction following it is much less steep, than those appearing in the previous case.

The air/CO_2 irregular patterns

The irregular refraction region for the air/CO_2 problem is considerably less complex. The only pertinent limiting angles are α_e and α_a (and α_A for $\xi < 0{\cdot}37$), and, as may be seen in figure 13, the curves for these, along with that for α_{sr}, are crowded together in a narrow band over most of the range of values of ξ. Nowhere is the angular interval between α_e and α_a (or α_A) large enough to permit an observable development of the irregular effect related solely to the former, before it is obscured by the rather prominent effect arising from the latter. Consequently, it is possible to observe only one type of irregular pattern for this problem—one that exhibits primarily the effect of exceeding the α_a-condition. This is a rather interesting case, however, since it displays the transition of the reflected rarefaction from a supersonic to subsonic phenomenon.

An example of the regular refraction pattern that exists at values of α just below α_a is shown in figure 14 f (plate 9). The irregular pattern that appears when α_a is exceeded follows in figure 14 g (plate 10). The principal changes to be noted concern the reflected rarefaction which, by the definition of α_a, now finds itself in a subsonic region. *RR* is no longer a centred wave,

but its leading edge has advanced into region (2), having climbed a short distance up the back of the incident shock *I*. (This intersection of the leading edge of *RR* on *I* subtends an angle at the corner which is approximately equal to α_a.) That portion of *I* that is overtaken by this rarefaction edge is weakened by it, and consequently curved backward slightly, causing it to make a smaller angle with the interface. The back edge of the rarefaction remains fixed at the intersection point. With these exceptions, the remainder of the fields (2) and (3) are uniform, as in regular refraction.

As α is increased further into the irregular range, the situation described above changes in magnitude only, with no other noticeable effects appearing.

The pattern shown in figure 14g was obtained with the back plate set normal to the transmitted shock. To illustrate how the corner effect from a less favourable boundary arrangement can confuse the refraction process, consider figure 14h (plate 11), which was obtained with the back plate set normal to the incident shock. In addition to the effects observed in the preceding pattern, there now appears a compression region behind the reflection—a feature which was totally absent in the other cases. Apparently this results from the draining of the excess pressure behind *TR* across the interface into the upper region (3), in which the compression can travel fast enough to reach the reflected wave. Some of this effect even extends back across the interface into the region (4) behind *T*, making it also non-uniform. The relief of the pressure behind *TR* is evidenced by the strong rarefaction following it. From another point of view, the shock *TR* can be considered to be refracting, irregularly, at the CO_2/air interface, producing a configuration not unlike that seen for air/CH_4 at glancing incidence (cf. figure 14e, plate 8).

The interpretation of the irregular patterns

From the experiments we know that each irregular refraction pattern is a pseudo-stationary equilibrium configuration; that is, the pattern grows linearly with time†. As such, the process can be treated as a steady state when expressed in distance/time coordinates. A formal theory of this interaction would have to derive the steady-state configuration from basic principles and initial conditions, just as was done for regular refraction. In this case, though, the assumed models would need to be quite complex, and the resulting computations correspondingly complicated. However, since we are dealing with a pseudo-stationary problem, some qualitative predictions can be made from perturbation considerations. From the experiments we have seen that the various configurations that develop as the angle of incidence is increased are related to one another in a continuous fashion, forming, as it were, a sequence, or evolution of patterns, rather than exhibiting any abrupt changes in detail. Hence, it should be possible to infer the nature of any one of them from a knowledge of an adjacent pattern, and consideration of the flow conditions that necessitate the change.

As an illustration, consider first the one observable irregular pattern for air/CO_2. The regular pattern observed for α just below α_a is shown in

figure 14 f (plate 9). Now, perturb this stable configuration slightly by increasing α until it is larger than α_a and then readjust the pattern accordingly until a new equilibrium condition is achieved, as follows.

When α exceeds α_a, the gas flow in region (2) becomes subsonic relative to the reflected rarefaction *RR*. Therefore, the Prandtl–Meyer wave, which requires sonic flow normal to all its radial characteristics, can no longer exist as such. Instead, the leading edge of the rarefaction is free to run ahead into region (2). Consequently, this front, remaining straight but no longer centred at the intersection point *X*, will overrun part of the incident shock *I*. If α is not too much greater than α_a, the expansion will still be sufficient to return the flow to sonic velocity behind *RR*, and the trailing edge will retain its centred position.

That portion of *I* near the interface that has been overrun by the rarefaction will now be weaker and hence more inclined to the incoming flow there. The effect, thus, is to curve *I* from the interface up to the intersection with the rarefaction front, causing it to be incident at a smaller angle on the interface. The pattern just constructed is essentially that observed experimentally (figure 14 g, plate 10).

A similar line of reasoning can be applied to the series of air/CH_4 irregular refraction patterns. The first critical condition is associated with the α_c-limit, the violation of which results in the most subtle, yet probably the most significant, of all the irregular effects. If we make α slightly larger than α_c, we impose upon the reflected shock *RS* and the transmitted shock *T* incompatible pressure and deflection conditions. The essence of the situation is that, if we required *RS* and *T* to meet the pressure requirements ($p_3 = p_4$), the outflows in regions (3) and (4) would be convergent.

A clue to the resolution of this paradox can be taken from a distantly related situation. In the problem of the supersonic aerofoil, for a given flight velocity, there is a limiting body angle beyond which a straight bow shock cannot deflect the flow parallel to the surfaces. For cases above this limit, the observed behaviour is that the bow shock becomes stronger near the leading edge, and less inclined to the flow there. This stronger shock produces a subsonic rather than supersonic region behind it, in which subsonic region the necessary flow deflection is taken care of continuously. (Strictly speaking, it cannot be continuous right in the corner between the shock and the boundary. Here the 'continuous' variation must be condensed into an infinitesimal region—a common type of subsonic singularity, cf. subsonic flow over a sharp corner.) This subsonic region is clearly an expansion, and is most severe where the shock is strongest. If the body angle is increased yet further, the bow wave detaches from the leading edge, and advances into the oncoming flow.

The reflected shock in the supercritical refraction pattern apparently cures its deflection difficulty by essentially the same process, that is, it becomes stronger and less inclined to the inflow, and in so doing produces a subsonic region behind it which handles the deflection and presssure adjustment in a continuous fashion (see figure 15).

This mechanism can only exist as shown over a small range of α. As α is increased further, the gas flow in region (2) relative to the reflection becomes less supersonic, and this reflected strong shock must become more normal to it to maintain its strength. Beyond the situation where it is just normal to the inflow, it has no other course than to leave the intersection point and advance into region (2), much as the bow wave detaches from the aerofoil. This, of course, is just the α_A-limit, beyond which a new irregular pattern occurs.

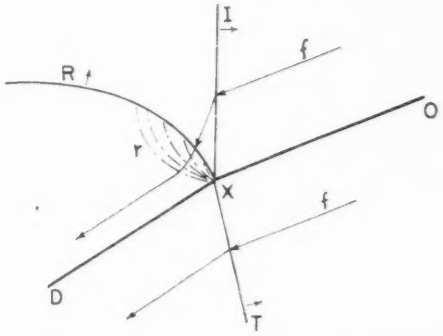

Figure 15. The α_r-adjustment. The reflected shock R becomes stronger near the interface, and is followed immediately by a steep subsonic rarefaction zone, which completes the necessary flow deflection and pressure adjustment.

That the process described above is far from insignificant is clear from the observed patterns of figure 14 b (plate 5) which show the great increase in strength of RS near the interface, and the sharp rarefaction region behind it. It is also impressive to compare the measured magnitude of this shock front near the interface with the reflected wave strengths in regular refractions (see figure 16).

It would seem only reasonable that some process like that developed above would likewise be expected in connection with the transmitted shock—to help out, as it were, with the flow deflection problem. Yet it remains a curious point in this case that there is no observable participation of the transmitted shock, and the flow behind it, in this readjustment process. As far as can be seen from the interferograms, T remains straight and unchanged in strength, and the field behind it remains very nearly uniform even though a rather drastic process is taking place in the adjacent region. Even the deflected interface seems totally unperturbed.

The α_A-adjustment for the air/CH_4 problem follows directly from the α_r-configuration just discussed. When α exceeds α_A, the gas flow in region (2) is no longer fast enough with respect to RS, even when normal to it, to maintain it at the required strength. As in the corresponding case for air/CO_2, RS will then advance into region (2) at a speed sufficient to maintain the necessary gas inflow on itself. In so doing, RS overtakes a portion of I,

thereby strengthening it, and establishing a pattern quite similar to a Mach reflection (cf. figure 14c, plate 6). The difference in entropy change for the gas crossing I and then RS, and that crossing the stem, necessitates a slipstream from the triple point. This slipstream is observed experimentally and is valuable in the interpretation of the patterns, since it assumes the direction of the local flow velocity.

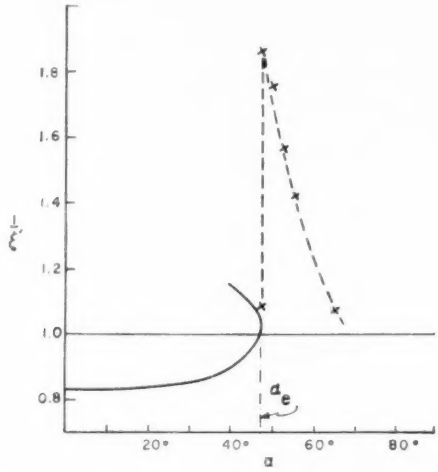

Figure 16. Strength of reflected wave front ($1/\xi'$) *vs* angles of incidence (α) for air/CH_4 with $\xi = 0{\cdot}30$. Solid line follows regular refraction solutions. Crosses mark experimentally observed strengths. Note the extreme maximum immediately following α_e.

The postulated pattern is quite efficient in relieving the critical conditions that necessitated the alterations. The stem shock is normal to the interface and strong enough to leave a subsonic region behind it, the combination of which handles the deflection of the flow near the interface quite adequately. The reflected wave is now somewhat removed from the interface, and no longer need deflect the flow behind it to be exactly parallel to the outflow from T, since there is a subsonic transition between regions (3) and (4). That this is indeed the case may be seen in figure 14c (plate 6) where the slipstream from the triple point, which follows the local flow direction, is clearly not parallel to the deflected interface. The less strenuous deflection requirements on RS are reflected in a lessening of its strength, quite sharply, as α increases (cf. figure 16).

For $\xi = 0{\cdot}30$, the limit α_{λ} is closely followed by α_i, which then is the last pertinent critical angle. However, for the weak shocks ($\xi = 0{\cdot}85$), α_i precedes α_{λ} by 13° and therefore produces a much more clearly defined effect. For this reason we will construct the α_i pattern at $\xi = 0{\cdot}85$, with the understanding that a similar situation must occur for the stronger shocks

also. At $\xi = 0{\cdot}85$, the previous pattern was that developed for $\alpha > \alpha_e$ (cf. figure 14 b, plate 5). As α is increased past α_t, the transmitted shock (which by definition of α_t now makes an angle of $\alpha'' = 90°$ with the interface) finds itself in a region where the inflow velocity is too small for its shock strength. To remedy this, the shock runs ahead in region (5), no longer maintaining contact with the intersection point (cf. figure 17 a). In so doing, however, a pressure difference is set up across the interface between the intersections of I and T. This of course requires a compression signal to be sent upward into (1) ahead of I, and, simultaneously, a rarefaction downward behind T (figure 17 b). The effect of the compressed region ahead of I is to curve I forward, causing it to make a larger angle of incidence with the interface (figure 17 c). The region behind this curved portion of I

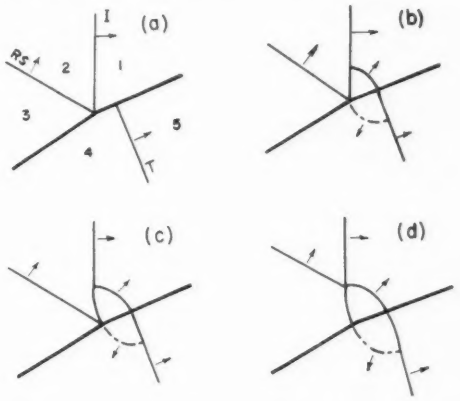

Figure 17. The α_t-adjustments. (a) The transmitted shock T leaves the intersection point and runs ahead into region (5). (b) This causes a compression front to propagate into region (1), ahead of the incident shock I, and simultaneously, a rarefaction front to advance down into region (4) behind T. (c) Consequently, T is weakened near the interface, while I travels more rapidly into the gas passed over by the compression. (d) The region behind the curved portion of I is now subsonic, hence the reflected shock RS runs ahead into region (2), until it reaches supersonic flow again, that is, behind the straight portion of I.

is no longer uniform. In particular, it is no longer supersonic with respect to the reflection, since the angle of incidence of this stem is past the α_A-limit. The process adopted in a case like this, as we have already seen in other cases, is for the reflection to advance into (2), climbing the back of I to the point where an adequate flow normal to itself is available, which in this case should be near the start of the curvature of I (figure 17 d).

The rarefaction that advances into (4) will weaken T somewhat, thereby reducing the inflow requirements slightly. This feature tends to stabilize the situation, in a sense restraining T from getting too far ahead. The

equilibrium situation finds T—a finite shock, followed by a region of compression to p_4—running just slightly ahead of the intersection point of I. The pattern that actually occurs for $\alpha > \alpha_i$ (figure 14 d, plate 7) corresponds to this equilibrium configuration.

If α is increased further, the inflow velocity in region (5) becomes subsonic ($\alpha > \alpha_j$), in which case there is nothing to prevent T from degenerating completely into a continuous compression, the front of which will run ahead with velocity a_5. The resulting other adjustments will be qualitatively the same as those described above for the α_i case, although the interaction region will now be much larger. This is the configuration displayed in figure 14 e (plate 8).

The process cannot proceed to this extreme in the stronger shock case, since the velocity of the configuration along the interface is more rapid, and hence the inflow deficit on T is relatively less significant†.

Figure 18 (plate 12) shows the α_i effect for $\xi = 0{\cdot}30$. Note that even at this large α (65°), T is only slightly ahead of the incident stem. One of the most interesting features of this picture is that the stem has been deformed by the precursor compression in such a way that it is actually incident at $\alpha > 90°$! As a consequence of this, the flow behind it temporarily has an upward component, and the interface is seen to be deflected up above its original position for a short distance.

It is clear from even such a sketchy analysis as that outlined above that the irregular patterns have a significance beyond their specific application to the refraction problem. In addition to providing some basis for empirical treatment of the irregular refraction regime, they are an abundant source of information on various shock interactions and flow field configurations which, in many cases, would be difficult to observe by more *ad hoc* experiments. In a sense, each irregular refraction process acts as a matrix in which are embedded, for our convenient observation, interactions between shock and shock, shock and rarefaction, shock and contact surface, shock and subsonic region, and many others, all existing in their 'natural' state. Such interactions are the fundamental elements of most complex shock processes, and whatever understanding of them can be acquired from this source should aid in the comprehension of other involved processes in which they also participate.

In this survey we have included at least one example of every type of irregular pattern we have observed, and it now appears that extension of the study to other gas combinations would not produce any configurations fundamentally different from those shown here. Such an extension would not be without value, however, since the order of occurrence of the effects and the quantitative nature of the various separate interactions can be significantly varied by the proper choice of gases. In fact, it is this possibility of using different gas combinations that promises the necessary breadth of range for the use of irregular refraction patterns as display cases for aerodynamic interactions.

This work has been supported by the Office of Naval Research. The author would also like to record here his indebtedness to Professor Walker Bleakney, whose insight, experience, and encouragement were indispensable to this project. Likewise, to his former colleagues at the Shock Wave Laboratory at Princeton University, and to his wife, the author expresses his gratitude.

References

Bitondo, D. 1950 Experiments on the amplification of a plane shock wave, Technical Report no. 7, Institute of Aerophysics, University of Toronto.

Bleakney, W. & Griffith, W. C. 1954 *Amer. J. Phys.* **22,** 597.

Fletcher, C., Taub, A. H. & Bleakney, W. 1951 *Rev. Mod. Phys.* **23,** 271.

Polachek, H. & Seeger, R. J. 1951 *Phys. Rev.* **84,** 922.

Stoner, R. G., Woodbridge, C. L. & Davies, E. B. 1952 Experimental observation of the interaction of shock waves at boundaries between various gases, Parts I and II, Pennsylvania State College Technical Report.

Taub, A. H. 1947 Some numerical results on refraction of plane shocks, Technical Report II–1, Department of Physics, Princeton University.

Taub, A. H. 1951 *Phys. Rev.* **77,** 51.

Supersonic flow past a bluff body with a detached shock Part II Axisymmetrical body

By W. CHESTER

Department of Mathematics, University of Bristol

(*Received* 20 *August* 1956)

SUMMARY

This paper considers the flow at high Mach number behind the curved shock formed when a supersonic stream impinges on an axisymmetrical body with a rounded nose.

The solution is obtained as a double expansion in

$$\delta = (\gamma-1)/(\gamma+1),$$

where γ is the adiabatic index, and M^{-2}; the expansion is developed to within terms of order $(\delta+M^{-2})^3$.

Expressions are obtained for the distance between the body and the shock, the radius of curvature of the shock compared with that of the body, and the pressure distribution on the body.

INTRODUCTION AND FUNDAMENTAL EQUATIONS

The technique evolved in Part I (Chester 1956) is used here to investigate supersonic flow past a blunt-nosed axisymmetrical body. The exposition is less detailed, for the ideas involved are essentially those of the previous paper.

The common axis of the body and of the shock wave formed ahead of it is in the direction of the uniform flow upstream of the shock. The x-coordinate is measured along this axis from an origin at the vertex of the shock. The radial coordinate is denoted by y.

Upstream of the shock the velocity, pressure and density are denoted by $(V,0)$, p_0, ρ_0 respectively. Corresponding quantities in the region of disturbed flow behind the shock are (Vu, Vv), $\rho_0 V^2 p$ and $\rho_0 \rho(\gamma+1)/(\gamma-1)$; as before, γ is the adiabatic index.

The equations of conservation of mass, momentum and entropy are, with $(\gamma-1)/(\gamma+1) = \delta$,

$$\left.\begin{aligned} \frac{\partial}{\partial x}(\rho u y) + \frac{\partial}{\partial y}(\rho v y) &= 0; \\ u\frac{\partial u}{\partial x} + v\frac{\partial u}{y\partial} &= -\frac{\delta}{\rho}\frac{\partial p}{\partial x}; \\ u\frac{\partial v}{\partial x} + v\frac{\partial v}{\partial y} &= -\frac{\delta}{\rho}\frac{\partial p}{\partial y}; \\ u\frac{\partial}{\partial x}(p\rho^{-\gamma}) + v\frac{\partial}{\partial y}(p\rho^{-\gamma}) &= 0. \end{aligned}\right\} \tag{1}$$

The first of these equations implies the existence of a stream function ψ such that $\delta\psi_y = \rho uy$, $\delta\psi_x = -\rho vy$. In the uniform flow ahead of the shock, $\psi = \frac{1}{2}y^2$ and is continuous across the shock. On the body, $\psi = 0$.

With the independent variables transformed to (ψ, y), equations (1) become

$$\left.\begin{aligned} y\frac{\partial p}{\partial \psi} - \frac{\partial u}{\partial y} &= 0; \\ u^2+v^2+(1+\delta)p/\rho &= 1+(1-\delta)\delta^{-1}M^{-2}; \\ \frac{\partial}{\partial\psi}\left(\frac{u}{v}\right)+\delta\frac{\partial}{\partial y}\left(\frac{1}{\rho vy}\right) &= 0; \\ p\rho^{-\gamma} &= f(\psi), \end{aligned}\right\} \tag{2}$$

where f is an arbitrary function of ψ.

We consider the particular case of a paraboloidal shock with unit radius of curvature at the nose. The equation of the shock profile is then $x = \frac{1}{2}y^2$, and the shock transition relations give the following boundary conditions to be satisfied on $\psi = \frac{1}{2}y^2$:

$$\left.\begin{aligned} u &= 1-(1-\delta)\left\{\frac{1}{1+y^2}-M^{-2}\right\}; \\ v &= (1-\delta)y\left\{\frac{1}{1+y^2}-\mathrm{M}^{-2}\right\}; \\ p &= (1-\delta)\left\{\frac{1}{1+y^2}-\frac{\delta M^{-2}}{1+\delta}\right\}; \\ \rho &= \frac{1}{1+(1-\delta)\delta^{-1}M^{-2}(1+y^2)}. \end{aligned}\right\} \tag{3}$$

From these equations it follows that

$$f(\psi) = (1-\delta)\left\{\frac{1}{1+2\psi}-\frac{\delta M^{-2}}{1+\delta}\right\}\{1+(1-\delta)\delta^{-1}M^{-2}(1+2\psi)\}^{(1+\delta)/(1-\delta)}. \tag{4}$$

From the third of equations (2) we also have

$$\frac{u}{v} = \delta\frac{\partial}{\partial y}\int_{\psi}^{\frac{1}{2}y^2}\left(\frac{1}{\rho vy}\right)d\psi + \left(\frac{u}{v}-\frac{\delta}{\rho v}\right)_{\psi=\frac{1}{2}y^2}. \tag{5}$$

Equations (3) then give

$$\frac{u}{v} = y+\delta\frac{\partial}{\partial y}\int_{\psi}^{\frac{1}{2}y^2}\left(\frac{1}{\rho vy}\right)d\psi; \tag{6}$$

and, hence, the equation of the body is

$$x = \tfrac{1}{2}y^2+\delta\int_{0}^{\frac{1}{2}y^2}\left(\frac{1}{\rho vy}\right)d\psi. \tag{7}$$

As in Part I, it is not difficult to show that equation (6) includes automatically the stand-off distance between the body and the shock.

Basic solution

When $\delta = M^{-2} = 0$, equation (4) becomes

$$f(\psi) = \frac{1}{1+2\psi} + \delta^{-1}M^{-2},$$

and equations (2) are easily solved using the boundary conditions (3). The results are

$$\left.\begin{aligned} u = yv &= \frac{(2\psi)^{1/2}y}{(1+2\psi)^{1/2}(1+y^2)^{1/2}}, \qquad p = \frac{A}{2y(1+y^2)^{3/2}}, \\ \rho &= \frac{(1+2\psi)A}{2y(1+y^2)^{3/2}\{1+\delta^{-1}M^{-2}(1+2\psi)\}}, \end{aligned}\right\} \tag{8}$$

where

$$A = [(2\psi)^{1/2}(1+2\psi)^{1/2} - \sinh^{-1}(2\psi)^{1/2} + y(1+y^2)^{1/2} + \sinh^{-1}y]. \tag{9}$$

The next step is to improve this approximation so as to obtain expressions for the velocity components which are uniformly valid as $\psi \to 0$. The expressions for u/v, p and ρ do not require modification; and so we have, correct to the *first* order of small quantities,

$$\begin{aligned} \frac{p}{\rho} = f(\psi)\rho^{\gamma-1} &= f(\psi)\{1+2\delta\log\rho\} \\ &= \frac{1}{1+2\psi}\Bigg[1+\delta^{-1}M^{-2}(1+2\psi)-\delta-2M^{-2}(1+2\psi)+ \\ &\qquad +2\{\delta+M^{-2}(1+2\psi)\}\log\left\{\frac{A(1+2\psi)}{2y(1+y^2)^{3/2}}\right\}\Bigg]. \end{aligned} \tag{10}$$

This expression for p/ρ is substituted in the second of equations (2) to give

$$u^2+v^2 = \frac{1}{1+2\psi}\left[2\psi - 2(d+2\psi M^{-2})\log\left\{\frac{A(1+2\psi)}{2y(1+y^2)^{3/2}}\right\}\right], \tag{11}$$

where $d = \delta + M^{-2}$.

Equation (11) is now solved in conjunction with $u = vy$, and all terms which are *uniformly* $O(d)$ are discarded. The following relations are then obtained:

$$u = yv = \frac{y(2\psi+dB)^{1/2}}{(1+y^2)^{1/2}(1+2\psi)^{1/2}}, \tag{12}$$

where

$$B = 2\log\left\{\frac{2y(1+y^2)^{3/2}}{y(1+y^2)^{1/2}+\sinh^{-1}y}\right\}. \tag{13}$$

First-order approximation

From equations (8) and (12), we can now obtain the following expression for $\delta/\rho v$, which is uniformly correct as far as terms which are $O(d)$:

$$\frac{\delta}{\rho v} = \frac{2y(1+y^2)^2(d+2\psi M^{-2})}{A(1+2\psi)^{1/2}(2\psi+dB)^{1/2}}. \tag{14}$$

We can then obtain a first approximation to the equation of the body by the substitution of (14) in (7). The result is

$$x = \tfrac{1}{2}y^2 + 2d(1+y^2)^2 \int_0^{\frac{1}{2}y^2} \frac{d\psi}{(2\psi)^{1/2}(1+2\psi)^{1/2}A} + \\ + M^{-2}(1+y^2)^2 \log\left\{\frac{2y(1+y^2)^{1/2}}{y(1+y^2)^{1/2}+\sinh^{-1}y}\right\} - \frac{2d^{3/2}B^{1/2}(1+y^2)^2}{y(1+y^2)^{1/2}+\sinh^{-1}y}. \quad (15)$$

Note that equation (15) contains terms which are $O(d)^{3/2}$, and is in fact correct to within $O(d^2)$.

To obtain the velocity components we must first calculate u/v from (6) which gives, correct to within $O(d^2)$,

$$u/v = y(1+g) + 2d\psi y^{-2}(1+y^2)^{1/2}(1+2\psi)^{1/2}(2\psi+dB)^{-1/2}, \quad (16)$$

where

$$g = -2d\psi y^{-2}(1+y^2)^{1/2}(1+2\psi)^{1/2}(2\psi+dB)^{-1/2} + \\ + \frac{\partial}{\partial y}\Big[2d(1+y^2)^2 \int_{\psi}^{\frac{1}{2}y^2} \frac{d\psi}{(2\psi)^{1/2}(1+2\psi)^{1/2}A} + \\ + M^{-2}(1+y^2)^2 \log\{2y(1+y^2)^{1/2}A^{-1}\} - \\ - \frac{2d(1+y^2)^2}{y(1+y^2)^{1/2}+\sinh^{-1}y}\{(2\psi+dB)^{1/2} - (2\psi)^{1/2}\}\Big]. \quad (17)$$

The form of the expression for u/v anticipates the fact that, near $y = 0$,

$$u \sim 2\delta\psi/\rho y^2 \sim 2d\psi/y^2$$

(the argument is similar to the corresponding one in Part I). Hence we may write

$$u = U + 2d\psi/y^2, \quad (18)$$

where U is $O(y^2)$ near $y = 0$. Equation (16) then gives

$$U/v = y(1+g); \quad (19)$$

and the singular term in (16) has now disappeared.

When these relations are substituted in (11) and the resulting equation solved for U, we find that

$$U = -\frac{2d\psi}{y^2} + y(1+2\psi)^{-1/2}(1+y^2)^{-1/2}\left(1+\frac{g}{1+y^2}\right)\times \\ \times\left[2\psi + 2(d+2\psi M^{-2})\log\left\{\frac{2y(1+y^2)^{3/2}}{A(1+2\psi)}\right\}\right]^{1/2}, \quad (20)$$

from which u and v are easily obtained using equations (14) and (15) respectively.

Finally the pressure is obtained by integration of the equation

$$\frac{\partial p}{\partial \psi} = \frac{1}{y}\frac{\partial u}{\partial y}$$

using the previously calculated expression for u and the boundary condition on $\psi = \frac{1}{2}y^2$ obtained from the last of equations (3). Although the variation of p with both ψ and y is required before the next approximation can be found, the complete expression is somewhat involved and we quote here

only the expansion for small values of y and $\psi = 0$. The basic terms are given exactly, but the rest of the terms have errors which are $O(y^6)$:

$$p = (1+y^2)^{-3/2}\left[\tfrac{1}{2}(1+y^2)^{1/2} + \frac{\sinh^{-1}y}{2y} + d\left(-\frac{1}{2} - \frac{1201}{252}y^2 + \frac{3277}{15120}y^4\right) + \right.$$
$$\left. + M^{-2}\left(1 + \frac{7}{18}y^2 + \frac{13741}{1080}y^4\right) + \left(\frac{8d}{3}\right)^{3/2}\left(\frac{4}{3}y^2 - \frac{3}{5}y^4\right)\right]. \quad (21)$$

Second-order approximation

The precautions referred to in Part I also apply here; otherwise the process is straightforward, and only the final results are given. Apart from the basic terms, fourth and higher powers of y have been ignored.

The equation of the body is

$$x = \left\{1 - \left(\frac{8d}{3}\right)^{1/2}\right\}d + \frac{26}{10}d^2 - dM^{-2} + M^{-4} -$$
$$- \frac{463}{168}d^2\left(\frac{8d}{3}\right)^{1/2} + \frac{13}{12}dM^{-2}\left(\frac{8d}{3}\right)^{1/2} - \frac{3}{2}M^{-4}\left(\frac{8d}{3}\right)^{1/2} +$$
$$+ \tfrac{1}{2}y^2\left[1 + \frac{19}{6}d + \frac{2}{3}M^{-2} - \frac{47}{15}d\left(\frac{8d}{3}\right)^{1/2} + \frac{11173}{840}d^2 - \frac{50}{21}dM^{-2} + \frac{23}{6}M^{-4} -\right.$$
$$\left. - \frac{2593}{126}d^2\left(\frac{8d}{3}\right)^{1/2} + \frac{287}{20}dM^{-2}\left(\frac{8d}{3}\right)^{1/2} - \frac{47}{10}M^{-4}\left(\frac{8d}{3}\right)^{1/2}\right]; \quad (22)$$

and the pressure on the body is given by

$$(1+y^2)^{3/2}p = \frac{1}{2}(1+y^2)^{1/2} + \frac{\sinh^{-1}y}{2y} - \frac{1}{2}d + M^{-2} + \frac{1}{8}d^2 - \frac{3}{2}dM^{-2} + \frac{3}{2}M^{-4} -$$
$$- y^2\left\{\frac{1201}{252}d - \frac{7}{18}M^{-2} - \frac{32}{9}d\left(\frac{8d}{3}\right)^{1/2} + \frac{10009633}{55440}d^2 + \frac{1}{252}dM^{-2} + \right.$$
$$\left. + \frac{725}{252}M^{-4} - \frac{3002}{189}d^2\left(\frac{8d}{3}\right)^{1/2} - \frac{40}{27}dM^{-2}\left(\frac{8d}{3}\right)^{1/2} - \frac{16}{3}M^{-4}\left(\frac{8d}{3}\right)^{1/2}\right\}. \quad (23)$$

Discussion of results

Although, for reasons given in Part I, the analysis is carried out for the case of a shock having unit radius of curvature at the nose, the following results have been corrected to apply to a body having unit radius of curvature at the nose.

Figures 1 and 2 show respectively the radius of curvature of the shock and the distance between the body and the shock along the axis of symmetry for various values of d. The isolated point in each figure is an experimental result given by Oliver (1956). The curves are calculated from equation (22), except for the broken parts which are simply extrapolations through values of d for which the convergence of (22) may not be satisfactory.

A comparison of corresponding expressions in Part I and II shows that the convergence is poorer in the axisymmetrical case. Nevertheless, one

or two general conclusions may be drawn. As in the two-dimensional problem, the stand-off distance seems to be virtually independent of M^{-2}, except in so far as this parameter influences d, and the single curve in figure 2 covers all cases.

As would be expected, under similar conditions both the radius of the shock and the stand-off distance are smaller in the axisymmetrical problem; a rough guide for the distance between the body and the shock is $2d$ in the two-dimensional case, and $\frac{3}{4}d$ in the axisymmetrical case.

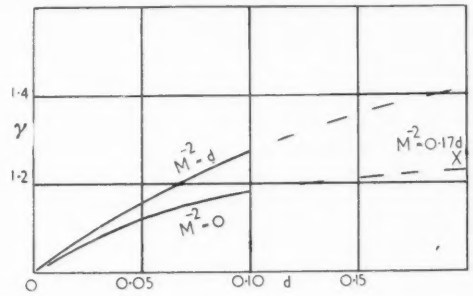

Figure 1. The radius of curvature of the shock on the axis of symmetry for various values of $d(=(\gamma-1)/(\gamma+1)+M^{-2})$. The unit of length is the radius of curvature of the body on the axis of symmetry. The cross denotes an experimental result.

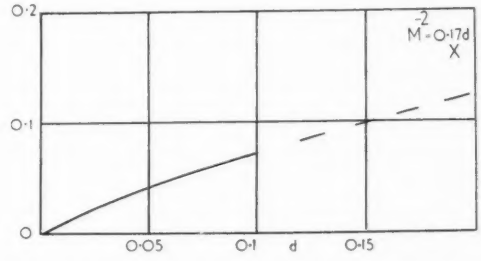

Figure 2. The distance between the body and the shock along the axis of symmetry for various values of $d(=(\gamma-1)/(\gamma+1)+M^{-2})$. The unit of length is the radius of curvature of the body on the axis of symmetry. The cross denotes an experimental result.

Because of the large factor multiplying d^2 (compared with the multiplier of d) in the coefficient of y^2 in equation (23), the expression for p cannot be regarded as reliable save for very small values of d in the neighbourhood of 0·01.

When $d = M^{-2} = 0$, the pressure distribution on the body is known exactly, and the ordinate of the sonic point is 0·680 compared with the value 0·629 in the two-dimensional case. According to calculations based on equation (23), the initial tendency is for the ordinate to decrease as d increases (and $M^{-2} = 0$) in contrast to an increase in the two-dimensional

case (see Part I, figure 3), the ordinates agreeing in the two cases for a value of d around 0·02. But up to this value the decrease is only 0·3%, and the most that can be said is that initially there is no appreciable variation in the position of the sonic point.

Since the pressures on the body at the stagnation point and the sonic point are functions only of d and M^{-2} (see equations (29) and (30) of Part I), it follows that, with similar conditions, the pressures are the same at these corresponding points in the two-dimensional and axisymmetrical cases. Hence we may deduce that for sufficiently small values of d, the pressure distribution in the two cases do not differ appreciably in the neighbourhood of the nose.

References

Chester, W. 1956 *J. Fluid Mech.* **1**, 353.
Oliver, R. E. 1956 *J. Aero. Sci.* **23**, 177.

An inequality concerning the production of vorticity in isotropic turbulence

By R. BETCHOV

Department of Aeronautics, The Johns Hopkins University, Baltimore

(*Received* 1 *May* 1956)

SUMMARY

An inequality is demonstrated involving the rate of production S of mean-square vorticity in isotropic turbulence and a factor γ which may be said to allow for intermittency or for the non-vanishing of fourth-order cumulants. An extreme state, corresponding to equality of this relationship, occurs if $S = 0{\cdot}64$ and $\gamma = 2{\cdot}14$. The experimental values are $S = 0{\cdot}4$ and $\gamma = 4$. Another kinematical relation shows that the mechanism of vorticity production resembles collision between fluid particles rather than the swirling of contracting jets.

1. INTRODUCTION

When the motion of a fluid is turbulent, the fluctuations of the vorticity are of major importance. For isotropic conditions they are directly related to energy dissipation by viscosity. They also show a sufficient degree of isotropy and homogeneity in general to justify the corresponding simplifications of the theory.

These fluctuations obey a system of equations in which the pressure does not appear and thereby the degree of complication is reduced. According to these equations, viscosity tends to eliminate vorticity, by a well-understood process. These equations also show that the mean-square vorticity can be increased by inertial effects. This aspect of the problem is still somewhat mysterious. What determines this production of vorticity and how does it occur?

The problem has been stated in terms of correlation functions, but this procedure leads to a number of unknowns always larger than the number of equations.

The Fourier transforms of the correlations can be introduced, amounting to a spectral analysis of a sample of turbulent flow. They lead to a relation between vorticity production and the rate of energy transfer from large eddies to small eddies. Each hypothesis concerning energy transfer has thus been followed by an evaluation of the rate of production of vorticity.

In this paper, we investigate the largest rate of production of vorticity compatible with the requirements of isotropy, homogeneity and incompressibility. We find an upper bound for the rate of vorticity production, although it depends upon a fourth-order mean value and therefore does

not constitute an absolute maximum. Comparison with old and new experimental data indicates that a turbulent flow produces vorticity at about 50% of this limiting rate. It is quite possible that dynamical effects are responsible for this factor and that we are confronted by an extreme state of affairs, characteristic of turbulent flows.

2. Fundamental inequality

We intend to establish an inequality valid at every point of an incompressible flow and at every instant. We shall use cartesian coordinates x_i, denote the velocity vector by u_i, and write $u_{i,j}$ for $\partial u_i/\partial x_j$. The condition of incompressibility, with the usual convention about summation of repeated indices, is

$$u_{j,j} = 0. \tag{1}$$

We can write $u_{i,j} = s_{ij} + r_{ij}$, where s_{ij} is the symmetric rate of strain tensor and r_{ij} the antisymmetric vorticity tensor. At any point and instant, we can find the principal axes of s_{ij} and, on referring to these axes, we have:

$$u_{i,j} = \begin{vmatrix} a & C & -B \\ -C & b & A \\ B & -A & c \end{vmatrix}, \tag{2}$$

where a, b, c are the eigenvalues of s_{ij} and A, B, C are half the vorticity components in the directions of the principal axes. In the sequel we shall designate the directions associated with a, b, c as the a-axis, b-axis and c-axis. Furthermore, we shall adopt the convention

$$|a| \geqslant |b| \geqslant |c|. \tag{3}$$

By (1) we have

$$a + b + c = 0, \tag{4}$$

and consequently b and c must be of the same sign and a and b of opposite sign.

We shall make use of the general Cauchy inequality (Hardy *et al.* 1952)

$$(a^3 + b^3 + c^3)^2 \leqslant (a^2 + b^2 + c^2)(a^4 + b^4 + c^4) \tag{5}$$

with equality if $a = b = c$. We shall also use the following identities, obtained by raising both sides of (4) to powers 2, 3 and 4,

$$\left.\begin{aligned} a^2 + b^2 + c^2 &= -2(ab + bc + ca), \\ a^3 + b^3 + c^3 &= 3abc, \\ a^4 + b^4 + c^4 &= \tfrac{1}{2}(a^2 + b^2 + c^2)^2. \end{aligned}\right\} \tag{6}$$

Values of a, b and c for which the two sides of (5) are nearly equal are excluded by the incompressibility condition. Indeed, when a, b and c satisfy (4), the ratio of the left-hand side to the right-hand side of (5) has a maximum value of $\frac{1}{3}$ at $-a = 2b = 2c$. This allows a factor $\frac{1}{3}$ to be inserted on the right-hand side of (5), and so, with the use of (6), we have

$$|abc| \leqslant \frac{1}{3\sqrt{6}}(a^2 + b^2 + c^2)^{3/2}. \tag{7}$$

It is known that the set of eigenvalues of a tensor is invariant to transformations of the coordinates; therefore each term of (7) is invariant. Indeed, each term can be expressed by invariants such as $s_{ij}s_{ij}$ or $s_{ij}s_{jk}s_{ki}$. Consequently (7) remains valid if we pass to a fixed system of coordinates, independent of the orientation of the *a*-, *b*-, and *c*-axes. We now consider an ensemble of points of the fluid, each with its own set of eigenvalues with respect to these fixed axes, and average both sides of (7). We can use a space, a time or an ensemble average. Then, with $\langle\ \rangle$ indicating the average, we have

$$|\langle abc\rangle| \leqslant \frac{1}{3\sqrt{6}}\,\langle(a^2+b^2+c^2)^{3/2}\rangle. \tag{8}$$

The right-hand side of (8) cannot be measured by conventional methods and comparison with experimental results is not possible unless we introduce a modified inequality. We can write a single inequality involving N sets of eigenvalues, viz.

$$\left(\sum_{n=1}^{N} a_n^3+b_n^3+c_n^3\right)^2 \leqslant \left(\sum_{1}^{N} a_n^2+b_n^2+c_n^2\right)\left(\sum_{1}^{N} a_n^4+b_n^4+c_n^4\right) \tag{9}$$

By taking (4) and (6) into account, and introducing the average as a limit for large N, the inequality (9) becomes

$$|\langle abc\rangle| \leqslant \frac{1}{3\sqrt{3}}\,\langle a^2+b^2+c^2\rangle^{1/2}\langle a^4+b^4+c^4\rangle^{1/2}. \tag{10}$$

The right-hand side of (8) is always less than or equal to the right-hand side of (10), with equality if a, b and c do not fluctuate. If, in addition, $a=-2b=-2c$, the two sides of (10) are equal. In view of (6), the ratio of right-hand sides of (8) and (10) depends only upon the probability distribution of $a^2+b^2+c^2$. In the case of a Gaussian probability distribution of $a^2+b^2+c^2$, the right-hand side of (8) is only 8% smaller than that of (10). In general, this ratio is close to unity, unless the probability distribution has a pronounced peak at the origin. Thus, the inequality (10) is not much weaker than (8).

3. Relations with measurable quantities

The various invariants occurring in (10) can be measured with a single hot-wire anemometer. This has been done in the turbulence produced by a grid obstructing a parallel flow of air. The hot-wire is located sufficiently far down-stream to give some guarantee of isotropic conditions, and its orientation is normal to the mean flow. The turbulence passes by the wire with a mean velocity about one hundred times larger than the velocity fluctuations, and consequently the time derivative of the hot-wire signal corresponds reasonably well to the space derivative of the velocity. With index 1 denoting the direction of mean flow, this means that the differentiated signal is proportional to $u_{1,1}$.

Let us find the relation between $u_{1,1}$ and the invariants of (10). At any particular instant, the hot-wire responds to a fluid particle whose principal

axes of rate of strain can be specified. Let ϕ be the angle between the 1-axis and the a-axis (latitude) and ψ be the angle between the c-axis and a direction normal to the a-axis and 1-axis (longitude). It then follows from tensor calculus that

$$u_{1,1} = a\cos^2\phi + b\cos^2\psi\,\sin^2\phi + c\sin^2\psi\sin^2\phi. \tag{11}$$

The vorticity does not contribute to this particular signal, but this is peculiar to the component $u_{1,1}$,

In the course of time the hot-wire is coincident with different fluid particles and the angles ϕ and ψ vary as well as the eigenvalues a, b, c. The eigenvalues are absolute quantities. Consequently, if the turbulence is isotropic, the angles must be statistically independent of the eigenvalues. To clarify this point let us consider all fluid particles for which $a = 1$, $b = -0{\cdot}7$, $c = -0{\cdot}3$. If, in the average over these particles, we find a definite orientation of the principal axis, we can use the numbers 1, $-0{\cdot}7$, $-0{\cdot}3$ to specify a direction. Such a direction would remain invariant to a rotation of the coordinates and this would reveal a lack of isotropy. Therefore, we must admit that, for any set of values of a, b, c, the orientation of the principal axis are random; that is, we have statistical independence of eigenvalues and orientations.

With $(1/4\pi)\sin\phi\,d\phi\,d\psi$ as the probability of finding ϕ and ψ inside a small solid angle, and statistical independence, we find

$$\langle u_{1,1}^2\rangle = \frac{2}{15}\,\langle a^2 + b^2 + c^2\rangle. \tag{12}$$

The same method can be used to demonstrate

$$\langle u_{1,1}^3\rangle = \frac{24}{105}\,\langle abc\rangle, \tag{13}$$

$$\langle u_{1,1}^4\rangle = \frac{8}{105}\,\langle a^4 + b^4 + c^4\rangle. \tag{14}$$

Some of these results have been derived by others from correlation functions. When the following non-dimensional parameters are introduced,

$$S = -\frac{\langle u_{1,1}^3\rangle}{\langle u_{1,1}^2\rangle^{3/2}}, \qquad \gamma = \frac{\langle u_{1,1}^4\rangle}{\langle u_{1,1}^2\rangle^2}, \tag{15}$$

the inequality (10) can be expressed as:

$$|S| \leqslant \frac{2}{\sqrt{21}}\,\gamma^{1/2}. \tag{16}$$

For normally distributed velocities we have $\gamma = 3$, and in that case $|S| \leqslant 0{\cdot}756$.

In the extreme case $-a = 2b = 2c =$ constant, we find by (12), (13) and (14), $\gamma = 2{\cdot}14$, $|S| = 0{\cdot}638$. Proudman & Reid (1954) calculated the value of S with the assumptions of no viscosity, zero initial triple correlations and a relation between three-point quadruple velocity correlations and double correlations appropriate for normal probability distribution. They found $S = 0{\cdot}78$, and by (16) this implies $\gamma \geqslant 3{\cdot}2$. This seems to

mean that the four-point quadruple correlations could not satisfy exactly a similar relation with double correlations, since this would imply $\gamma = 3$.

4. Experimental results

The numerous measurements of S and γ by Townsend (1947, 1948, 1951) gave $S = 0{\cdot}38$, $\gamma = 4$. Later Stewart (1951) found values of S decreasing with increasing Reynolds number of the turbulence, in the range $S = 0{\cdot}5$ to $0{\cdot}3$. From the measurements of $\langle \partial^2 u_1 / \partial x_1^2 \rangle$ by Liepmann *et al.* (1951) one can find S, by making use of the vorticity equation. The resulting values of S increase from 0·4 to 0·5 with increasing Reynolds numbers.

The author measured S and γ for a variety of meshes and with improved electronic devices in the low-turbulence wind tunnel of the University of Maryland. The hot-wire signal was carefully compensated for thermal inertia. A simple low-pass filter was used to avoid excessive electronic noise, and it was verified that the filter did not affect the measurements of mean cubes.

To measure mean squares and mean cubes, I used chains of biased diodes. For mean fourth power, I first obtained the instantaneous square with a quarter-square multiplier using four chains of diodes.

The first grids used were of 2·5 cm mesh, with 38 and 66% open area and air velocities of 2 to 20 m/sec. The wire was located at distances from 30 to 100 mesh lengths from the grid. The results consistently indicated $S = 0{\cdot}4 \pm 0{\cdot}1$, without systematic variation.

With a grid of 0·6 cm mesh, 21% open area and a wind of 4 m/sec I found $S = 0{\cdot}4 \pm 0{\cdot}05$ at distances of 20 to 150 mesh lengths. With a first grid of 2·5 cm and 54% open area, followed at 125 cm downstream by a second grid of 1·25 cm and 76% open area, I found $S = 0{\cdot}4$ at a distance of 200 cm from the first grid. When several strips of paper tape were added to the first grid the turbulence was considerably altered thereby, but S was found to be unchanged.

In a crude pipe flow and in the wake behind a cylinder, I again found $S = 0{\cdot}4$. The central part of a turbulent boundary layer gave the same result.

Only a few measurements of γ were made, and they indicate $\gamma = 4 \pm 0{\cdot}5$.

The constancy of S is remarkable, and holds at Reynolds numbers lower than those for which Kolmogoroff's theory might be expected to be valid. Comparison with the inequality (16) shows that the experimental value of $S/\gamma^{1/2}$ corresponds roughly to 50% of the maximum permissible value. With $\gamma = 4$, the inequality requires $|S| \leqslant 0{\cdot}872$.

5. Production of vorticity

We shall now introduce the dynamical equations. With additional indices to indicate successive derivatives, we write the Navier–Stokes equations as

$$\partial u_i / \partial t + u_k u_{i,k} - \nu u_{i,kk} = -P_i/\rho, \tag{17}$$

where ν is the kinematical viscosity, P the pressure and ρ the density. After differentiating with respect to x_j, multiplication by $u_{i,j}$, summation in i and j, and averaging we obtain

$$\frac{\partial}{\partial t}\langle u_{i,j}u_{i,j}\rangle + 2\langle u_k u_{i,j}u_{i,kj}\rangle + 2\langle u_{i,j}u_{i,k}u_{k,j}\rangle - \\ -2\nu\langle u_{i,j}u_{i,jkk}\rangle = -\frac{1}{\rho}\langle u_{i,j}P_{ij}\rangle. \quad (18)$$

For the first term we can write, with reference to (2),

$$\langle u_{i,j}u_{i,j}\rangle = \langle a^2+b^2+c^2\rangle + 2\langle A^2+B^2+C^2\rangle. \quad (19)$$

We now consider the invariant $\langle u_{i,j}u_{j,i}\rangle$. In homogeneous and incompressible flow, we have

$$\langle u_{i,j}u_{j,i}\rangle = \frac{\partial}{\partial x_j}\langle u_i u_{j,i}\rangle = 0, \quad (20)$$

giving the following relation between the mean-square vorticity and the mean-square rate of strain:

$$\langle a^2+b^2+c^2\rangle = 2\langle A^2+B^2+C^2\rangle. \quad (21)$$

The invariant $\langle u_k u_{i,j}u_{i,jk}\rangle$ also vanishes, either by homogeneity or by isotropy. Also, for the same reasons, $\langle P_{ij}u_{i,j}\rangle = 0$. The viscous term can be related to the vorticity or the rate of strain, and can also be written as

$$\langle u_{i,j}u_{i,jkk}\rangle = -\langle u_{i,jk}u_{i,jk}\rangle. \quad (22)$$

The invariant $\langle u_{i,j}u_{i,k}u_{k,j}\rangle$ can be written as $\langle u_{i,j}u_{j,k}u_{i,k}\rangle$, where the sequence of indices must be noted. With the use of (2), it becomes

$$\langle u_{i,j}u_{j,k}u_{i,k}\rangle = \langle a^3+b^3+c^3\rangle - \langle aA^2+bB^2+cC^2\rangle. \quad (23)$$

Let us consider the invariant $\langle u_{i,j}u_{j,k}u_{k,i}\rangle$, where the index sequence is now different. This quantity vanishes because it can be expressed as the divergence of a vector;

$$\langle u_{i,j}u_{j,k}u_{k,i}\rangle = \frac{\partial}{\partial x_i}\langle u_{i,j}u_{j,k}u_k - \tfrac{1}{2}u_i u_{k,j}u_{j,k}\rangle = 0. \quad (24)$$

Equation (24) is a relation imposed by homogeneity, and with the use of (2) it becomes

$$\langle a^3+b^3+c^3\rangle = -3\langle aA^2+bB^2+cC^2\rangle. \quad (25)$$

This relation is comparable with (21) in that it is purely kinematical. The right-hand side describes the stretching of vortex lines, as discussed by Taylor (1938).

We can now use relations (19), (21), (22), (23), and (25) and rewrite the dynamical equation (18) as

$$\frac{\partial}{\partial t}\langle A^2+B^2+C^2\rangle = -\langle abc\rangle - \tfrac{1}{4}\nu\langle u_{i,jk}u_{i,jk}\rangle. \quad (26)$$

The viscous term is always positive and indicates dissipation of vorticity. Production of mean-square vorticity occurs if $\langle abc\rangle < 0$, which is equivalent to $S > 0$. Our inequalities therefore specify a maximum rate of

production of vorticity with a limit determined by mean square and mean fourth powers of the eigenvalues.

Let us examine the effect of intermittency of the flow. We will say that the flow is intermittent if $u_{i,j} \equiv 0$ in a variety of large and well defined regions, occupying a fraction α of the space filled by the fluid. The distribution of these regions can be isotropic and homogeneous and they can eventually have a size comparable with the integral scale of the turbulence. The quantities S and γ can be measured as previously or similar quantities S' and γ' can be obtained by averaging only over those regions where $u_{i,j}$ fluctuates. It follows from (15) that $S' = \sqrt{(1-\alpha)}S$ and $\gamma' = (1-\alpha)\gamma$. Hence $S'/\sqrt{\gamma'}$ is independent of α, and this means that the presence of γ in (16) allows for possible intermittency of the flow.

The factor γ' is related to quadruple four-point correlations, and one could perhaps assume that, within the regions of finite $u_{i,j}$, the fourth order cumulants vanish. This would give $\gamma' = 3$. Observation of turbulent flows suggests that γ and *a fortiori* γ' are not very different from 3, and that $u_{i,j}$ is mildly intermittent. This means that S could not exceed a value of about 0·9 without serious intermittency or without non-zero fourth order cumulants.

6. A remark on vorticity production

From (6) and (25), we have the important relation

$$-\langle abc \rangle = \langle aA^2 + bB^2 + cC^2 \rangle.$$

In a different form, this relation was first written by Townsend (1951). We must remember that b and c are of the same sign and that a is the largest eigenvalue. Thus abc has the sign of a and, for production of vorticity, we must have a predominance of points at which $a < 0$.

If $a < 0$, the flow behaves locally as a jet parallel to the a-axis and impinging on a wall represented by the b- and c-axes. The dynamic equations show that A (the vorticity component normal to the wall) is attenuated, and that B and C are amplified. If this situation lasts long enough, we shall find, for any initial vorticity, that $aA^2 + bB^2 + cC^2 > 0$. This situation is therefore such that both sides of (27) are positive. If $a > 0$, the flow behaves locally as if it were entering a contraction cone. A small fluid sphere is deformed into a cigar-shaped ellipsoid. Only A is amplified, and if this situation lasts long enough, it will contribute positively to the right-hand side of (27) and negatively to the left-hand side.

It is clear, therefore, that production of vorticity is associated essentially with $a < 0$ and amplification of B and C. This suggests that the most important processes associated with production of vorticity and energy transfer resemble a jet collision and not the swirling of a contracting jet.

7. Remark on continuity

So far, we have not mentioned any requirement of continuity, and the existence of second derivatives of the velocity has been assumed implicitly.

This question is of major interest, especially in the case of very small viscosity. Let us consider the extreme case of our inequality, that is, $a = -2b = -2c =$ constant. Equations (21) and (25) impose some restrictions on the vorticity, and it turns out that they involve only $\langle A^2 \rangle$ and $\langle B^2 + C^2 \rangle$. This leaves a great freedom in the choice of the vorticity and the orientation of the principal axes. However, this does not guarantee that we can connect smoothly the values of $u_{i,j}$ at a point with its values at some other point. When the viscosity is very small the momentum equation can conceivably include large values of $u_{i,kk}$, but there may be a limit to the type and magnitude of the viscous terms. This leads to the following question: Is it possible to construct a velocity field with maximum $\langle abc \rangle$, isotropic and homogeneous properties and such that it satisfies the momentum equations? In the limit of vanishing viscosity discontinuities of $u_{i,j}$ occur, and we can ask whether the condition $a = -2b = -2c =$ constant makes the flow everywhere discontinuous or whether we can choose the other components of $u_{i,j}$ in such a way that the discontinuities occur only along isolated surfaces (shear layers). The answer to such questions could very well lead to a lower maximum value of S and eventually close the gap between experiments and theory.

References

Hardy, G. H., Littlewood, J. E. & Polya, G. 1952 *Inequalities*. Cambridge University Press.

Liepmann, H. W., Laufer, J. & Liepmann, K. 1951 On the spectrum of isotropic turbulence, *Nat. Adv. Comm. Aero., Wash., Tech. Note* no. 2473.

Proudman, I. & Reid, W. H. 1954 On the decay of a normally distributed and homogeneous turbulent velocity field, *Proc. Roy. Soc.* A, **247,** 163.

Stewart, R. W. 1951 Triple velocity correlations in isotropic turbulence, *Proc. Camb. Phil. Soc.* **47,** 146.

Taylor, G. I. 1938 Production and dissipation of vorticity in a turbulent fluid, *Proc. Roy. Soc.* A, **164,** 15.

Townsend, A. A. 1947 Experimental evidence for the theory of local isotropy, *Proc. Camb. Phil. Soc.* **44,** 560.

Townsend, A. A. 1948 Local isotropy in wake of a cylinder, *Aust. J. Sci. Res.* A, **1,** 161.

Townsend, A. A. 1951 On the fine-scale structure of turbulence, *Proc. Roy. Soc.* A, **208,** 534.

The almost-rigid rotation of viscous fluid between concentric spheres

By IAN PROUDMAN
Trinity College, Cambridge

(*Received* 30 *April* 1956)

SUMMARY

Two concentric spheres are supposed to rotate about the same axis with almost the same angular velocity, so that the viscous stresses over the surfaces of the spheres induce a flow which may be represented by a small perturbation superimposed upon a rigid body rotation of the fluid as a whole. The governing equations are therefore linearized in the magnitude of the perturbation, and it appears that the validity of this linearization is independent of the Reynolds number of the primary rotation. Attention is then restricted to the case in which the Reynolds number is large, the principal object of the note being to exemplify some of the properties of rotating systems at large Reynolds numbers in terms of a particularly simple mathematical model.

It is found that the cylindrical surface that touches the inner sphere (the axis being the axis of rotation) is a singular surface in which velocity gradients are very large. Everywhere outside this cylinder, the fluid rotates as a rigid body with the same angular velocity as the outer sphere. Inside the cylinder, the velocity distribution in the central (inviscid) core of the motion is shown to be determined by the velocity distribution in the boundary layers over the spheres, and explicit solutions are obtained for all these velocity distributions. The mechanics of the cylindrical shear layer itself is also discussed, though no explicit solution is obtained in this case.

1. INTRODUCTION

In the literature relating to rotating systems in fluid dynamics, very little attention has been paid to problems in which the configuration of the boundaries is such that the flow may be represented by a small perturbation superimposed upon a rigid body rotation of the (incompressible) fluid as a whole. Indeed, the only relevant work of which I am aware is that of Squire (1953) and Stewartson (1953). Squire considered the flow due to a rotating disc when the fluid at a great distance from the disc is rotating as a rigid body about the same axis with almost the same angular velocity, and Stewartson considered the similar problem in which two discs rotate about the same axis with almost the same angular velocity. In both these

problems, the potential value of the basic approximation was, perhaps, somewhat obscured by the fact that the general form of the exact solutions of the Navier–Stokes equations had previously been found by Batchelor (1951). The peculiar property of the general class of flows under discussion is, in fact, that the governing equations become linear in a manner that is independent of the Reynolds number, and the much greater tractability of linear equations leads to the expectation that substantial analytical progress can be made in such problems. A discussion of many of the interesting properties of rotating systems is undoubtedly prohibited by the linearization, but this is obviously not true of all such properties. In particular, the phenomenon of flow at large Reynolds numbers being governed by linear equations is of real interest, and may be expected to yield useful information concerning the behaviour of boundary layers in rotating systems.

The present note is concerned with the particular problem in which two concentric spheres rotate rapidly about the same axis with slightly different angular velocities. In such a system, it is clear that the viscous stresses over the boundaries must induce a secondary flow, and the principal purpose of the note is to examine the properties of this secondary flow when the Reynolds number is large.

2. The governing equations

Let the radii of the inner and outer spheres be a and αa, respectively, and let the corresponding angular velocities be Ω and $\Omega(1+\epsilon)$, where ϵ is very small. Let (r', θ, ϕ) denote spherical polar coordinates in which the line $\theta = 0$ coincides with the axis of rotation, and let u', v', w', be the corresponding components of velocity (see figure 1).

By symmetry, all dynamical variables must be independent of ϕ, so that the incompressibility condition may be integrated in terms of a stream function ψ', where

$$u' = \frac{1}{r'^2 \sin\theta}\frac{\partial\psi'}{\partial\theta}, \qquad v' = -\frac{1}{r'\sin\theta}\frac{\partial\psi'}{\partial r'}. \tag{2.1}$$

Then, writing

$$w' = \frac{\chi'}{r'\sin\theta}, \tag{2.2}$$

the Navier–Stokes equations of steady motion become (see Goldstein 1938, ch. 3)

$$\frac{2\chi'}{r'^2\sin^2\theta}\left[\frac{\partial\chi'}{\partial r'}\cos\theta - \frac{1}{r'}\frac{\partial\chi'}{\partial\theta}\sin\theta\right] - \frac{1}{r'^2\sin\theta}\frac{\partial(\psi', D^2\psi')}{\partial(r',\theta)} + \\ + \frac{2D^2\psi'}{r'^2\sin^2\theta}\left[\frac{\partial\psi'}{\partial r'}\cos\theta - \frac{1}{r'}\frac{\partial\psi'}{\partial\theta}\sin\theta\right] = \nu D^4\psi', \tag{2.3}$$

and

$$-\frac{1}{r'^2\sin\theta}\frac{\partial(\psi', \chi')}{\partial(r',\theta)} = \nu D^2\chi', \tag{2.4}$$

where

$$D^2 = \frac{\partial^2}{\partial r'^2} + \frac{\sin\theta}{r'^2}\frac{\partial}{\partial\theta}\left(\frac{1}{\sin\theta}\frac{\partial}{\partial\theta}\right). \tag{2.5}$$

The boundary conditions for equations (2.3) and (2.4) are :

$$\left.\begin{aligned} r' = a, \qquad & \frac{\partial \psi'}{\partial r'} = \psi' = 0, \qquad \chi' = \Omega a^2 \sin^2\theta \ ; \\ r' = \alpha a, \qquad & \frac{\partial \psi'}{\partial r'} = \psi' = 0, \qquad \chi' = \Omega(1+\epsilon)\alpha^2 a^2 \sin^2\theta. \end{aligned}\right\} \tag{2.6}$$

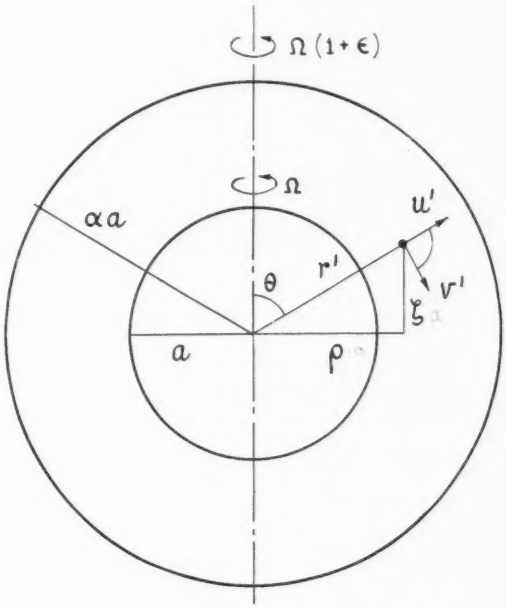

Figure 1. Notation.

When $\epsilon = 0$, the exact solution of the problem is obviously the rigid body rotation represented by

$$\psi' = 0, \qquad \chi' = \Omega r'^2 \sin^2\theta.$$

Hence, when ϵ is non-zero but small, it is reasonable to write

$$\psi' = \epsilon a^3 \Omega \psi, \qquad \chi' = \Omega r'^2 \sin^2\theta + \epsilon a^2 \Omega \chi, \tag{2.7}$$

and retain only terms of the first order in ϵ. Thus, introducing the dimensionless variable

$$r = r'/a, \tag{2.8}$$

the dynamical equations (2·3) and (2·4) reduce to

$$2\left(\frac{\partial \chi}{\partial r}\cos\theta - \frac{1}{r}\frac{\partial \chi}{\partial \theta}\sin\theta\right) = \frac{1}{R} D^4 \psi, \tag{2.9}$$

$$-2\left(\frac{\partial \psi}{\partial r}\cos\theta - \frac{1}{r}\frac{\partial \psi}{\partial \theta}\sin\theta\right) = \frac{1}{R} D^2 \chi, \tag{2.10}$$

where D^2 is the same operator as (2.5), but with r' replaced by r, and R is the Reynold's number given by

$$R = \frac{a^2\Omega}{\nu}. \tag{2.11}$$

The boundary conditions become

$$\left.\begin{aligned} r = 1, \quad & \frac{\partial\psi}{\partial r} = \psi = 0, \quad \chi = 0, \\ r = \alpha, \quad & \frac{\partial\psi}{\partial r} = \psi = 0, \quad \chi = \alpha^2 \sin^2\theta. \end{aligned}\right\} \tag{2.12}$$

The equations (2.9) and (2.10) form the basis of the present note.

It is worth noting here that the approximation leading to (2.9) and (2.10) is somewhat analogous to the approximation introduced by Oseen (1910) in problems of uniform streaming past obstacles. For, in both cases, a linear approximation to the inertia terms in the Navier–Stokes equation is made. In Oseen's case, however, it is an immediate (kinematic) consequence of the boundary conditions that the approximate form of the inertia terms is invalid in the neighbourhood of the obstacle, so that the approximation is spatially uniform only if the Reynolds number is very small. In the present case no such troubles seem to arise, since the boundary conditions are kinematically consistent with the linearization over the whole field of flow, and the Reynolds number of the primary motion remains a significant parameter on which there is no immediately obvious restriction. Nevertheless, when the Reynolds number is very large, the possibility that intense velocity gradients in the secondary flow might invalidate the linearization must not be ignored. This last point will be a matter for subsequent examination.

Although the spherical polar coordinates are particularly suited to the geometry of the boundaries, many aspects of the natural dynamical behaviour of the system at large Reynolds numbers are of a much more two-dimensional nature than the boundary conditions suggest. It will therefore be useful to set out here the governing equations in terms of the cylindrical coordinates (see figure 1)

$$\rho = r\sin\theta, \qquad \zeta = r\cos\theta. \tag{2.13}$$

Thus, (2.9) and (2.10) become

$$2\frac{\partial\chi}{\partial\zeta} = \frac{1}{R}D^4\psi, \tag{2.14}$$

and

$$-2\frac{\partial\psi}{\partial\zeta} = \frac{1}{R}D^2\chi, \tag{2.15}$$

where

$$D^2 = \frac{\partial^2}{\partial\rho^2} - \frac{1}{\rho}\frac{\partial}{\partial\rho} + \frac{\partial}{\partial\zeta^2}. \tag{2.16}$$

3. The boundary layers over the spheres

When the Reynolds number is very large, viscous forces must be negligible over the whole field of flow, except, possibly, in the neighbourhood of certain singular surfaces. The cylindrical polar equations (2.14)

and (2.15) then show that, apart from such surfaces, the solutions must take the simple form

$$\psi = \psi(\rho), \qquad \chi = \chi(\rho), \tag{3.1}$$

and since it is clearly impossible to satisfy the viscous boundary conditions (2.12) with such functions, it follows that the singular surfaces must indeed exist in this problem.

Now, it is natural in the first place to suppose that the singular surfaces take the form of conventional boundary layers over the two spherical boundaries. Thus, taking the case of the inner sphere first, the usual boundary layer approximations in the dynamical equations (2.9) and (2.10) lead to the equations

$$2\frac{\partial\chi}{\partial r}\cos\theta = \frac{1}{R}\frac{\partial^4\psi}{\partial r^4}, \qquad -2\frac{\partial\psi}{\partial r}\cos\theta = \frac{1}{R}\frac{\partial^2\chi}{\partial r^2}. \tag{3.2}$$

In view of the large velocity gradients implied by the approximate equations (3.2), it is then proper to enquire whether these equations are consistent with the original linearization in ϵ. Returning, therefore, to the exact dynamical equations (2.3) and (2.4), the neglected inertia terms in the first of these equations are

$$\epsilon^2 a\Omega^2\left[\frac{2\chi}{r^2\sin^2\theta}\left\{\frac{\partial\chi}{\partial r}\cos\theta - \frac{1}{r}\frac{\partial\chi}{\partial\theta}\sin\theta\right\} - \frac{1}{r^2\sin^2\theta}\frac{\partial(\psi, D^2\psi)}{\partial(r,\theta)} + \right.$$
$$\left. + \frac{2D^2\psi}{r^2\sin^2\theta}\left\{\frac{\partial\psi}{\partial r}\cos\theta - \frac{1}{r}\frac{\partial\psi}{\partial\theta}\sin\theta\right\}\right],$$

which, on the assumption that a boundary layer exists at $r = 1$, reduce to

$$\epsilon^2 a\Omega^2\left[\frac{2\cos\theta}{\sin^2\theta}\chi\frac{\partial\chi}{\partial r} - \frac{1}{\sin\theta}\left(\frac{\partial\psi}{\partial\theta}\frac{\partial^3\psi}{\partial r^3} - \frac{\partial\psi}{\partial r}\frac{\partial^3\psi}{\partial r^2\partial\theta}\right) + \frac{2}{\sin^2\theta}\frac{\partial\psi}{\partial r}\frac{\partial^2\psi}{\partial r^2}\right].$$

Thus, since we may assume

$$\psi = O(R^{-1/2}), \qquad \chi = O(1),$$
$$\partial/\partial r = O(R^{1/2}), \qquad \partial/\partial\theta = O(1),$$

the order of magnitude of the neglected terms is

$$\epsilon^2 a\Omega^2 R^{1/2}.$$

The order of magnitude of the inertia term retained in the first of equations (3.2), on the other hand, is

$$\epsilon a\Omega^2\frac{\partial\chi}{\partial r}\cos\theta \quad \text{or} \quad \epsilon a\Omega^2 R^{1/2}.$$

Hence the neglected terms are smaller by a factor ϵ than those retained, and the presence of large velocity gradients does not affect the basic approximation. The argument may not, of course, apply near particular values of θ, notably near the equator. Similar remarks apply to the other dynamical equation.

The property of the equations (3.2) that is chiefly responsible for the success of this investigation is that they are both *ordinary* differential equations. This remarkable circumstance possibly embodies a point of

where D^2 is the same operator as (2.5), but with r' replaced by r, and R is the Reynold's number given by

$$R = \frac{a^2\Omega}{\nu}. \tag{2.11}$$

The boundary conditions become

$$\left.\begin{aligned} r = 1, \quad & \frac{\partial\psi}{\partial r} = \psi = 0, \quad & \chi = 0, \\ r = \alpha, \quad & \frac{\partial\psi}{\partial r} = \psi = 0, \quad & \chi = \alpha^2 \sin^2\theta. \end{aligned}\right\} \tag{2.12}$$

The equations (2.9) and (2.10) form the basis of the present note.

It is worth noting here that the approximation leading to (2.9) and (2.10) is somewhat analogous to the approximation introduced by Oseen (1910) in problems of uniform streaming past obstacles. For, in both cases, a linear approximation to the inertia terms in the Navier–Stokes equation is made. In Oseen's case, however, it is an immediate (kinematic) consequence of the boundary conditions that the approximate form of the inertia terms is invalid in the neighbourhood of the obstacle, so that the approximation is spatially uniform only if the Reynolds number is very small. In the present case no such troubles seem to arise, since the boundary conditions are kinematically consistent with the linearization over the whole field of flow, and the Reynolds number of the primary motion remains a significant parameter on which there is no immediately obvious restriction. Nevertheless, when the Reynolds number is very large, the possibility that intense velocity gradients in the secondary flow might invalidate the linearization must not be ignored. This last point will be a matter for subsequent examination.

Although the spherical polar coordinates are particularly suited to the geometry of the boundaries, many aspects of the natural dynamical behaviour of the system at large Reynolds numbers are of a much more two-dimensional nature than the boundary conditions suggest. It will therefore be useful to set out here the governing equations in terms of the cylindrical coordinates (see figure 1)

$$\rho = r\sin\theta, \qquad \zeta = r\cos\theta. \tag{2.13}$$

Thus, (2.9) and (2.10) become

$$2\frac{\partial\chi}{\partial\zeta} = \frac{1}{R}D^4\psi, \tag{2.14}$$

and

$$-2\frac{\partial\psi}{\partial\zeta} = \frac{1}{R}D^2\chi, \tag{2.15}$$

where

$$D^2 = \frac{\partial^2}{\partial\rho^2} - \frac{1}{\rho}\frac{\partial}{\partial\rho} + \frac{\partial}{\partial\zeta^2}. \tag{2.16}$$

3. The boundary layers over the spheres

When the Reynolds number is very large, viscous forces must be negligible over the whole field of flow, except, possibly, in the neighbourhood of certain singular surfaces. The cylindrical polar equations (2.14)

and (2.15) then show that, apart from such surfaces, the solutions must take the simple form

$$\psi = \psi(\rho), \qquad \chi = \chi(\rho), \tag{3.1}$$

and since it is clearly impossible to satisfy the viscous boundary conditions (2.12) with such functions, it follows that the singular surfaces must indeed exist in this problem.

Now, it is natural in the first place to suppose that the singular surfaces take the form of conventional boundary layers over the two spherical boundaries. Thus, taking the case of the inner sphere first, the usual boundary layer approximations in the dynamical equations (2.9) and (2.10) lead to the equations

$$2\frac{\partial\chi}{\partial r}\cos\theta = \frac{1}{R}\frac{\partial^4\psi}{\partial r^4}, \qquad -2\frac{\partial\psi}{\partial r}\cos\theta = \frac{1}{R}\frac{\partial^2\chi}{\partial r^2}. \tag{3.2}$$

In view of the large velocity gradients implied by the approximate equations (3.2), it is then proper to enquire whether these equations are consistent with the original linearization in ϵ. Returning, therefore, to the exact dynamical equations (2.3) and (2.4), the neglected inertia terms in the first of these equations are

$$\epsilon^2 a\Omega^2\left[\frac{2\chi}{r^2\sin^2\theta}\left\{\frac{\partial\chi}{\partial r}\cos\theta - \frac{1}{r}\frac{\partial\chi}{\partial\theta}\sin\theta\right\} - \frac{1}{r^2\sin^2\theta}\frac{\partial(\psi, D^2\psi)}{\partial(r,\theta)} + \right.$$
$$\left. + \frac{2D^2\psi}{r^2\sin^2\theta}\left\{\frac{\partial\psi}{\partial r}\cos\theta - \frac{1}{r}\frac{\partial\psi}{\partial\theta}\sin\theta\right\}\right],$$

which, on the assumption that a boundary layer exists at $r = 1$, reduce to

$$\epsilon^2 a\Omega^2\left[\frac{2\cos\theta}{\sin^2\theta}\chi\frac{\partial\chi}{\partial r} - \frac{1}{\sin\theta}\left(\frac{\partial\psi}{\partial\theta}\frac{\partial^3\psi}{\partial r^3} - \frac{\partial\psi}{\partial r}\frac{\partial^3\psi}{\partial r^2\partial\theta}\right) + \frac{2}{\sin^2\theta}\frac{\partial\psi}{\partial r}\frac{\partial^2\psi}{\partial r^2}\right].$$

Thus, since we may assume

$$\psi = O(R^{-1/2}), \qquad \chi = O(1),$$
$$\partial/\partial r = O(R^{1/2}), \qquad \partial/\partial\theta = O(1),$$

the order of magnitude of the neglected terms is

$$\epsilon^2 a\Omega^2 R^{1/2}.$$

The order of magnitude of the inertia term retained in the first of equations (3.2), on the other hand, is

$$\epsilon a\Omega^2\frac{\partial\chi}{\partial r}\cos\theta \quad \text{or} \quad \epsilon a\Omega^2 R^{1/2}.$$

Hence the neglected terms are smaller by a factor ϵ than those retained, and the presence of large velocity gradients does not affect the basic approximation. The argument may not, of course, apply near particular values of θ, notably near the equator. Similar remarks apply to the other dynamical equation.

The property of the equations (3.2) that is chiefly responsible for the success of this investigation is that they are both *ordinary* differential equations. This remarkable circumstance possibly embodies a point of

principle which might have been anticipated on general grounds. It is, of course, a consequence of the linearization that the entire secondary flow must be reversible. In particular, this reversibility must be true of the flow in the boundary layers. Now, the boundary layer flow in an axial plane presumably involves a general mass flux from the poles to the equator, or *vice versa*, depending on whether ϵ is negative or positive (for the inner sphere). Hence, if one regards this flow as being determined by conditions just outside the boundary layer, together with an initial condition represented by the fact that the flow is of some generalized 'stagnation' type at the poles (say), then the corresponding solution at the equator must be such that, when used as an initial condition for the reversed flow, it yields an identical flow pattern. This would appear to impose a severe integral condition on the flow in the boundary layers, and by far the most attractive method of satisfying this condition is to suppose that the velocity profile at each value of θ is determined independently. That such is the case is shown by (3.2), and the explanation given seems at least a possible one.

One integration of (3.2) gives

$$\left.\begin{aligned} 2\cos\theta(\chi-\chi_0) &= \frac{1}{R}\frac{\partial^3\psi}{\partial r^3}, \\ -2\cos\theta(\psi-\psi_0) &= \frac{1}{R}\frac{\partial\chi}{\partial r}, \end{aligned}\right\} \tag{3.3}$$

where ψ_0 and χ_0 are functions of θ only, which are determined by conditions at the outer edge of the boundary layer. From (3.3) it follows that

$$\frac{\partial^4}{\partial r^4}(\psi-\psi_0) = -4R^2\cos^2\theta(\psi-\psi_0), \tag{3.4}$$

so that a suitable measure of distance from the boundary is

$$\eta = (r-1)(R\cos\theta)^{1/2} \quad (0 \leqslant \theta < \tfrac{1}{2}\pi). \tag{3.5}$$

The four independent solutions of (3.4) are then of the form

$$\exp\{(\pm 1 \pm i)\eta\},$$

and the bounded solution for ψ that has a double zero at $\eta = 0$ is

$$\psi = \psi_0\{1-e^{-\eta}(\cos\eta+\sin\eta)\}. \tag{3.6}$$

The corresponding solution for ψ follows immediately from the first of equations (3.3), and is

$$\chi = \chi_0 - 2(R\cos\theta)^{1/2}\psi_0 e^{-\eta}\cos\eta \tag{3.7}$$

Then, since χ must also vanish at $\eta = 0$, we must have

$$\chi_0 = 2(R\cos\theta)^{1/2}\psi_0. \tag{3.8}$$

The formulae (3.5) to (3.8), which represent the explicit solution for the flow in a three-dimensional boundary layer, were first obtained by Ekman (1902). Actually, Ekman considered the flow near a rotating disc when the relative flow at a great distance from the disc is a uniform stream, but, to the order of the boundary layer approximation, this flow is clearly identical with the flow near the spherical boundaries of the present problem. Since

the boundary layer is very thin, each element of the surface of the sphere may be regarded as a large disc rotating with the normal component $\Omega \cos\theta$ of the angular velocity of the sphere, and the relative velocity outside the boundary layer is locally a uniform stream.

The most striking feature of the solution is the oscillatory approach to conditions in the 'inviscid' core of the motion (the 'Ekman spiral'). The same feature appeared, of course, in Squire's and Stewartson's solutions for the flow near a rotating disc. Another point of interest is the explicit formula (3.5) for the thickening of the boundary layer towards the equator. Very close to the equator this thickening becomes very rapid, and when $\frac{1}{2}\pi - \theta = O(R^{-1})$ the boundary layer approximation clearly breaks down altogether.

It should also be noted at this stage that the relation (3.8), which is demanded by the viscous mechanics of the boundary layer on the inner sphere, implies a relation between the functions ψ and χ throughout the whole of that part of the core of the motion which lies within the cylinder $\rho = 1$ (i.e. the cylinder that touches the inner sphere). The reason for this is the form (3.1) that the solution must take in the absence of viscous forces. Actually, it is not strictly correct to apply the first of the results (3.1) without further explanation because (3.8) ensures that $\psi = O(R^{-1/2})$ which vanishes in the limit of infinite Reynolds number. The strictly 'inviscid' solution is therefore

$$\psi = 0, \qquad \chi = (\rho).$$

But, of course, when $\psi = O(R^{-1/2})$ and $\chi = O(1)$, it is still true that the viscous terms in the dynamical equation (2.15) are negligible in the core of the motion, so that the first of the results (3.1) is still valid. In this restricted sense, the motion in the core is 'inviscid', and we may write

$$\psi = \psi_0(\rho), \qquad \chi = \chi_0(\rho). \tag{3.9}$$

Since $\rho = \sin\theta$ on the inner sphere, it then follows that $\psi_0(\sin\theta)$ and $\chi_0(\sin\theta)$ are the functions of θ only that appear in (3.3), so that the condition (3.8) becomes

$$\chi_0(\rho) = 2R^{1/2}(1-\rho^2)^{1/4}\psi_0(\rho) \quad (\rho < 1). \tag{3.10}$$

The analysis of the motion in the boundary layer on the outer sphere is substantially the same. Here, the integration of (3.2) gives

$$\left.\begin{aligned} 2\cos\theta\{\chi - \chi_0(\alpha\sin\theta)\} &= \frac{1}{R}\frac{\partial^3\psi}{\partial r^3}, \\ -2\cos\theta\{\psi - \psi_0(\alpha\sin\theta)\} &= \frac{1}{R}\frac{\partial\chi}{\partial r}, \end{aligned}\right\} \tag{3.11}$$

where ψ_0 and χ_0 have the same meanings as in (3.9), since $\alpha\sin\theta$ is the value of ρ on the outer sphere. Then, introducing the variable

$$\eta' = (\alpha - r)(R\cos\theta)^{1/2}, \tag{3.12}$$

the relevant solution for ψ is

$$\psi = \psi_0(\alpha\sin\theta)\{1 - e^{-\eta'}(\cos\eta' + \sin\eta')\}, \tag{3.13}$$

and the corresponding solution for χ is

$$\chi = \chi_0(\alpha \sin\theta) + 2(R\cos\theta)^{1/2}\psi_0(\alpha\sin\theta)e^{-\eta'}\cos\eta'. \tag{3.14}$$

Moreover, the boundary conditions (2.12) require that $\chi = \alpha^2\sin^2\theta$ over the outer sphere $\eta' = 0$, so that (3.14) gives

$$\alpha^2\sin^2\theta - \chi_0(\alpha\sin\theta) = 2(R\cos\theta)^{1/2}\psi_0(\alpha\sin\theta). \tag{3.15}$$

Now, the result (3.15) provides a relation between the functions ψ_0 and χ_0 which must be satisfied throughout the entire core of the motion. Thus,

$$\rho^2 - \chi_0(\rho) = 2R^{1/2}\left(1-\frac{\rho^2}{\alpha^2}\right)^{1/4}\psi_0(\rho), \tag{3.16}$$

without restriction on the value of ρ. In the region $\rho < 1$, therefore, the two relations (3.10) and (3.16) uniquely determine the functions ψ_0 and χ_0, and the relevant formulae are readily found to be

$$\psi_0(\rho) = \frac{\rho^2}{2R^{1/2}}\left\{\left(1-\frac{\rho^2}{\alpha^2}\right)^{1/4} + (1-\rho^2)^{1/4}\right\}^{-1}, \tag{3.17}$$

and

$$\chi_0(\rho) = \rho^2(1-\rho^2)^{1/4}\left\{\left(1-\frac{\rho^2}{\alpha^2}\right)^{1/4} + (1-\rho^2)^{1/4}\right\}^{-1}. \tag{3.18}$$

The result (3.18) is particularly interesting inasmuch as it is an explicit example of a velocity distribution of order R^0 being determined by viscous mechanics in a case where R is large. The manner in which this takes place in the present problem is, of course, very simple. In the core of the motion, the streamlines in an axial plane are parallel to the axis of rotation, so that fluid leaving the boundary layer on one sphere round the circle $\rho = \rho_0$ must enter the boundary layer on the other sphere round a circle of the same radius. This is one essential connection between the boundary layers on the two spheres. The other essential connection arises from the fact that the azimuthal velocity in the core is also a function only of the radial distance from the axis of rotation, and must be such that the associated centrifugal and coriolis forces are just sufficient to require the same mass flux from *both* boundary layers at any particular value of ρ.

It follows from (3.18) that the cylindrical surface $\rho = 1$ must be another singular surface of the motion. It is true that the formula (3.18) is not valid for values of ρ close to unity, but this cannot affect the deduction that velocity gradients become very large at such values of ρ. Thus, it seems likely that viscosity must again be taken into account near this surface.

The problem of finding the distribution of ψ_0 and χ_0 for values of ρ greater than unity is slightly different, because the result (3.10) is no longer relevant. It may be replaced, however, by the symmetry condition that $\psi = 0$ over the equatorial plane $\zeta = 0$. Hence, either the equatorial plane is also a singular surface of the motion (so that ψ at $\zeta = 0$ is not equal to $\psi_0(\rho)$), or else

$$\psi_0(\rho) \equiv 0 \quad \text{for all } \rho > 1. \tag{3.19}$$

As regards the former possibility, the appropriate boundary layer approximations in the cylindrical polar equations (2.14) and (2.15) yield the equations

$$2R\frac{\partial\chi}{\partial\zeta} = \frac{\partial^4\psi}{\partial\zeta^4}, \qquad -2R\frac{\partial\chi}{\partial\zeta} = \frac{\partial^2\chi}{\partial\zeta^2},$$

so that

$$\frac{\partial^4}{\partial\zeta^4}\{\psi-\psi_0(\rho)\} = -4R^2\{\psi-\psi_0(\rho)\}.$$

But there are clearly no solutions of this last equation that remain bounded for all values of ζ (both positive and negative), so that (3.19) appears to be the relevant deduction. It follows immediately from (3.16) that

$$\chi_0(\rho) \equiv \rho^2 \quad \text{for all } \rho > 1, \tag{3.20}$$

which shows that the whole of the fluid outside the cylinder containing the inner sphere rotates as a rigid body with the same angular velocity as the outer sphere. There is, of course, no boundary layer over the portion of the outer sphere that bounds this rigid body rotation.

There now remains the problem of finding the motion in the free shear layer near the surface $\rho = 1$. This problem is discussed in the following section.

4. The cylindrical shear layer

In the immediate neighbourhood of the surface $\rho = 1$, velocity gradients with respect to ρ must surely be very much greater than those with respect to ζ, so that it is again permissible to make a boundary layer type of approximation in the governing equations. Thus, the equations (2.14) and (2.15) may be written, approximately,

$$2R\frac{\partial\chi}{\partial\zeta} = \frac{\partial^4\psi}{\partial\rho^4}, \qquad -2R\frac{\partial\psi}{\partial\zeta} = \frac{\partial^2\chi}{\partial\rho^2}. \tag{4.1}$$

However, the approximate equations (4.1), unlike those governing the motion in the boundary layers over the spheres, are not always consistent with the linearization in ϵ. For, if the exact equations of motion are written in cylindrical polar coordinates and a shear layer is supposed to exist at $\rho = 1$, it is a simple matter to show that the neglected terms on the left hand sides of the first and second of equations (4.1) are

$$\epsilon R\left(2\chi\frac{\partial\chi}{\partial\zeta} + \frac{\partial\psi}{\partial\rho}\frac{\partial^3\psi}{\partial\rho^2\partial\zeta} - \frac{\partial\psi}{\partial\zeta}\frac{\partial^3\psi}{\partial\rho^3}\right)$$

and

$$\epsilon R\left(\frac{\partial\psi}{\partial\rho}\frac{\partial\chi}{\partial\zeta} - \frac{\partial\psi}{\partial\zeta}\frac{\partial\chi}{\partial\rho}\right),$$

respectively. Then, if δ is the thickness of the layer, and if χ is assumed to be $O(1)$ throughout the layer (χ is actually equal to the azimuthal velocity when $\rho = 1$), the orders of magnitude of these terms are

$$\epsilon R\left(1+\frac{\psi^2}{\delta^3}\right) \quad \text{and} \quad \frac{\epsilon R\psi}{\delta},$$

respectively. Hence, comparing the second of these estimates with the second of equations (4.1), the validity of the linearization is certainly dependent upon the condition that ϵ/δ should be small. Thus, if $\delta \to 0$ as $R \to \infty$, the equations (4.1) cannot refer to the limit $R \to \infty$ for fixed small ϵ. However, if, as seems likely, the orders of magnitude of ψ, χ and δ, are determined only by R when ϵ is small, the equations should apply to the limit* $\epsilon \to 0$ for fixed large R. In this sense, the linearized equations (4.1) will be assumed to be valid.

Now, it appears that the boundary layer type of approximation leading to (4.1) is the only feature that the shear layer has in common with conventional boundary layers. It does not seem to be possible, for instance, to have a shear layer of this kind in which dynamical variables are of the same order of magnitude as in ordinary boundary layers. For, if that were the case, we should have

$$\psi = O(R^{-1/2}), \qquad \chi = O(1),$$

together with the information that the thickness of the layer is $O(R^{-1/2})$. But, with these orders of magnitude, the first of equations (4.1) reduces to

$$\frac{\partial^4 \psi}{\partial \rho^4} = 0,$$

and, quite apart from the dynamical unlikelihood of a layer with negligible acceleration in an axial plane, this equation does not possess solutions that are bounded as $(\rho - 1)R^{1/2} \to \pm \infty$.

Again, it might be thought that the orders of magnitude must be such that viscous and inertia forces are comparable in both equations of motion. This would at least correspond in principle, if not in detail, to the mechanics of an ordinary three-dimensional boundary layer. Under these circumstances, elimination of ψ from the equations (4.1) gives

$$-4R^2 \frac{\partial^2 \chi}{\partial \zeta^2} = \frac{\partial^6 \chi}{\partial \rho^6},$$

from which it follows immediately that the thickness of the layer must be $O(R^{-1/3})$, and hence, from (4.1), that

$$\psi/\chi = O(R^{-1/3}). \tag{4.2}$$

Now, it must surely be the case that $\chi = O(1)$ throughout the layer, so that (4.2) gives $\psi = O(R^{-1/3})$, which implies a general mass flux by the velocity components in an axial plane of the same order of magnitude. But an important *raison d'etre* of the shear layer is to carry fluid from the boundary layer on one sphere to that on the other, and *this* mass flux is only $O(R^{-1/2})$. The conclusion would have to be, therefore, that, to the order of the boundary layer approximation, the total mass flux parallel to the axis of rotation was zero, and this would imply that there was a substantial 'return flow' in the shear layer. I have not been able to show that such a situation is impossible, but the assumption of comparable viscous and inertia forces does seem to

* A somewhat easier limiting process to realize in any practical arrangement.

be a most unnatural method of attempting to satisfy the conditions of the problem.

The only acceptable alternatives appear to be those in which the orders of magnitude of ψ and χ in the layer are those suggested by the boundary conditions, namely

$$\psi = O(R^{-1/2}), \qquad \chi = O(1), \tag{4.3}$$

and the thickness of the layer is sufficiently large to ensure that viscous forces are comparable with inertia forces in either only one, or possibly neither, of the dynamical equations (4.1). Taking first the case in which the mechanics is not entirely inviscid, it is a simple matter to see that the equation in which viscous forces are appreciable must be the second of equations (4.1); from which it follows that the thickness of the layer is $O(R^{-1/4})$. The governing equations may therefore be written

$$\frac{\partial \chi}{\partial \zeta} = 0, \qquad -2\frac{\partial \psi'}{\partial \zeta} = \frac{\partial^2 \chi}{\partial \rho'^2}, \tag{4.4}$$

where

$$\rho' = (\rho - 1)R^{1/4} \tag{4.5}$$

and

$$\psi' = \psi R^{1/2}. \tag{4.6}$$

If this interpretation of the mechanics is correct, it appears that viscous layers in rotating systems can have an entirely different structure from ordinary boundary layers. This structure is a highly anisotropic one in which viscous forces oppose only the rotary motion, so that the motion in planes containing the axis of rotation remains 'inviscid'. In the special problem under discussion, the inviscid nature of the flow in an axial plane provides a neat explanation of how it is that fluid travels from one sphere to the other within a layer which remains thin. The essential point is that the layer is sufficiently thick, and the velocity sufficiently small, to make viscous forces negligible.

The general solution of (4.4) is easily seen to be

$$\left.\begin{aligned} \chi &= F(\rho'), \\ \psi' &= -\tfrac{1}{2}\zeta F''(\rho') + G(\rho'), \end{aligned}\right\} \tag{4.7}$$

where F and G are arbitrary functions of ρ', and F'' is the second derivative of F. The form of these arbitrary functions is presumably determined by conditions at the points $\zeta = 0$ and $\zeta = (\alpha^2 - 1)^{1/2}$ where the shear layer joins the boundary layer on the spheres. Unfortunately, the solution for the flow in the neighbourhood of these points lies outside the scope of the boundary layer approximations, and would require a much more comprehensive analysis of the motion than I have been able to make. However, it can at least be shown that the structure of the solution (4.7) is consistent with the boundary conditions as $\rho' \to \pm\infty$. As $\rho' \to +\infty$, the motion must tend to the rigid body rotation represented by (3.19) and (3.20), so that we must have

$$F(\infty) = 1, \qquad G(\infty) = 0.$$

As $\rho' \to -\infty$, on the other hand, the boundary conditions are found by writing $\rho = 1$ in the formulae (3.17) and (3.18). In this way we get

$$F(-\infty) = 0, \qquad G(-\infty) = \frac{1}{2}\left(1 - \frac{1}{\alpha^2}\right)^{-1/4}.$$

It may then be noted that $F''(\rho') \to 0$ as $\rho' \to \pm\infty$, so that the dependence of the solution (4.7) on ζ disappears as the inviscid regions are approached.

The remaining possibility is that the mechanics of the shear layer is entirely inviscid. This clearly corresponds to the case in which the thickness of the layer is of greater order of magnitude than $R^{-1/4}$. In such a case, both the thickness of the layer and the velocity distribution within it (now of the simple form (3.9)) would presumably be determined by conditions near the joins of the shear layer with the boundary layers over the spheres.

It would seem that the only satisfactory way of deciding which, if either, of the preceding two mechanical structures is correct is to determine the asymptotic form, for large Reynolds numbers, of the exact solution of the linearized equations (2.9) and (2.10).

I am indebted to Mr W. W. Wood for several helpful comments on an earlier draft of this paper.

References

Batchelor, G. K. 1951 *Quart. J. Mech. Appl. Math.* **4**, 29.
Ekman, V. W. 1902 *Nyt. Mag. Naturv.* **40**, 1.
Oseen, C. W. 1910 *Ark. f. Mat. Astr. og Fys.* **6**, no. 29.
Squire, H. B. 1953 *Aero. Res. Counc., Lond., Rep.* no. 16,021.
Stewartson, K. 1953 *Proc. Camb. Phil. Soc.* **49**, 333.

The speed of drifting bodies in a stream

By J. R. D. FRANCIS
Imperial College, London

(*Received* 12 *May* 1956)

SUMMARY

The speed of free floating bodies on the surface of a water stream in a sloping channel has been found to be sensibly the same as the mean speed of the layer of water in which the bodies are floating, contrary to some recorded opinions.

It is sometimes believed that a ship drifting in a river without power or sail travels faster than the mean speed of the layer of water in which it is floating; it is said that the relative speed of the water past the rudder enables the ship to be steered. Prandtl (1952, p. 179) for example says "The boat, in fact, hurries ahead of the water, and gets enough way on her to be steered ".

The basis of the belief is that the weight force W of the ship is directed vertically downwards, but that the hydrostatic buoyancy force on the ship is directed at right angles to planes of equal pressure, that is, normal to the free surface. Since the surface in a river in uniform flow is inclined by friction at an angle i to the horizontal, it follows that a component force Wi ($i \doteqdot \sin i$ for usual slopes) acts on the ship in a direction down the surface slope. This component force is balanced in steady motion by the hydrodynamic drag force due to the relative motion between ship and water. Alternatively, it is believed that a ship travels faster than the equivalent volume of water because there is an exchange of momentum by turbulent motions across the boundaries of the water. Since the mean speed of the stream decreases with depth, the exchange of momentum causes a resistive force to be exerted on the water volume. The solid boundary of the ship prevents this exchange, so that the only forces on the ship restraining the down-gradient motion are shear stresses caused by the motion of the ship relative to its surroundings, it being tacitly assumed that the flow and pressures in the surroundings are not affected by the replacement of the water volume by the ship. If, in fact, the solid boundary modifies the flow in the neighbourhood, then the forces on it may be quite unlike those at the boundaries of the same volume of water. The buoyancy force on the ship may not then be normal to the free surface, so that the down-hill force can no longer be so easily found.

It is difficult to show if ships do indeed travel faster than their surroundings; for the effect must be small in slow flowing rivers (with small i), and it is clearly imprudent to allow a ship to drift unrestrainedly in a fast and turbulent river (which has a larger i). It is more practical

to test the existence of this relative velocity on a cylinder floating with its axis vertical in a stream. Such floats are sometimes used by engineers to determine the speed of a river, and it may be desirable to ascertain if there is any systematic error in using them for this purpose.

The force W on such a cylinder of diameter d and length l when floating in a fluid of density ρ is $W = \frac{1}{4}\pi d^2 l\rho g$. If the cylinder is moving at a velocity u_{rel} relative to its surroundings, then the drag force F on it is approximately that which the same cylinder would experience if it was travelling at the same speed relative to still water. On this approximation, $F = C_d dl(\frac{1}{2}\rho u_{rel}^2)$; and, equating F to the downstream component of W, we have

$$C_d dl(\tfrac{1}{2}\rho u_{rel}^2) = \tfrac{1}{4}\pi d^2 l\rho g i,$$

where C_d is the coefficient of drag of the cylinder. It is convenient to substitute the frictional properties of the river channel for the variable i, and one empirical formula used by engineers is

$$\bar{u} = C\sqrt{(mi)},$$

where C is a coefficient (Chezy's coefficient) predominantly determined by the roughness of the channel, $\bar{u}$ is the mean velocity, and m is the hydraulic mean depth, i.e. the cross-sectional area divided by the wetted perimeter of the channel (equal to the depth if the channel is wide). Substituting for i in the previous equation, we obtain

$$\frac{u_{rel}}{\bar{u}} = \frac{1}{C}\sqrt{\left(\frac{\pi g d}{2mC_d}\right)}.$$

It will be seen from this equation that a high value of u_{rel} should be obtained in rough-walled channels (having a low value of C) and with cylinders having a large d/m ratio. Engineer's floats may be cylinders of about 3 in. diameter, and might well be used in a typical river of depth $m = 10$ ft., $C = 100$ ft.$^{1/2}$ sec^{-1}. The equation shows that the theoretical value of $u_{rel}/\bar{u}$ is about 0·01; it is probable that this small increase of velocity (if it exists at all) is hidden by experimental error and by the large-scale turbulence of the stream.

The point may be better investigated in a laboratory channel which can be made to have a great roughness, and experiments have been so made in the Civil Engineering Laboratories of Imperial College. Systematic roughness elements, of a type proposed by Denil and tested by White & Nemenyi (1942), were arranged on the bottom of a glass sided channel 11 m long and 30 cm wide. These roughnesses are zigzag walls 1·6 cm high running across the channel. From alternate 90° angles, longitudinal walls of the same height connect one wall with the next, 7·5 cm upstream or downstream. The bed of the channel may be tilted so that it is parallel to the surface of the water. Four floats were made, all circular cylinders ballasted to float to a draft of 2·5 cm with their axes vertical. A quantity of 0·00652 m^3 sec^{-1} was made to flow down the channel; and it was found that if the bed was inclined at $i = 1/271$, the depth was constant at 7·5 cm above the top of the roughness. Under these conditions, $C = 21$ m$^{1/2}$ sec^{-1} for

$\bar{u} = 0{\cdot}286$ m/sec. The theoretical value of $u_{rel}/\bar{u}$ for each cylinder is given in table 1. In this table the coefficients of drag have been taken as those applicable to cylinders whose length-diameter ratio is double that of the cylinders tested, so as to allow for the three-dimensional flow round the lower end (Goldstein 1938, p. 439).

Float diameter (cm) :	6·3	1·9	0·7	0·2
Calculations				
Length/diameter	0·4	1·3	3·6	12·5
Drag coefficient	0·6	0·7	0·8	0·95
$u_{rel}/\bar{u}$	0·270	0·137	0·078	0·038
u_{rel} (cm/sec)	7·7	3·9	2·2	1·1
Observations				
Number of successful drifts	20	21	22	16
Mean time to traverse 2·88 m (sec)	6·83	6·90	6·80	6·89
Mean deviation (sec)	±0·24	±0·31	±0·25	±0·24
Mean speed (m/sec)	0·421	0·417	0·423	0·418

Table 1. Calculated and measured velocities of cylinders 2·5 cm long drifting in a stream of mean velocity 0·286 m/sec.

The observed speeds of the floats are also shown in table 1. They were timed to the nearest 1/10 sec with a stopwatch calibrated in 1/100 sec, over a 2·88 m length of the channel, starting 5 m downstream of the channel inlet and finishing 3 m upstream of the outlet. The floats were released 1 m upstream of the starting line in mid-stream; and, if the float later drifted so that its axis came outside of the middle third of the channel, its time was disregarded. Only about 1 float in 6 drifted successfully within the middle third.

It will be seen that the calculation predicts that the largest cylinder should travel some 6·6 cm/sec faster than the smallest, but that the observations do not disclose any significant difference in speed for the large range of d/m used.

It is, however, possible that *all* the cylinders drifted at the same speed relative to the upper 2·5 cm of water, in which they all were immersed. Two tests were made to explore this possibility. In the first, drops of dye were put into the stream just ahead and around the largest cylinder. On no occasion did the cylinder appear to overtake the dye and to float into clear water. If the relative velocity exists, then it should have overtaken at 7·7 cm/sec, a speed easily observed.

In the second test, carried out concurrently with the timing of the floats over the 2·88 m test distance, the mean speed of the upper 2·5 cm of water was measured by a current meter. This was a paddlewheel, 30 cm radius, rotating on a horizontal axis, with light aluminium blades immersed

to a depth of 2·5 cm. The part of the wheel in the air was protected from draughts. The meter was calibrated before and after the test by towing it through still water. The mean speed of the water was found five times during the timing of the floats both upstream and downstream of the test length. The mean water speed so obtained was 0·420 m/sec; this was close to the mean speed of all the floats (0·420 m/sec ± 0·017 m/sec mean deviation of 79 observations).

It therefore appears that the floats were in fact travelling, as nearly as could be measured, at the same speed as the water; and that the 'hurrying ahead' of the float was either not present at all, or was much smaller than predicted. Perhaps the presence of shear in a stream rearranges the hydrostatic pressure on the float, so that the resultant upthrust exactly balances the weight force; in this respect, a drifting body therefore appears to affect the flow in the surrounding fluid. This is fortunate, for many experiments in fluid mechanics are carried out using particles of near neutral buoyancy as tracers. If the gradient effect had been real, then systematic errors would occur if pressure gradients occurred. In meteorology, pilot balloons would not travel with the wind; since the atmospheric pressure gradient is at right angles to the wind, a sideways component would be given to the balloon, giving a false direction. The above experiments should not be taken to apply to a flow which has a surface gradient but no shear, in which case a floating object might possibly move relative to the water down the gradient.

If, as was mentioned at the beginning, ships can indeed be steered while drifting down a river, then a possible explanation independent of the 'hurrying ahead' effect may be that the ship's draft is nearly the same as the depth of the river. The lower part of the rudder is therefore in water which is considerably retarded by the boundary layer of the river bed. The ship travels at the mean speed of the upper layers, which is faster, so that there is relative motion over the rudder and the ship is steered. The effect will be enhanced if the ship is of small draft, with a rudder projecting well below its bottom. Tests carried out in the laboratory channel show in fact that a model boat can be steered when drifting if it has such a deep rudder. It cannot be steered if the same rudder is arranged so that it does not project below the boat.

I am indebted to Professor C. M. White, who pointed out that Prandtl's statement was untested.

References

Prandtl, L. 1952 *Essentials of Fluid Dynamics*. London: Blackie.

White, C. M. & Nemenyi, P. 1942 Appendix to *Report of Committee on Fish Passes*. Inst. Civ. Eng., London.

Goldstein, S. (Ed.) 1938 *Modern Developments in Fluid Mechanics*. Oxford University Press.

Outline of a theory of turbulent shear flow

By W. V. R. MALKUS

Woods Hole Oceanographic Institution, Woods Hole, Massachusetts

(*Received* 4 *June* 1956)

SUMMARY

In this paper the spatial variations and spectral structure of steady-state turbulent shear flow in channels are investigated without the introduction of empirical parameters. This is made possible by the assumption that the non-linear momentum transport has only stabilizing effects on the mean field of flow. Two constraints on the possible momentum transport are drawn from this assumption: first, that the mean flow will be statistically stable if an Orr–Sommerfeld type equation is satisfied by fluctuations of the mean; second, that the smallest scale of motion that can be present in the spectrum of the momentum transport is the scale of the marginally stable fluctuations of the mean. Within these two constraints, and for a given mass transport, an upper limit is sought for the rate of dissipation of potential energy into heat. Solutions of the stability equation depend upon the shape of the mean velocity profile. In turn, the mean velocity profile depends upon the spatial spectrum of the momentum transport. A variational technique is used to determine that momentum transport spectrum which is both marginally stable and produces a maximum dissipation rate. The resulting spectrum determines the velocity profile and its dependence on the boundary conditions. Past experimental work has disclosed laminar, 'transitional', logarithmic and parabolic regions of the velocity profile. Several experimental laws and their accompanying constants relate the extent of these regions to the boundary conditions. The theoretical profile contains each feature and law that is observed. First approximations to the constants are found, and give, in particular, a value for the logarithmic slope (von Kármán's constant) which is within the experimental error. However, the theoretical boundary constant is smaller than the observed value. Turbulent channel flow seems to achieve the extreme state found here, but a more decisive quantitative comparison of theory and experiment requires improvement in the solutions of the classical laminar stability problem.

INTRODUCTION

The significant difficulty encountered in the theoretical study of fluid turbulence is the non-linearity of the equations of motion. The classical inquiries (e.g. Goldstein 1938), which are concerned with gross spatial

features of the flow, avoid dealing with non-linearity by deducing macroscopic laws from the observations. The more recent statistical inquiries (e.g. Batchelor 1953), which are mainly restricted to homogeneous fields of motion, deal with non-linearity by various hypotheses concerning the transfer of energy from one scale of motion to another. The emphasis in these latter studies is on the local random aspects of turbulence and on those regions of the spectrum of turbulence far removed from external energy sources. Hence the spatial variations and spectral structure of momentum and heat transport, which are intimately coupled to the energy sources, receive little theoretical attention.

In this paper the emphasis is on the statistical organization of turbulent fields rather than on their statistical randomness. Hence the momentum and heat transport of a steady-state turbulent field and the dependence of these transports on boundary conditions are of primary concern. However, this will not be a detailed mechanistic study. Indeed, there is little hope that exact time-dependent solutions of the non-linear equations describing turbulence can be found. Here, as in past work, an assumption specifying the role of the non-linear processes will be made. This particular assumption is a negative one, specifying what the non-linear processes can not do. In this way the class of possible turbulent fields is restricted. The determination of an extreme member of this class reduces the mathematical problem to tractable linear form without the introduction of empirical parameters. This absence of empirical parameters permits a rigorous appraisal of the validity of the assumption. Indeed, if the quantitative solutions to the problem are to compare favourably with the observations, the assumption must embody all the significant restraints imposed by the equations of motion.

The particular physical situation to be discussed is the fully turbulent flow in channels. This flow has been studied experimentally for many years. Hence it is an excellent testing ground for theoretical models. The model evolved here has its origin in conventional laminar stability theory. Therefore a brief restatement of the conclusions of this theory is of value.

The stability of a time-independent state of a fluid field can be established by study of the growth or decay of superimposed infinitesimal disturbances. If any disturbance releases a larger amount of potential energy from the pressure field than it dissipates through the action of viscosity, it will grow. The mathematical formulation of this kind of problem usually leads to a linear characteristic value equation. The external conditions which delimit the range of stability of the initial time-independent state of the fluid are determined by the minimum characteristic value. In simple shearing flow a disturbance can abstract energy from the pressure field only through the agency of viscous stress. Hence, in this case, viscosity plays the double role of permitting the growth of disturbances and also dissipating them.

When a disturbance achieves finite amplitude, its non-linear interaction with the initial motion alters both this motion and the disturbance.

First-order stability theory tells one nothing of this alteration, while inclusion of the non-linear interaction in the problem leads to such intractable mathematics that even second-order effects have seldom been investigated. However, the physics of the non-linear effects is fairly clear. The disturbance must grow until its alteration of the initial motion reduces the rate of release of potential energy to the rate of dissipation of this energy. If the disturbance is an aperiodic turbulent motion rather than another steady laminar motion, the equalization of rates of energy release and dissipation must still occur on the average. In either the laminar or turbulent case, alteration of the initial motion is accomplished by the transport of heat or momentum, whichever was responsible for the instability. Hence the most important aspects of the non-linear interaction of disturbance and initial motion are those advective terms which readjust the energy sources of the disturbance.

In the new 'stability' that is achieved, the finite-amplitude disturbance can be looked upon as the stabilizing sink of energy for the destabilizing energy source in the pressure field. It will be assumed that this is so on the average even in the fully developed steady-state turbulence, i.e. that the mean non-linear momentum transport terms in the equations of motion are entirely stabilizing, and that the only energy source for those disturbances which enter into the mean momentum transport is the pressure field of the mean motion.

In the first section, a limiting 'statistical stability' condition on the spatial structure of the mean momentum transport is found as a consequence of this assumption. The momentum transport is then resolved into a spatial spectrum whose smallest scale of motion is the scale of the smallest statistically unstable motion. The determination of the particular spectrum satisfying these stability constraints and the boundary conditions, and also releasing the largest amount of potential energy, leads to an unusual formal problem. In this problem the non-constant cofficients of a linear characteristic value equation are varied under constraints to determine a minimum least characteristic value, also the corresponding minimum least characteristic function and the optimum form of the non-constant coefficients.

The second section outlines a variational approach designed to find these optimal functions and constants; i.e. to find the momentum transport spectrum and mean velocity profile which lead to a marginally stable mean field of maximum dissipation rate. Considerable use is made of the knowledge acquired in the past thirty years about solutions of the laminar stability equation for shearing flow. A first approximation to the spectrum is found, and a comparison is made between this theoretical extreme and the observations.

The concluding section describes other more detailed tests of this work by comparison with recent channel flow data, e.g. the observation of a smallest scale of motion. An attempt to rationalize the basic assumption of the theory raises questions concerning the uniqueness of solutions to the equations of motion, while the apparent existence of extreme states in

turbulent fields suggests an explicit statistical mechanical origin. Finally, the application of this approach to quite different turbulent phenomena is outlined.

1. Formulation of a tractable problem

This is a study of the steady-state fully evolved three-dimensional turbulence observed between fixed parallel surfaces. Here 'fully evolved' will mean both that the Reynolds number (based on the channel half-width and the average velocity) is far above its value for marginal stability, and that there are no variations of moments of the fluctuating field in the downstream direction. In figure 1 the coordinate frame is chosen so that the x direction is the direction of the mean velocity U, which in turn is some unknown function of the cross-stream direction z. The 'mean' will be defined here as an average in the y direction (perpendicular to the plane of figure 1). It is assumed that the effect of the distant y boundaries on real flows does not influence the nature of the motion far from those boundaries. Hence the remainder of this work deals with parallel surfaces of infinite extent.

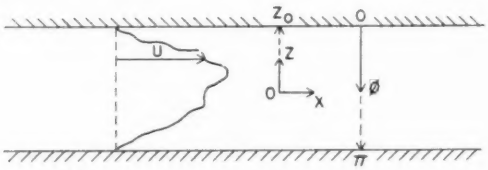

Figure 1. Coordinates chosen to describe flow between parallel surfaces.

It is also assumed in general that compressibility, heating effects and non-linear viscous effects are unimportant in the experimental situation. Therefore the equations of motion and continuity are

$$\frac{D\mathbf{v}}{Dt} = -\frac{1}{\rho}\nabla P + \nu\nabla^2\mathbf{v} \qquad \text{and} \qquad \nabla\cdot\mathbf{v} = 0, \tag{1.1}$$

where D/Dt is the substantial derivative, P the pressure, ρ the fixed density, ν the constant kinematic viscosity, and $\mathbf{v}$ the velocity vector.

A first concern will be the determination of statistical stability constraints imposed on the steady-state flow by these equations.

As implied by the name, statistical stability means the constancy in time of some space (or ensemble) average of the field of motion. Here an investigation will be made of the time dependence of the quantity

$$\bar{\mathbf{v}}(x,z,t) = \left[\frac{1}{2y_0}\int_{-y_0}^{+y_0}\mathbf{v}\,dy\right]_{y_0\to\infty} = \mathbf{v}-\mathbf{v}'. \tag{1.2}$$

Future use of the bar will indicate the mean with respect to y, as in (1.2). Expanding (1.1) with the aid of (1.2), one may write

$$\frac{\partial\bar{\mathbf{v}}}{\partial t}+\frac{\partial\mathbf{v}'}{\partial t}+\bar{\mathbf{v}}\cdot\nabla\bar{\mathbf{v}}+\bar{\mathbf{v}}\cdot\nabla\mathbf{v}'+\mathbf{v}'\cdot\nabla\bar{\mathbf{v}}+\mathbf{v}'\cdot\nabla\mathbf{v}' = -\frac{1}{\rho}\nabla P+\nu\nabla^2\bar{\mathbf{v}}+\nu\nabla^2\mathbf{v}',$$

and

$$\nabla\cdot\bar{\mathbf{v}}+\nabla\cdot\mathbf{v}' = 0. \tag{1.3}$$

The mean value of (1.3) is then

$$\frac{\partial \bar{\mathbf{v}}}{\partial t} + \bar{\mathbf{v}} \cdot \nabla \bar{\mathbf{v}} + \overline{\mathbf{v}' \cdot \nabla \mathbf{v}'} = -\frac{1}{\rho} \nabla_2 \bar{P} + \nu \nabla_2^2 \bar{\mathbf{v}}$$

and

$$\nabla_2 \cdot \bar{\mathbf{v}} = 0, \tag{1.4}$$

where ∇_2 indicates the two-dimensional (x, z) del operator. Subtracting (1.4) from (1.3), one obtains

$$\frac{\partial \mathbf{v}}{\partial t} + (\bar{\mathbf{v}} \cdot \nabla \mathbf{v}' + \mathbf{v}' \cdot \nabla \bar{\mathbf{v}}) + (\mathbf{v}' \cdot \nabla \mathbf{v}' - \overline{\mathbf{v}' \cdot \nabla \mathbf{v}'}) = -\frac{1}{\rho}(\nabla P - \nabla_2 \bar{P}) + \nu \nabla^2 \mathbf{v}',$$

and

$$\nabla \cdot \mathbf{v}' = 0. \tag{1.5}$$

Now if the mean flow is to be stable and independent of x, i.e. if $\bar{\mathbf{v}} = U(z)\mathbf{i}$, then if follows from (1.4) that

$$\left[-\nu \frac{\partial^2 U}{\partial z^2}\right]\mathbf{i} + \left[\frac{1}{\rho}\frac{\partial P}{\partial x}\right]\mathbf{i} + \left[\frac{1}{\rho}\frac{\partial P}{\partial z}\right]\mathbf{k} = -\left[\frac{\partial}{\partial z}\overline{w'u'}\right]\mathbf{i} - \left[\frac{\partial}{\partial z}\overline{w'^2}\right]\mathbf{k}, \tag{1.6}$$

where $\mathbf{i}$ and $\mathbf{k}$ are unit vectors in the x and z directions respectively, and u' and w' are the components of $\mathbf{v}'$ in the x and z directions respectively. Equation (1.6) is, of course, the usual equation for the mean flow. Integrating the $\mathbf{k}$ equation, one finds that $\bar{P}/\rho + \overline{w'^2} = \bar{P}_0/\rho$, where $\bar{P}_0$ is the pressure at either fixed surface; and since $\partial \overline{w'^2}/\partial x = 0$ (no variation of mean flow moments in the x direction), then $\partial \bar{P}/\partial x = \partial \bar{P}_0/\partial x$. Integrating the $\mathbf{i}$ equation, one finds that, since there must be no torque on the fluid as a whole,

$$-\left(\frac{1}{\rho}\frac{\partial \bar{P}_0}{\partial x}\right)z = \nu\beta + \overline{w'u'} = \tau = \tau_0 \frac{z}{z_0}, \tag{1.7}$$

where $\beta = -\partial U/\partial z$, and $\tau_0 = -\left(\frac{1}{\rho}\partial \bar{P}_0/\partial x\right)z_0$ is the stress per unit mass at the fixed surface. Equation (1.7) specifies the spatial relation of the mean gradient and the mean momentum transport. Thus it is basic to the following work.

However, the stability of any particular mean flow is not assured unless an arbitrary mean disturbance disappears in a finite time. If we take

$$\bar{\mathbf{v}} = U(z)\mathbf{i} + \epsilon \bar{\mathbf{v}}_1(x, z, t) + \epsilon^2 \bar{\mathbf{v}}_2(x, z, t) + \ldots,$$

and

$$\bar{P} = \bar{P}(x, z) + \epsilon \bar{P}_1(x, z, t) + \epsilon^2 \bar{P}_2(x, z, t) + \ldots, \tag{1.8}$$

where ϵ is a constant parameter, then $\bar{\mathbf{v}}_1$, $\bar{P}_1$, $\bar{\mathbf{v}}_2$,, $\bar{P}_2$, etc. must all decay in time for an arbitrary choice of ϵ. From (1.4), the zeroth-order terms in ϵ give (1.6). The first-order ϵ terms in (1.4) are

$$\frac{\partial \bar{\mathbf{v}}_1}{\partial t} + U\frac{\partial \bar{\mathbf{v}}_1}{\partial x} + \left(\bar{\mathbf{v}}_1 \cdot \mathbf{k}\frac{\partial U}{\partial z}\right)\mathbf{i} - \nu \nabla_2^2 \bar{\mathbf{v}}_1 + \frac{1}{\rho}\nabla_2 \bar{P}_1 = -[\Delta \overline{\mathbf{v}' \cdot \nabla \mathbf{v}'}]$$

and

$$\nabla_2 \cdot \bar{\mathbf{v}}_1 = 0, \tag{1.9}$$

where $[\Delta \overline{\mathbf{v}' \cdot \nabla \mathbf{v}'}]$ signifies any first-order change that occurs in the mean non-linear stress due to the complex interaction in (1.5) of $\bar{\mathbf{v}}_1$ and $\bar{P}_1$ with

the field of finite fluctuations. If arbitrary $\bar{\mathbf{v}}_1$ and $\bar{P}_1$ are to decay in time, equation (1.9) places restrictions on the form and amplitude of $U(z)$, and hence, through (1.7), on the form and amplitude of $\overline{w'u'}$.

At this point in the analysis, the mechanistic assumption that $\overline{\mathbf{v}' \cdot \nabla \mathbf{v}'}$ plays only a stabilizing role is introduced. The conditions placed on stable forms of $U(z)$ and $\overline{w'u'}$ will be at least as severe as the actual case if the assumed stabilizing effect of $[\Delta\overline{\mathbf{v}' \cdot \nabla \mathbf{v}'}]$ is neglected. Then, with $[\Delta\overline{\mathbf{v}' \cdot \nabla \mathbf{v}'}]$ set equal to zero, equation (1.9) assumes the familiar linear form of the equation for the disturbance of a time-independent shearing flow. Here, however, the problem is to find the entire class of U, for given boundary conditions, which lead to marginally stable $\bar{\mathbf{v}}$ and $\bar{P}$.

Taking the curl of (1.9) to remove the pressure term, and assuming that

$$\bar{\mathbf{v}}_1 \cdot \mathbf{k} = \Phi(z) \exp i(\alpha/z_0)[x - (cU_m)t], \tag{1.10}$$

one may write

$$\left(\frac{U}{U_m} - c\right)\left(\frac{\partial^2\Phi}{\partial(z/z_0)^2} - \alpha^2\Phi\right) - \frac{\partial^2(U/U_m)}{\partial(z/z_0)^2}\Phi = \frac{i}{\alpha R}\left(\frac{\partial^4\Phi}{\partial(z/z_0)^4} - 2\alpha\frac{\partial^2\Phi}{\partial(z/z_0)^2} + \alpha^4\Phi\right), \tag{1.11}$$

where α/z_0 is the downstream wave number of the disturbance of the mean, cU_m is its phase velocity, U_m is the z-averaged mean velocity, and $R = z_0U_m/\nu$ is the Reynolds number. Equation (1.11) is called the Orr–Sommerfeld equation (Orr 1906–7, Sommerfeld 1908), and has been studied for many years to determine initial instability criterion for a given laminar U. Its appearance in a problem of fully turbulent flow is due in part to the present special assumption and in part to the vanishing of explicit interaction terms between $\bar{\mathbf{v}}$ and $\mathbf{v}'$ in (1.4).

In his study of equation (1.11), Heisenberg (1924) has shown that for a given R some smallest scale of motion (largest α) is unstable. (This is also established in equation (2.41) of this paper.) In addition if $\overline{w'u'}$ is entirely stabilizing, it cannot produce motions requiring greater destabilizing force than that available in the mean flow. Hence a second consequence of the assumption is that the spectrum of $\overline{w'u'}$ cannot contain a scale of motion smaller than twice the scale of the smallest marginally stable motion according to (1.11). (We specify 'twice' since $\overline{w'u'}$ is a product of the fluctuation velocities.)

This restriction on the spectrum of $\overline{u'w'}$ is, through (1.7), a restriction on the possible spatial structure of U. Hence the class of possible U is doubly restricted by the marginal solutions of the stability equation (1.11). Within this class, for a given U_m, one function leads to the release of more potential energy per unit time than any other. This function can be thought of as the 'most stable' in the sense that any alteration of it will increase the potential energy available to disturbances. Ignorance of the detailed mechanisms of momentum transport permits one to hope that this extreme state is approached in the observed turbulence. Hence in the remainder of this section a tractable formal problem for the extreme is posed.

In the steady state, the rate of release of potential energy equals the rate at which mechanical work is done by the shearing stresses, and this equals the rate at which energy is dissipated into heat by the action of viscosity. Hence

$$(\beta\tau)_m = \nu\left[\overline{\left(\frac{\partial \mathbf{v}}{\partial x}\right)^2} + \overline{\left(\frac{\partial \mathbf{v}}{\partial y}\right)^2} + \overline{\left(\frac{\partial \mathbf{v}}{\partial z}\right)^2}\right]_m, \tag{1.12}$$

where $(\partial\mathbf{v}/\partial x)^2 = (\partial\mathbf{v}/\partial x).(\partial\mathbf{v}/\partial x)$, etc., the subscript m again indicates an average value in the z direction, and

$$(\beta\tau)_m = \tau_0(\beta z/z_0)_m = \tau_0\,\beta_0 \tag{1.13}$$

from (1.7). Also

$$\beta_0 = \frac{1}{2z_0}\int_{-z_0}^{+z_0}\beta\frac{z}{z_0}\,dz = -\frac{zU}{2z_0}\bigg|_{-z_0}^{+z_0} + \frac{1}{2z_0}\int_{-z_0}^{+z_0}\frac{U}{z_0}\,dz = \frac{U_m}{z_0}. \tag{1.14}$$

Hence the total rate of dissipation per unit mass, $\tau_0 U_m$, will be a maximum for a given U_m when τ_0 is a maximum. In a non-dimensional form, a maximum for $(z_0/\nu)(\tau_0/U_m)$ is sought for a given $(z_0/\nu)U_m = R$. However, it is convenient to invert this problem and seek the minimum Reynolds number associated with a marginally stable solution to (1.11), holding $(z_0/\nu)(\tau_0/U_m)$ constant. This latter quantity is proportional to the ratio of the actual dissipation rate and the dissipation rate which would result from a laminar parabolic flow with the same U_m. Indeed, it is readily shown that

$$(\tau_0)_{\text{laminar}} = 3\nu\beta_0. \tag{1.15}$$

Hence the ratio

$$\frac{\tau_0}{(\tau_0)_{\text{laminar}}} = \frac{1}{3}\left(\frac{z_0}{\nu}\right)\left(\frac{\tau_0}{U_m}\right) = \frac{\beta(z_0)}{3\beta_0} \tag{1.16}$$

will be held constant during the minimization of R. The other variables in (1.11) for which optimum values will be sought are α, c and the mean velocity U. There are, however, certain geometric and boundary constraints on U which first must be determined.

One notes that since $u = v = w = 0$ and $\partial w/\partial z = 0$ (from $\nabla . \mathbf{v} = 0$) at the boundary surfaces z_0 and $-z_0$, then

$$u'w' = \frac{\partial\overline{u'w'}}{\partial z} = \frac{\partial^2\overline{u'w'}}{\partial z^2} = 0,$$

at z_0 and $-z_0$. Hence, from (1.7), we have

$$\beta = \frac{1}{\nu}\left(\tau_0\frac{z}{z_0} - \overline{u'w'}\right) = -\frac{\partial U}{\partial z}; \quad \text{thus} \quad \beta(z_0) = \frac{\tau_0}{\nu}, \quad \beta(-z_0) = -\frac{\tau_0}{\nu};$$

$$\frac{\partial\beta}{\partial z} = \frac{\tau_0}{\nu z_0} - \frac{1}{\nu}\frac{\partial\overline{u'w'}}{\partial z} = -\frac{\partial^2 U}{\partial z^2}: \quad \text{thus} \quad \frac{\partial\beta}{\partial z}(z_0) = \frac{\partial\beta}{\partial z}(-z_0) = \frac{\tau_0}{\nu z_0};$$

$$\frac{\partial^2\beta}{\partial z^2} = -\frac{1}{\nu}\frac{\partial^2\overline{u'w'}}{\partial z^2} = -\frac{\partial^3 U}{\partial z^3}: \quad \text{thus} \quad \frac{\partial^2\beta}{\partial z^2}(z_0) = \frac{\partial^2\beta}{\partial z^2}(-z_0) = 0; \tag{1.17}$$

and also $U = 0$ at z_0 and $-z_0$.

Yet another constraint on U arises from certain general conclusions regarding the stability of solutions of (1.11). It has been found (Heisenberg

1924, Lin 1945–46) that a necessary, but not sufficient, requirement for stable solutions at large Reynolds numbers is that the curvature of the mean flow be always of the same sign. A type of instability called 'inflexional' can result if this is not the case. Hence one further requires of U that

$$-\frac{\partial^2 U}{\partial z^2} = \text{const.} \times d^2, \tag{1.18}$$

where d is a real quantity. It is convenient to define the dimensionless quantity

$$\mathcal{U} = \frac{U}{U_m}, \tag{1.19}$$

and choose the constant in (1.18) so that

$$\frac{\partial^2 \mathcal{U}}{d\phi^2} = -\frac{12}{\pi^2}\frac{\tau_0}{(\tau_0)_L} d^2 = -K d^2, \tag{1.20}$$

where $\phi = \frac{1}{2}\pi . (1 - z/z_0)$ (see figure 1). In terms of ϕ, the boundary conditions on d^2, for equations (1.17), may be expressed as follows:

$$\left.\begin{aligned}
&(a) \quad \left(\frac{\partial d^2}{\partial \phi}\right)_0 = \left(\frac{\partial d^2}{\partial \phi}\right)_\pi = 0; \\
&(b) \quad (d^2)_0 = (d^2)_\pi = 1; \\
&(c) \quad \frac{1}{\pi}\int_0^\pi d^2\, d\phi = 1; \\
&(d) \quad \frac{2}{\pi^2}\int_0^\pi \phi\, d^2\, d\phi = 1, \qquad \text{or} \qquad \int_{-z_0}^{+z_0} z\, d^2\, dz = 0.
\end{aligned}\right\} \tag{1.21}$$

The definitional constraint $\pi^{-1}\int_0^\pi \mathcal{U}\, d\phi = 1$ may be written

$$\frac{2}{\pi^3}\int_0^\pi \phi^2 d^2\, d\phi = 1 - \frac{4}{\pi^2 K}. \tag{1.22}$$

Now (*d*) of (1.21) is just the requirement that d^2 be symmetric; accordingly, equation (1.22) may be written

$$\frac{1}{K} = \int_0^{\frac{1}{2}\pi} \left(\phi - \frac{\phi^2}{\pi}\right) d^2\, d\phi. \tag{1.23}$$

From (1.7) we have

$$\frac{\overline{u'w'}}{\tau_0} = \frac{2}{\pi}\int_0^\phi (d^2 - 1)\, d\phi. \tag{1.24}$$

Hence the spatial spectrum of the momentum transport is determined by d^2. We have also

$$\mathcal{U} = K\left\{\tfrac{1}{2}\pi\phi - \phi\int_0^\phi d^2\, d\phi + \int_0^\phi \phi d^2\, d\phi\right\}. \tag{1.25}$$

The final constraint on U is due to the requirement that the field of transporting motions, $\overline{u'w'}$, has some smallest scale, eventually to be determined by the stability equation. This constraint is introduced by

the requirement that d has some smallest scale n_0, that is

$$d = \sum_{n=0}^{n_0} Y_n \psi_n(\phi), \tag{1.26}$$

where $\psi_n(\phi)$ is some real orthogonal set of functions satisfying the appropriate boundary and symmetry conditions, and the Y_n are arbitrary real amplitudes.

The formal linear problem may now be stated: First, for any U satisfying $-(\partial^2 U/\partial z^2) \geqslant 0$, find from the Orr–Sommerfeld equation (1.11) the smallest scale of motion and the relation between R, α and c for marginal stability. Second, expressing U in terms of the d from (1.18) and taking some convenient set ψ_n, vary Y_n, subject to the constraints (1.21) and (1.23), to find the minimum R for constant K. This analysis is undertaken in the next section.

2. A variational solution to the stability problem

The stability equation (1.11) has been studied since 1908. A recent interesting inquiry (Lin 1945–46) contains, as a partial list, seventy references. A first purpose in all these papers was to establish the Reynolds number for the initial instability of laminar flow. Only an outline of this theory will be given here.

For a given velocity profile U, the Orr–Sommerfeld equation determines a relation $c = c(\alpha, R)$ for each solution Φ. For R and α real, and c complex, this single relation can be separated into a real and imaginary part. For marginal stability the imaginary part of c is zero and this determines $R = R(\alpha)$, the curve of marginal stability. For each point on this curve the real part of the relation $c = c(\alpha, R)$ determines the corresponding value of c. No complete solution has yet been found. However, asymptotic solutions of equation (1.11) for large values of αR have proved adequate in the study of initial laminar instability (and should be much better for the turbulence problem since αR is orders of magnitude larger). Recent quantitative work rests on the relations*:

$$\left(\Phi_3 \Big/ \frac{\partial \Phi_3}{\partial \phi}\right)_{\phi=0} = \phi_c F(\eta), \tag{2.1}$$

where Φ_3 is the highly oscillatory part of the asymptotic Φ, and ϕ_c is that value of ϕ at which $U = c$;

$$\eta = [(1+\lambda)(1-\gamma)^{1/3}] \cdot (\tfrac{1}{4}\pi^2 K)^{-2/3} c(\alpha R)^{1/3}, \tag{2.2}$$

where

$$\gamma = \frac{2}{\pi}\int_0^{\phi_c} d^2\, d\phi, \qquad \frac{\lambda}{1+\lambda} = \frac{1}{\phi_c}\int_0^{\phi_c}\left(\frac{2}{\pi}\int_0^{\phi} d^2\, ds\right) d\phi; \tag{2.3}$$

and

$$F(\eta) = \frac{\displaystyle\int_{+\infty}^{-\eta} d\xi' \int_{+\infty}^{\xi'} \xi^{1/2} d\xi H_{1/3}^{(1)}[\tfrac{2}{3}(i\xi)^{3/2}]}{\displaystyle -\eta \int_{+\infty}^{-\eta} \xi^{1/2} d\xi H_{1/3}^{(1)}[\tfrac{2}{3}(i\xi)^{3/2}]} \equiv 1 - \frac{1}{J(\eta)}.$$

* Lin's equations (6.28), (6.29), and (12.32) correspond to (2.1), (2.2), and (2.4) in the notation used here.

The function $F(\eta)$ was first numerically calculated by Tietjens. Lin has improved and extended this calculation, of which relevant results appear in table 1 below.

η	2·6	2·8	3·0	3·2	3·4	3·6	3·8
$F_i(\eta)$	0·07203	0·12220	0·17391	0·22520	0·27193	0·30705	0·32130
$J_i(\eta)$	0·31558	0·46043	0·54872	0·58082	0·56401	0·51074	0·43560
$F_r(\eta)$	0·52773	0·49952	0·46456	0·41947	0·36110	0·28802	0·20352

Table 1

A first relation imposed by the boundary conditions on the several parts of the asymptotic Φ is written

$$J_i(\eta) = -\tfrac{1}{2}\pi^2 K(1-2\lambda)\left[\frac{\partial^2 U/\partial\phi^2}{(\partial U/\partial\phi)^3}\right]_{\phi=\phi_c} = 2\phi_c d_c^2[(1+\lambda)(1-\gamma)]^{-3} = v(c), \quad (2.4)$$

where the primary contribution to $v(c)$ is due to the pole of equation (1.11) at $U = c$, and where λ, as will be justified *a posteriori*, is assumed to be very small. The value of ϕ_c is determined from (2.4) at the first interception of $v(c)$ and $J_i(\eta)$. Equations (2.1), (2.2) and (2.4) can then be used to determine αR as a function of c; hence they determine $(\alpha R)_{\min}$ and the corresponding c. An important characteristic of the $R(\alpha)$ curve, used since Heisenberg first developed this approach, is that the value of R at $(\alpha R)_{\min}$ is very close to the minimum value of R. This property of $R(\alpha)$ will also be used here to find $R_{\min}$. The real task of recent work has been the evaluation of α from the complicated second relation imposed by the boundary conditions on the asymptotic Φ. This will be avoided here through the use of an integral condition for stability discussed later in this section.

Turning now to the turbulence problem, one notes that the scale of motion in Φ is determined by the imaginary part of the derivative of Φ. The largest value of this derivative will occur in the sharp shear zone at the boundary. Hence

$$n_0 = \left|\left(\frac{1}{\Phi_3}\frac{\partial\Phi_3}{\partial\phi}\right)_i\right|_{\phi=0}. \quad (2.5)$$

Then, from (2.1), one may write

$$\xi_c = \frac{1}{F_i(\eta)}. \quad (2.6)$$

where $\xi_c = n_0\phi$. Equation (2.4) is now written

$$(d^2/n_0)_c = \tfrac{1}{2}[(1+\lambda)(1-\gamma)]^3 J_i(\eta)F_i(\eta). \quad (2.7)$$

To determine $(\alpha R)_{\min}$, Heisenberg first observed that for $\partial(\alpha R)/\partial c = 0$, one has from (2.2) and (2.4)

$$\eta J_i'(\eta) = cv'(c), \quad (2.8)$$

and

$$(\alpha R)_{\min} = (\tfrac{1}{4}\pi^2 K)^2\left(\frac{\eta_0}{c}\right)^3 1/(1+\lambda)^3(1-\gamma), \quad (2.9)$$

where η_0 is that η which satisfies (2.8), and where the small spatial variation of $(1+\lambda)^3(1-\gamma)$ has been neglected. Hence, if the Y_n in the expansion of d^2, equation (1.26), are constrained to satisfy (2.7) and (2.8), the resulting profile will be both marginally stable and continuously at $(\alpha R)_{\min}$, no matter what further variations of Y_n are made.

Now a convenient orthonormal set $\psi_n(\phi)$ which automatically satisfies (*a*) and (*d*) of (1.21) is

$$\psi_n(\phi) = \sqrt{2}\cos 2n\phi, \qquad \psi_0(\phi) = 1, \tag{2.10}$$

where n is any integer. Hence, to satisfy (*b*) and (*c*) of (1.21), we must have

$$\sum_{n=0}^{\frac{1}{2}n_0} Y_n^2 = 1, \tag{2.11}$$

and

$$\left(\sum_{n=0}^{\frac{1}{2}n_0} Y_n\right)^2 = \tfrac{1}{2}. \tag{2.12}$$

Equation (1.23) may be written

$$\frac{1}{K} = \sum_{n=0}^{\frac{1}{2}n_0}\sum_{m=0}^{\frac{1}{2}n_0} B_{nm}\, Y_n\, Y_m, \tag{2.13}$$

where

$$B_{nm} = \int_0^{\pi/2}\left(\phi - \frac{\phi^2}{\pi}\right)[\cos 2(n+m)\phi + \cos 2(n-m)\phi]\, d\phi.$$

Also from (1.24) and (2.10) the momentum transport spectrum is

$$\frac{\overline{u'w'}}{\tau_0} = \sum_{n=1}^{n_0} T_n \sin 2n\phi,$$

where

$$T_n = \frac{1}{2n}\sum_{x=-\frac{1}{2}n_0}^{\frac{1}{2}n_0} Y_{|x|}\, Y_{|n-x|}. \tag{2.14}$$

It is now possible to write down a complete set of equations optimizing Y_n for a minimum $(\alpha R)_{\min}$. However, not only is this a most complicated problem, but its solution will be as approximate as the stability criteria. Thus, to establish the more significant physical consequences of the extreme state, the spectrum Y_n will be approximated to roughly the same extent that Φ is in equation (2.1). This approximation of the optimum Y_n will be done in two ways: First, only the consequences of Y_n at large n_0 will be considered, so that in expansions in powers of $1/n_0$ only the first term will be kept. Second, rather than optimize each Y_n separately, optimization will be made between sets of Y_n which satisfy the conditions (2.7), (2.8), (2.10) and (2.11).

Although other trial functions may converge more rapidly to the optimum dissipation rate, a simple power series has many mathematical advantages. Hence Y_n is expanded as

$$Y_n = \frac{A}{\sqrt{n_0}}\left[1 + \frac{C_1}{(n_0/2)}\, n + \frac{C_2}{(n_0/2)^2}\, n^2 + \frac{C_3}{(n_0/2)^3}\, n^3 + \ldots\right]. \tag{2.15}$$

To have even one free parameter for a variational optimization, Y_n must

have five free parameters. Therefore Y_n in (2.15) will be terminated at the n^3 term, leaving A, n_0, C_1, C_2 and C_3 to be determined. From (2.15) and (1.26) one finds that

$$d = \frac{A}{(2n_0)^{1/2}}\Bigg[\Bigg\{1 + \frac{\sin(n_0+1)\phi}{\sin\phi}\Bigg\} + \frac{C_1}{(n_0/2)}\Bigg\{\left(\frac{n_0}{2}+1\right)\frac{\sin(n_0+1)\phi}{\sin\phi} - \\ - \frac{1}{2}\frac{(1-\cos(n_0+1)\phi)}{\sin^2\phi}\Bigg\} + \frac{C_2}{(n_0/2)^2}\Bigg\{\left(\frac{n_0}{2}+1\right)^2\frac{\sin(n_0+1)\phi}{\sin\phi} + \\ + \frac{(n_0+3)}{2}\frac{\cos(n_0+2)\phi}{\sin^2\phi} - \frac{1}{2}\frac{\sin(n_0+3)\phi}{\sin^3\phi}\Bigg\} + \\ + \frac{C_3}{(n_0/2)^3}\Bigg\{\left(\frac{n_0}{2}+1\right)^3\frac{\sin(n_0+1)\phi}{\sin\phi} + \frac{3}{2}\left(\frac{n_0+1}{2}\right)^2\frac{\cos(n_0+1)\phi\cos\phi}{\sin^2\phi} - \\ - \frac{3}{4}\left(\frac{n_0+1}{2}\right)\frac{\sin(n_0+1)\phi(1+\cos^2\phi)}{\sin^3\phi} + \frac{1}{4}\frac{(1+2\cos^2\phi)}{\sin^4\phi} - \\ - \frac{1}{8}\frac{\cos(n_0+1)\phi\cos\phi(5+\cos^2\phi)}{\sin^4\phi}\Bigg\}\Bigg], \tag{2.16}$$

where the various sums, $\sum_{n=0}^{\frac{1}{2}n_0} n\cos 2n\phi$, etc., have been performed by the calculus of finite differences. In keeping with the requirement of large n_0, it is convenient to divide d^2 into a function describing its complicated transition region near the boundary and a function which is important away from the boundary. These are

$$(d^2/n_0)_{\phi \sim 1/n_0} = \frac{A^2}{2}\left[1 + C_0\frac{\sin(n_0+1)\phi}{\sin\phi}\right]^2, \tag{2.17}$$

and

$$(d^2/n_0)_{\phi\sim 1/n_0} = \frac{A^2}{2\xi^2}\Bigg[C_0\sin\xi + C_1\Bigg\{-\frac{(1-\cos\xi)}{\xi}\Bigg\} + C_2\Bigg\{2\frac{\cos\xi}{\xi} - \frac{2\sin\xi}{\xi^2}\Bigg\} + \\ + C_3\Bigg\{3\frac{\cos\xi}{\xi} - 6\frac{\sin\xi}{\xi^2} + 6\frac{(1-\cos\xi)}{\xi^3}\Bigg\}\Bigg] = \frac{A^2}{2\xi^2}L^2(\xi), \tag{2.18}$$

where $C_0 = 1 + C_1 + C_2 + C_3$, and $\xi = n_0\phi$. Hence equation (2.7) becomes

$$AL(\xi_c) = [(1+\lambda)(1-\gamma)]^{3/2}[J_i(\eta_0)/F_i(\eta_0)]^{1/2}. \tag{2.19}$$

Moreover, if one neglects the variations of $[(1+\lambda)(1-\gamma)]^{3/2}$ with ξ_c, equation (2.8) becomes

$$\frac{L'(\xi_c)}{L(\xi_c)} = \tfrac{1}{2}F_i(\eta_0)\left[1 + \frac{\eta_0 J_i'(\eta_0)}{J_i(\eta_0)}\right]. \tag{2.20}$$

Equation (2.12) can be summed to give

$$2 = -C_1 - \tfrac{2}{3}C_2 - \tfrac{1}{2}C_3 \tag{2.21}$$

to the zeroth order in $1/n_0$, while (2.11) is summed as

$$2 = A^2\{1 + C_1 + \tfrac{1}{3}(2C_2 + C_1^2) + \tfrac{1}{2}(C_1C_2 + C_3) + \\ + \tfrac{1}{5}(2C_1C_3 + C_2^2) + \tfrac{1}{3}C_2C_3 + \tfrac{1}{7}C_3^2\}. \tag{2.22}$$

Then equations (2.6), (2.19), (2.20), (2.21) and (2.22) are five relations between six independent variables A, C_1, C_2, C_3, η_0 and ξ_c. A choice for ξ_c, say, determines the other five. Actually, λ and γ are small quadratic functions of these independent variables, from equation (2.3). However, to a zeroth approximation they may be assumed to be zero, their values then computed for each ξ_c and these values used for a first approximation of A, C_1, C_2, C_3 at each ξ_c.

Before resolving these algebraic relations the remainder of the problem will be discussed. From (2.9) we have

$$(\alpha R)_{\min} = \tfrac{1}{2}\pi K^2\left(\frac{n_0}{K}\frac{\eta_0}{\xi_c}\right)^3\frac{1}{(1-\gamma)}\,; \tag{2.23}$$

i.e. $C(1+\lambda) = \frac{1}{2}\pi K/\xi_c$. Hence the dependence of n_0/K on

$$\xi_c = \xi_c(A, C_1, C_2, C_3, \eta_0)$$

must be found in order to determine that ξ_c (say $\underline{\xi_c}$) which makes $(\alpha R)_{\min}$ a minimum. Following this, to determine the relation between n_0 and R, α must be determined. Now α, the down-stream wave number, bears some (probably fixed) relation to $\frac{1}{2}\pi n_0$, the cross-stream wave number, say

$$\tfrac{1}{2}\pi n_0 = r\alpha. \tag{2.24}$$

(If $r = 1$, the smallest 'eddy' would be circular; if $r = 10$ the smallest 'eddy' would be a 10 to 1 ellipse with major axis parallel to the boundary.) Then from (2.6) and (2.23) it follows that

$$R_{\min} = \frac{r}{(1-\gamma)}\left(\frac{\eta_0}{\underline{\xi_c}}\right)^3\left(\frac{n_0}{K}\right)n_0. \tag{2.25}$$

Hence a determination of the ratio r establishes the relation $R = R(n_0)$.

To interpret the various formulae in conventional experimental terms, it is convenient to define a 'boundary Reynolds number':

$$R_{\mathrm{B}} = \frac{sU_s}{\nu}\,, \tag{2.26}$$

where s is a distance proportional to z_0/n_0, say $s = z_0/n_0$, and U_s is the velocity that would be due to the initial gradient at that distance from the boundary. So defined, equation (2.26) may be written as

$$R_{\mathrm{B}} = \frac{\pi^2}{4}\frac{RK}{n_0^2}\,, \quad \text{or} \quad n_0 = \frac{z_0}{\nu}\frac{1}{\sqrt{R_{\mathrm{B}}}}\,U_\tau, \quad \text{or} \quad \frac{n_0}{K} = \frac{\pi^2}{4}\frac{1}{\sqrt{R_{\mathrm{B}}}}\frac{U_m}{U_\tau}, \tag{2.27}$$

where $U_\tau = \sqrt{\tau_0}$ is the conventional 'friction velocity', in terms of which most data have been described. From (2.27) and (2.25) we have

$$R_{\mathrm{B}} = \frac{\pi^2}{4}\frac{r}{(1-\gamma)}\left(\frac{\eta_0}{\underline{\xi_c}}\right)^3. \tag{2.28}$$

Finally, to find n_0/K and the velocity profile as functions of

$$\xi_c = \xi_c(A, C_1, C_2, C_3),$$

equations (1.23) and (1.26) may be integrated using (2.17) and (2.18). From

(1.26), (2.17), and (2.18), it follows that

$$\frac{n_0}{K} = \int_0^{\frac{1}{2}\pi} \left(\phi - \frac{\phi^2}{\pi}\right) d^2 n_0 \, d\phi \doteq \int_0^{\frac{1}{2}\pi - \epsilon} \left(\frac{\pi}{4} - \frac{\theta^2}{\pi}\right) (d^2 n_0)_{\phi >> 1/n_0} d\theta + \\ + \int_0^{n_0 \epsilon} \left(\xi - \frac{\xi^2}{n_0 \pi}\right) \left(\frac{d^2}{n_0}\right)_{\phi \sim 1/n_0} d\xi, \tag{2.29}$$

where $\theta = \frac{1}{2}\pi - \phi$, and $1/n_0 \ll \epsilon \ll 1$. For large n_0,

$$n_0/K = \tfrac{1}{2} A^2 [\tfrac{1}{2} C_0^2 (\ln \Gamma n_0 + 1) + \pi^2/12 + C], \tag{2.30}$$

where $\Gamma = 1{\cdot}78^+$ is Euler's constant, and

$$C = \frac{(2 \ln 2 + 1)}{2} (1 - C_0^2) + (2 \ln 2 - 1) \frac{C_2}{15} (2C_0 - 3 + \tfrac{1}{6} C_2) \tag{2.31}$$

after some condensation with the help of (2.21). From (1.25) and (2.18), the velocity field near the boundary may be determined in terms of sine and cosine integrals:

$$\frac{n_0}{K} \mathit{U} = \tfrac{1}{2}\pi\xi - \xi \int_0^{\xi} \left(\frac{d^2}{n_0}\right)_{\phi \sim 1/n_0} ds + \int_0^{\xi} s \left(\frac{d^2}{n_0}\right)_{\phi \sim 1/n_0} ds.$$

After rising linearly, as $\frac{1}{2}\pi\xi$, from the boundary, $n_0 \mathit{U}/K$ turns sharply through a 'transition' region to its asymptotic value

$$n_0 \mathit{U}/K = \tfrac{1}{2} A^2 [\tfrac{1}{2} C_0^2 (\ln 2\Gamma\xi + 1) + \pi^2/12 + C]. \tag{2.32}$$

From (1.23) and (2.17), direct integration gives

$$\frac{n_0}{K} (\mathit{U}_{\max} - \mathit{U}) = \tfrac{1}{2} A^2 [\tfrac{1}{2}\theta^2 - \tfrac{1}{2} C_0^2 \ln \cos\theta]. \tag{2.33}$$

Now combining (2.30), (2.32) and (2.33) with (2.27), one may write a theoretical form for the gross features of channel flow beyond the 'transition' region:

$$\frac{U}{U_\tau} = \sqrt{R_B} \left(\frac{AC_0}{\pi}\right)^2 \left[\ln \frac{(z_0 - z) U_\tau}{\nu} + \left\{\left(1 + \ln \frac{\pi\Gamma}{\sqrt{R_B}}\right) + \right.\right. \\ \left.\left. + \frac{2}{C_0^2} \left(\frac{\pi^2}{12} + C\right)\right\}\right], \tag{2.34}$$

$$\frac{U_{\max} - U}{U_\tau} = \sqrt{R_B} \left(\frac{AC_0}{\pi}\right)^2 \left[\ln \frac{1}{\cos\theta} + \frac{\theta^2}{C_0^2}\right]; \tag{2.35}$$

$$\frac{U_m}{U_\tau} = \sqrt{R_B} \left(\frac{AC_0}{\pi}\right)^2 \left[\ln \frac{z_0 U_\tau}{\nu} + \left\{\left(1 + \ln \frac{\Gamma}{\sqrt{R_B}}\right) + \right.\right. \\ \left.\left. + \frac{2}{C_0^2} \left(\frac{\pi^2}{12} + C\right)\right\}\right]. \tag{2.36}$$

Those readers familiar with the experimental literature will have recognized a 'velocity defect law' in equation (2.35) and a 'logarithmic boundary law' in (2.34). The usual empirical constants in these experimental laws depend here on the determination of $\xi_c = \xi_c(A, C_1, C_2, C_3, \eta_0)$ and the ratio r.

Returning to the algebraic problem of finding $\xi_c = \xi_c(A, C_1, C_2, C_3, \eta_0)$ from (2.6), (2.19), (2.20), (2.21) and (2.22), one notes that, for a particular

ξ_c, η_0 is determined from (2.6) and table 1. Resolving the other four equations, it is found that

$$C_1 = -2-\left(\frac{2}{3}+\frac{e_3}{2}\right)C_2+\tfrac{1}{2}Q; \qquad C_2 = QG_1-G_2; \qquad C_3 = Q+e_3\,C_2, \tag{2.37}$$

where

$$Q = \frac{e_1}{A}+e_2 = -\frac{q_2}{q_1}\pm\left[\left(\frac{q_2}{q_1}\right)^2-\frac{q_3}{q_1}\right]^{1/2},$$

$$q_1 = -e_5\,G_1-e_4\,G_1^2-\frac{11}{420}+\frac{2}{e_1^2},$$

$$q_2 = \tfrac{1}{2}\{e_5\,G_2+e_6\,G_1\}+e_4\,G_1\,G_2+\frac{1}{15}-\frac{2e_2}{e_1^2},$$

$$q_3 = -e_6\,G_2-e_4\,G_2^2-\frac{1}{3}+\frac{2e_2^2}{e_1^2};$$

also

$$G_1 = \frac{e_1'-1}{e_3-e_3'}, \qquad G_2 = \frac{e_1e_2-e_2'}{e_3-e_3'},$$

$$e_1 = \frac{[(1+\lambda)(1-\gamma)]^{3/2}[J_i(\eta_0)/2F_i(\eta_0)]^{1/2}}{(d_3-\frac{1}{2}d_1)},$$

$$e_2 = \frac{(2d_1-d_0)}{(d_3-\frac{1}{2}d_1)}, \qquad e_3 = \frac{(\frac{2}{3}d_1-d_2)}{(d_3-\frac{1}{2}d_1)},$$

$$e_4 = \left(\frac{2}{135}+\frac{7}{180}e_3+\frac{11}{420}e_3^2\right), \qquad e_5 = \left(\frac{7}{180}+\frac{11}{210}e_3\right),$$

$$e_6 = \left(\frac{1}{9}+\frac{2}{15}e_3\right), \qquad e_1' = \frac{\frac{1}{2}F_i(\eta)[1+\eta_0.J'(\eta_0)](d_3-\frac{1}{2}d_1)}{J(\eta_0)(d_3'-\frac{1}{2}d_1')}$$

$$e_2' = \frac{(2d_1'-d_0')}{(d_3'-\frac{1}{2}d_1')}, \qquad e_3' = \frac{(\frac{2}{3}d_1'-d_2')}{(d'-\frac{1}{2}d_1')};$$

and

$$L(\xi_c) = (d_0+C_1\,d_1+C_2\,d_2+C_3\,d_3), \qquad L'(\xi_c) = (d_0'+C_1\,d_1'+C_2\,d_2'+C_3\,d_3').$$

For each chosen ξ_c, the quantity $(n_0/K)(\eta_0/\xi_c)$ of equation (2.23) may be found from these relations and (2.30). However, the restriction that the first interception of $J_i(\eta)$ and $v(c)$, equation (2.4), determines ξ_c sets an upper limit on the ξ_c that may be chosen. Table 2 lists the computed values for $(n_0/K)(\eta_0/\xi_0)$, the corresponding values of γ and λ, and the maximum value of

$$I = AL(\xi)\xi^{1/2}\{[1+\lambda(\xi)].[1-\gamma(\xi)]\}^{3/2}/[J_i(\eta_0)]^{1/2}, \qquad \xi < \xi_c,$$

at several ξ_c on either side of this upper limit. When $I = 1$, $J_i(\eta)$ marginally

ξ_c	$\left(\frac{n_0}{K}\cdot\frac{\eta_0}{\xi_c}\right)_{n_0=10^5}$	$\left(\frac{n_0}{K}\cdot\frac{\eta_0}{\xi_c}\right)_{n_0=10^6}$	γ	λ	$I(\xi)$	ξ
6·00	14·87	30·14	0·095	0·045	0·846	$0{\cdot}93\pi$
$350^\circ = 6{\cdot}1086$	14·40	28·78	0·121	0·065	1·042	$0{\cdot}97\pi$
2π	13·84	27·80	0·183	0·114	1·375	$1{\cdot}05\pi$

Table 2

intercepts $v(c)$ at the smaller ξ. Hence, from a graph of table 2, the minimum value of $(n_0/K)(\eta_0/\xi_c)$ occurs at $\xi_c = \underline{\xi_c} = 6{\cdot}081$. Substitution of this ξ_c into the relations (2.37) gives

$$C_2 = 25{\cdot}67, \qquad Q = -1{\cdot}630, \qquad A^2 = 11{\cdot}43;$$

and

$$\frac{\eta_0}{\underline{\xi_c}} = 0{\cdot}4875, \qquad C_0^2 = 2{\cdot}308, \qquad C + \frac{\pi^2}{12} = -1{\cdot}908, \tag{2.38}$$

for

$$\gamma = 0{\cdot}114, \qquad \lambda = 0{\cdot}059.$$

The ratio r can be determined from the second relation imposed by the boundary conditions on the asymptotic Φ. (Equation (2.4) was the first relation.) However, this is a difficult task involving sums of series of integrals of functions of the optimum velocity profile. Instead, an integral condition for stability due to Synge (1938) will be used. Synge observed that multiplying the Orr–Sommerfeld equation (1.11) by $\Phi^* d\phi$, integrating from 0 to π and adding the resulting equation to its own complex conjugate leads to

$$I_2^2 + 2\alpha^2 I_1^2 + \alpha^4 I_0^2 = -\alpha R \mathscr{U}'(0) I_3 - \alpha R c_i (I_1^2 + \alpha^2 I_0^2), \tag{2.39}$$

where $I_0^2 = \int_0^\pi \Phi\Phi^* d\phi, \qquad I_1^2 = \int_0^\pi \Phi'\Phi^{*\prime} d\phi, \qquad I_2^2 = \int_0^\pi \Phi''\Phi^{*\prime\prime} d\phi,$

$$I_3 = \tfrac{1}{2} i \int_0^\pi (\mathscr{U}'/\mathscr{U}'(0))(\Phi'\Phi^* - \Phi\Phi^{*\prime})\, d\phi,$$

and the prime denotes differentiation with respect to ϕ. When Φ is stable, we have $c_i \leqslant 0$; hence

$$1/I_0^2 \int_0^\pi \left[1 + \frac{\mathscr{U}'(0)}{\alpha^3} R \left\{ \frac{i}{2} \frac{\mathscr{U}'}{\mathscr{U}'(0)} \left(\frac{\Phi'}{\Phi} - \frac{\Phi^{*\prime}}{\Phi^*} \right) + \right.\right.$$

$$\left.\left. + \frac{2}{\alpha^2} \left(\frac{\Phi'\Phi^{*\prime}}{\Phi\Phi^*} \right) \right] \Phi\Phi^*\, d\phi + \left(\frac{I_2}{\alpha^2 I_0} \right)^2 \geqslant 0. \tag{2.40}$$

A sufficient condition for stability is that the integral in (2.40) be greater than zero. If then $\Phi'/\Phi = A + iB$, this integral is positive definite when

$$[\mathscr{U}'(0)R]^2 = 8\alpha^4 M, \qquad M = \frac{\int_0^\pi (A^2 + B^2)\Phi\Phi^* d\phi \int_0^\pi \Phi\Phi^* d\phi}{\left[\int_0^\pi (\mathscr{U}'/\mathscr{U}'(0)) B \Phi\Phi^* d\phi \right]^2}. \tag{2.41}$$

Synge noted that, since $\int B^2 \Phi\Phi^* d\phi \int \Phi\Phi^* d\phi \geqslant \left[\int B\Phi\Phi^* d\phi \right]^2$, M in (2.41) must be greater than one. Hence, $[\mathscr{U}'(0)R]^2 = 8\alpha^4$ sets a lower limit on α for stable Φ. However, a closer condition can be set by using the asymptotic Φ to estimate M. Now at the boundary, $\phi = 0$, $A(0) \geqslant F_r(\eta_0)$ and $B(0) = F_i(\eta_0)$. From (2.38) and table 1, $F_r(\eta_0) = 0{\cdot}465$ and

$$F_i(\eta_0) = 0{\cdot}174.$$

Also from table 1 one sees that $F_r(\eta_0)/F_i(\eta_0)$ increases for smaller η (i.e. larger ϕ) through the range where $\mathscr{U}'/\mathscr{U}'(0)$ is large. Hence, in a conservative estimate, we have

$$\int_0^\pi (A^2 + B^2)\Phi\Phi^* d\phi \geqslant \left\{ 1 + \left[\frac{A(0)}{B(0)} \right]^2 \right\} \int_0^\pi B^2 \Phi\Phi^* d\phi,$$

and

$$M \geqslant \left[1 + \left(\frac{0{\cdot}465}{0{\cdot}174} \right)^2_{\delta} \right] \doteqdot 8.$$

Since the value of M will enter final formulae only as $M^{1/12}$, this represents

only a slight improvement on Synge's condition. An extension of the preceding analysis shows that $I_2/\alpha^2 I_0$ and $I_1/\alpha I_0$ approach zero for large α and larger R; hence using (2.41), we have

$$C_i \to -\left[\frac{\alpha}{R}\left(1-\frac{2}{\alpha^2}\right)^2\right] \to 0.$$

Equation (2.41) then becomes as accurate an estimate of the marginally stable α as one could hope to attain by the tedious method mentioned earlier.

Finally, equating the R in (2.41) and (2.23), one obtains

$$r=(1-\gamma)^{1/3}\left(\frac{\xi_c}{\eta_0}\right)(8M)^{1/6}=3{\cdot}94 \tag{2.42}$$

for $M = 8$, $\eta_0/\xi_c = 0{\cdot}4875$ and $\gamma = 0{\cdot}114$ from (2.38). Inserting the numerical results of (2.38) and (2.42) into (2.28) and the constants of (2.34) and (2.35), one obtains

$$R_B=\frac{\pi^2}{4}\frac{r}{(1-\gamma)}\left(\frac{\eta_0}{\xi_c}\right)^3=1{\cdot}271, \tag{2.43}$$

$$\sqrt{R_B}\left(\frac{AC_0}{\pi}\right)^2=3{\cdot}014; \qquad \text{e.v.}=3{\cdot}0\pm0{\cdot}1, \tag{2.44}$$

$$\left(1+\ln\frac{\pi\Gamma}{\sqrt{R_B}}\right)+\frac{2}{C_0^2}\left(\frac{\pi^2}{12}+C\right)=+1{\cdot}001; \qquad \text{e.v.}=1{\cdot}8\pm0{\cdot}1, \tag{2.45}$$

where e.v. means the experimental values recently determined by Laufer (1950).

The constant of equation (2.44) (inversely proportional to von Kármán's constant) is the most important in these results since it enters into every other relation. The 'logarithmic intercept' constant, equation (2.45), involves the relatively sensitive quantity C (equation (2.31)), perhaps accounting for the error in this determination. An observation of r will be discussed in the conclusion. The dissipation rate is inversely proportional to the square of U_m/U_τ, equation (2.36); hence it is larger than observed due to the error in C. However, at large R the percentage error due to C is small, and the dissipation rate approaches the observed curve.

It should be emphasized that an extension of the technique outlined here involves considerable computational labour. In addition, further variational freedom for the Y_n spectrum may necessitate the use of $R_{\min}$ rather than the approximate $(\alpha R)_{\min}$.

To summarize this section: All known gross qualitative features of turbulent flow in smooth channels result from an optimization of the dissipation rate subject to the mean stability constraints; a decisive quantitative comparison with the observations is not achieved primarily due to the mathematical difficulties encountered in finding a general solution to the Orr–Sommerfeld equation.

3. Conclusion

From a mathematical viewpoint the foregoing analysis is most laborious. The asymptotic solution to the Orr–Sommerfeld equation for a quite general U is described. Only then is U restricted to an optimal form.

However, the stability problem might be considerably simplified if the major restrictions on U imposed by the optimization could be made first. Some slight progress has been made along this line by performing constrained variations of U in the integral stability equations (2.39). This approach offers hope of a more complete understanding of the problem than the maze of formulae employed here permits.

On the physical side this work strongly supports the basic mechanistic assumption. Its validity can be tested by measuring the smallest scales of motion in the transport and energy spectra. Laufer (1950) has made time-spectra studies in channel flow from the boundaries to channel centre. The smallest scale of motion he detected in the energy spectrum was in the middle of the 'laminar' boundary region, and was twice as large as the observed thickness of this region. Since the energy spectrum has twice the maximum wave number of the velocity spectrum, this observation establishes that the minimum ellipticity of the smallest scale of motion is approximately four to one. Equation (2.42) gives a theoretical optimum value of 3·94. A more successful investigation of the detailed stability restrictions on the spectral transfer of energy may one day remove the assumption entirely.

Before leaving the topic of spectra, it should be noted that the spatial spectrum for the transport given by (2.14) differs in kind from the temporal spectra obtained by the experimentalist. In homogeneous turbulence, spatial and temporal spectra would be identical; but in this inhomogeneous and non-isotropic shear flow, the observed spectra are functions of position. The work presented here does not determine the temporal spectra and their spatial dependence, but does provide a framework for such an inquiry.

The apparent achievement of a statistical extreme state by the turbulent fluid raises questions of a different sort than those raised by the mechanistic assumption. It suggests that one observes the most probable of a large set of possible motions: that turbulent solutions to the equations of motion may be highly degenerate. If this is so, what determines the observed spatial and spectral structure of statistical observables, such as $\overline{\mathbf{v}'^2}$, not studied here? One might think that degeneracy implied the equal *a priori* probability of each solution, but the infinite series of higher order small corrections to the usual equations of motion remove degeneracies and couple the macroscopic field of motion to the underlying microscopic particle motion. Hence it is proposed that the probability of occurrence of a degenerate solution is directly proportional to its degree of disorganization, or entropy. The search for a useful measure of the disorganization of irreversible fluid processes involves sufficiently different formal techniques to necessitate separate discussion. However, even the usual thermostatic statistical mechanics suggests that a steady-state system with a fixed number of particles would have maximum 'entropy' when it has a maximum 'temperature' and when all the dynamic variables have, as nearly as possible, normal Gaussian distributions about their mean values. In steady-state shear flow, the mean temperature is a maximum relative to the boundary

temperature for a maximum rate of dissipation of potential energy into heat. Yet to achieve this first extreme the mean momentum transport must be highly organized, as studied in this paper. Hence a completely random distribution of either macroscopic or microscopic dynamic variables is not possible. A study of possible secondary extremes for partially constrained macroscopic observables of turbulent shear flow will be presented in another paper.

Finally, it is of interest that the techniques used here are of value in the study of other forms of turbulence. Many of the laminar stability equations developed for geophysical and astrophysical problems can serve as the foundation for determining the gross statistical features of their corresponding turbulent fields. Certain of these stability problems are much easier than the Orr–Sommerfeld problem. In particular this is true of turbulence due to thermal convection. With heat flux replacing momentum transport, mean temperature profile replacing the mean velocity profile, and Rayleigh's equation replacing the Orr–Sommerfeld equation, turbulent convection may be treated just as shear flow was here. Two earlier papers (Malkus 1954) report the initial results of such a study.

The author wishes to thank Dr G. E. R. Deacon, Director of the National Institute of Oceanography, Surrey, and Professor P. A. Sheppard of the Department of Meteorology, Imperial College, London, for their kindness to him during the year in England in which this work was undertaken. He is particularly indebted to Professor C. C. Lin of the Massachusetts Institute of Technology and to Dr G. K. Batchelor of Trinity College, Cambridge, for their comments on the stability problem. This work was performed under the auspices of the Office of Naval Research, and is contribution No. 804 from the Woods Hole Oceanographic Institution.

References

Batchelor, G. K. 1953 *The Theory of Homogeneous Turbulence*. Cambridge University Press.

Goldstein, S. (Ed.). 1938 *Modern Developments in Fluid Dynamics*, Vol. 2. Oxford University Press.

Heisenberg, W. 1924 *Ann. Phys.* **74,** 577–627.

Laufer, J. 1950 *Nat. Adv. Comm. Aero., Wash.*, no. 2123.

Lin, C. C. 1945–46 *Quart. Appl. Math.* **3,** 117–142, 218–234 & 277–301.

Malkus, W. V. R. 1954 *Proc. Roy. Soc.* A, **225,** 185–195 & 196–212.

Orr, W. M. F. 1906–7 *Proc. Roy. Irish Acad.* **27,** 9–26, 69–138.

Sommerfeld, A. 1908 *Proc. 4th Internat. Cong. Math., Rome*, 116–124.

Synge, J. L. 1938 *Semicent. Publ. Amer. Math. Soc.* **2,** 227–269.

On the motion of small spheroidal particles in a viscous liquid

By P. G. SAFFMAN
Trinity College, Cambridge

(*Received* 22 *May* 1956)

SUMMARY

Small spheroidal particles suspended in a sheared viscous liquid are sometimes observed to take up slowly preferred orientations, relative to the motion of the undisturbed liquid, which are independent of the initial conditions of release. These observations cannot be accounted for by the solution, obtained by Jeffery (1922), of the linearized Navier–Stokes equations. It is shown in this paper that the effect of the inertia of the liquid is to alter slowly the orbit of the particle in accordance with Jeffery's hypothesis that the particle ultimately moves in such a way that the dissipation of energy is a minimum, but that this effect is orders of magnitude too small to account for any of the experimental observations.

It is suggested that non-Newtonian properties of the liquid account for the observations. It is shown that the rate of orientation of a particle would then be independent of its size, and this prediction is verified experimentally. Other experimental evidence in support of this suggestion is also described.

Some remarks are also made about the possible effect of collisions between the particles when more than one particle is present.

1. INTRODUCTION

The slow motion of a small ellipsoidal particle in a uniformly sheared viscous fluid was examined by Jeffery (1922). The usual approximation was made that the acceleration (commonly called inertia) terms $\rho(\partial \mathbf{u}/\partial t + \mathbf{u}.\nabla \mathbf{u})$ in the hydrodynamical equations of motion may be neglected when the Reynolds number is sufficiently small. The approximate equations of motion

$$\mu \nabla^2 \mathbf{u} - \nabla p = 0, \qquad \operatorname{div} \mathbf{u} = 0, \tag{1}$$

were then solved with the boundary condition that $\mathbf{u} = \boldsymbol{\Omega} \wedge \mathbf{r}$ at the surface of the ellipsoid. Here, $\mathbf{u}$, p, μ and ρ denote respectively the velocity, pressure, viscosity and density of the liquid, $\boldsymbol{\Omega}$ is the angular velocity of the ellipsoid (to be found) and the origin of $\mathbf{r}$ is the centre of the ellipsoid. The angular velocity was determined by the condition that the total force and

couple on the body should vanish; this condition is valid since, as can be shown, the inertia of the body may be neglected to the same order in the Reynolds number as the approximation involved in (1).

The equations that determine the motion or orbit of the ellipsoid can be integrated when the ellipsoid is one of revolution. Let θ be the angle between the axis of symmetry of the spheroid and the direction of the vortex lines of the undisturbed shear, and let ϕ be the angle between the plane that contains the axis of symmetry and the direction of the vortex lines and a fixed plane containing the latter direction, that is, ϕ is the azimuthal angle of the axis of symmetry about the direction of the vortex lines. Then the orbit of the spheroid is given by the equations

$$\left.\begin{aligned}(a^2+b^2)\dot{\theta} &= \kappa(a^2-b^2)\sin\theta\cos\theta\sin\phi\cos\phi,\\ (a^2+b^2)\dot{\phi} &= \kappa(a^2\cos^2\phi+b^2\sin^2\phi),\end{aligned}\right\} \tag{2}$$

which have the solution

$$\left.\begin{aligned}\tan\phi &= \frac{a}{b}\tan\frac{\kappa abt}{a^2+b^2},\\ \tan\theta &= \frac{ab}{k(a^2\cos^2\phi+b^2\sin^2\phi)^{1/2}},\end{aligned}\right\} \tag{3}$$

where $2a$ is the length of the axis of symmetry, $2b$ is the length of the other principal axes, κ is the magnitude of the undisturbed shear, and k, the orbital parameter, is an arbitrary constant of integration that depends upon the initial conditions of release.

These equations show that the motion is periodic with the axis of symmetry describing a (non-circular) cone about the direction of the vortex lines, so that the motion is kinematically similar to that of a top. It also follows that the value of k, which specifies the particular orbit, is determined by the initial conditions, and there is no tendency for the spheroid to set itself so that its axes point in a particular direction or to choose a particular orbit, that is, there are no preferred orientations relative to the motion of the surrounding fluid that the spheroid will eventually take up irrespective of the initial conditions.

Jeffery did not consider the existence of this indeterminateness to be entirely satisfactory and expressed the opinion that a more complete investigation would reveal the existence of preferred orbits. In effect, the suggestion made was that over a short period of time the orbit is given accurately by equations (2) and (3), but that effects neglected in the analysis have a cumulative effect and slowly alter the orbit, so that eventually the particle is moving in a preferred orbit which is independent of the initial conditions. Jeffery suggested further that these preferred orbits would correspond to those solutions of the approximate equations of motion (1) for which the rate at which energy is dissipated by viscosity is a minimum. It was then shown that, according to this hypothesis, prolate spheroidal particles would tend to set themselves with the axis of symmetry parallel to the vortex lines

and would rotate about this axis with constant angular velocity, so that the whole motion is steady; and oblate spheroidal particles would tend to set themselves with an equatorial axis parallel to the vortex lines and would rotate about this axis with a variable angular velocity, so that the whole motion is periodic but not steady.

Several experiments have been performed in order to test the accuracy of equations (2) and (3) and to investigate whether preferred orbits do indeed exist. The results of these experiments, which will be described briefly in § 2, are not uniform. In some cases, preferred orbits do not appear to exist; in other cases, they do exist but are orbits of either minimum or *maximum* energy dissipation.

This question of preferred orbits is not without practical interest; for example, it is closely related to the viscosity of suspensions of non-spherical particles. It is the purpose of this paper to discuss some of the effects neglected by Jeffery in order to see whether there are any theoretical reasons why particles should take up preferred orbits in accordance with Jeffrey's hypothesis, and to suggest a possible explanation of the experimental results.

In § 3 we shall discuss the problem generally and show that many effects, such as those due to the inertia of the particle or the presence of rigid walls, need not be considered; and that the two most likely effects are the inertia of the liquid, which gives rise to the acceleration terms in the equations of motion, and non-Newtonian properties of the liquid. The rate at which the orbit of the particle is altered by the inertia of the liquid was calculated and the results are given in § 4. These results provide theoretical support for Jeffery's hypothesis, but are unable to account for any of the experimental observations since the predicted rates of orientation are orders of magnitude too small. It is suggested in § 5 that non-Newtonian properties of the liquid are responsible for the observed phenomena, and experimental evidence in support of this suggestion is described.

When more than one particle is present, as is the case for a suspension, there is a further effect to be considered, namely that of collisions and interactions between the particles (see Manley, Arlov & Mason 1955). In § 6, we shall give the results (mainly negative) of calculating the mechanics of the interaction between two particles whose separation is always large compared with their size, and discuss briefly the significance of these results and some intuitive ideas about the problem.

2. Relevant experimental results

Experiments using prolate and oblate spheroids were carried out by Taylor (1923). Binder (1939), Trevelyan & Mason (1951), and Manley & Mason (1956) describe experiments in which cylindrical rods of large aspect ratio were used (the aspect ratio is the ratio of the length to the diameter). In all these experiments, the particles were suspended in liquids contained between rotating concentric cylinders. This motion differs from the uniform shear of infinite extent envisaged by Jeffrey in the

existence of Coriolis forces, wall and end effects, and the fact that the shear in the neighbourhood of the particle is only approximately uniform. However, these effects can easily be shown to be negligible to the order considered by Jeffery, although their possible influence on the existence of preferred orbits has to be kept in mind (see §§ 3 and 4 below).

Taylor used aluminium spheroids in water-glass. He observed that, as far as he could tell, the spheroids moved as predicted by equations (2) and (3), and that, after about 20 minutes for the prolate spheroids and five minutes for the oblate ones (these figures correspond roughly to 180 complete revolutions for the prolate spheroids and 40 for the oblate ones), the spheroids took up orbits in accordance with Jeffery's hypothesis. In these experiments, $\kappa \doteqdot 1{\cdot}65\,\mathrm{sec}^{-1}$, $\epsilon \doteqdot 0{\cdot}5$ when $a \doteqdot 0{\cdot}13$ cm, and $\epsilon \doteqdot -0{\cdot}75$ when $a \doteqdot 0{\cdot}05$ cm. Here ϵ denotes the ratio $(a-b)/a$, sometimes called the 'ellipticity' of the spheroid. The viscosity of water-glass is very roughly 1,000 gm/cm sec.

Binder used particles of human hair suspended in glycerine. The orbits of the particles are described as being in qualitative agreement with equations (2) and (3), although there must be some discrepancy since these equations describe the motion of spheroids and not cylindrical rods. When the aspect ratio of the rods was less than 15, the rods orientated themselves along the vortex lines, in accordance with Jeffery's hypothesis, but when the aspect ratio was greater than 15, the rods set themselves perpendicular to the vortex lines in an orbit of maximum energy dissipation.

Trevelyan & Mason and Manley & Mason used cylindrical rods of glass, dacron, nylon and human hair in corn syrup. They verified equations (2) and (3) to a reasonable degree of accuracy considering that rods and not spheroids were used, but their observations of the existence of preferred orbits for a single particle are inconclusive. They sometimes observed a slow tendency for a particle to align itself along the vortex lines or to take up an orbit in which it was perpendicular to the vortex lines, but in other cases the orbit varied erratically with time. The manner in which the orbit varied appeared to be random and independent of the particle size, the aspect ratio, and the magnitude of the undisturbed shear.

Manley & Mason carried out also experiments with suspensions of particles of large aspect ratio. Suspensions in which the particles were initially distributed isotropically were sheared, and a statistical tendency was found for those orbits with large values of k to be favoured, that is, there was a tendency for particles to orientate themselves along the vortex lines.

3. The non-linearity of the problem

We shall now consider whether a theoretical treatment which uses the approximate equations (1) can explain these experimental observations or predict the existence of preferred orbits. In other words, when the perturbations due to the effect of rigid walls in the experimental apparatus, or the possibility that the shear is only approximately uniform, or any similar

alterations in the idealized external conditions envisaged by Jeffery, are taken into account using the approximate equations (1), does the orbit of the particle remain constant in time or alter slowly until a preferred orbit is reached?

Now equations (1) are linear and hence all pressures and stresses are proportional to the magnitude of the undisturbed shear and are therefore linear in κ. It follows that the equations determining the orbit are linear in κ, i.e. $\dot{\theta}$ and $\dot{\phi}$ are given by the products of κ and functions of θ and ϕ. The extra effects can be regarded as giving rise to perturbations of the orbit given by (3), and any variations of the orbit with time are then best represented by changes in the mean value of the orbital parameter k, where k can vary between 0 and ∞, being zero when the axis of symmetry is perpendicular to, and infinite when parallel with, the vortex lines, and the mean is taken over a complete revolution of the particle. On putting θ, as given by (3), in the expressions obtained for $\dot{\theta}$ and $\dot{\phi}$ when the extra effects are taken into account, and averaging over a complete revolution, we then obtain

$$\frac{1}{k}\frac{dk}{dt} = \kappa f(k), \tag{4}$$

where $f(k)$ depends on the shape but not the size of the particle and (as in all subsequent equations of this kind) k is to be understood as representing the average value over a complete revolution. Hence, if the shear is reversed, by, for example, the cylinders being rotated in opposite directions, then dk/dt will change sign; and if a preferred orbit exists in one case, a different preferred orbit will arise when the shear is reversed.

It follows immediately that, if the motion is such that the physical situation is unaltered by a reversal of the shear, then $f(k)$ must be zero and the particle rotates in a constant orbit. In other words, the use of equations (1) will predict that the orbit remains fixed unless there is a certain degree of asymmetry in the external conditions. (Another way of seeing this result is to note that, according to equations (1), the motion is reversible.) This result was indeed verified directly for the case of a spheroid near a rigid plane wall. The wall effect was calculated by a method due to Lorentz (1907), and the necessary modifications to (2) and (3) were found. It was found, as expected, that the mean value of k over one revolution remains constant.

Further, this argument also shows that the inertia of the particle may be neglected since the equations for the orbit, with the inertia of the particle taken into account, are linear in κ.

It is clear now that the question of preferred orbits is to some extent dependent on the design of the experimental apparatus. However, the Couette flow between rotating cylinders that was used in the experiments described in the previous section and with which we are primarily concerned possesses the necessary symmetry for the above result to be valid. Further, it is to be expected that flows for which the symmetry condition is not valid will be the exception rather than the rule; and even in these cases, the result

may still hold since the linearity of equations (1) and the consequent superposability of solutions enables the motion to be split into two parts, one of which is reversible and the other not, and the part that is not reversible may not produce a couple on the particle. For example, if account is taken of the relative velocity of particle and liquid owing to their different densities, this relative velocity does not change sign when the shear is reversed but the couple it produces on the particle is zero.

We must therefore look for non-linear terms that are neglected in (1). The first such terms that come to mind are the acceleration (inertia) terms and in the next section we shall examine their effect. We shall see, however, that the experimental phenomena cannot be explained in this way and some other non-linear effect must be sought. Non-Newtonian properties of the liquid give rise to non-linear effects and these will be discussed in § 5 together with some relevant experimental results.

There is, of course, the possibility that external effects of a random nature influence the orbits of the particles. It is difficult to understand the experiments with single particles by Manley & Mason (1956) in any other way. Indeed, they say that slow convection currents were present and regard these as the explanation of the randomness of their observations, and the opinion is expressed that the orbit would remain constant in the absence of such random effects. However, experiments that are capable of being repeated, such as those of Taylor or those described in § 5, cannot be explained in this way.

4. The inertia of the liquid

The full equations of motion of an incompressible liquid are

$$\rho \frac{D\mathbf{u}}{Dt} = -\nabla p + \mu \nabla^2 \mathbf{u}, \qquad \operatorname{div} \mathbf{u} = 0. \tag{5}$$

To calculate the effect of the acceleration terms by obtaining the complete solution of (5) is, in general, a problem of great difficulty, but we can by simple dimensional considerations obtain the order of magnitude of their effect. For $\rho(D\mathbf{u}/Dt)/\mu\nabla^2\mathbf{u}$ is of order R, where R denotes the Reynolds number $\kappa a^2/\nu$ ($\nu \equiv \mu/\rho$), and on making the plausible assumption that the extra stresses introduced when the acceleration terms are taken into account are smaller by a factor of order R than the stresses calculated neglecting these terms, we obtain for the rate of change of the orbit due to the inertia of the liquid

$$\frac{1}{k}\frac{dk}{dt} = \frac{a^2\kappa^2\epsilon}{\nu} g\left(\frac{k}{a}\right), \tag{6}$$

where $g(k/a)$ depends on the shape of the particle, and the factor $\epsilon\,(=(a-b)/a)$ has been introduced to emphasize the fact that dk/dt vanishes from considerations of symmetry when the particle is a sphere.

Now the sign of $g(k/a)$ is of interest in connection with Jeffery's hypothesis, and it is also not without value to have an estimate of its numerical magnitude. It was therefore decided to calculate this function by taking

account of the acceleration terms in (5) by means of an iterative procedure. That is, denoting the solution of (5) with $\rho D\mathbf{u}/Dt$ neglected by $\mathbf{u}^{(1)}$ and $p^{(1)}$, where $\mathbf{u}^{(1)} = \boldsymbol{\Omega} \wedge \mathbf{r}$ at the surface of the spheroid and $\mathbf{u}^{(1)}$ tends to the undisturbed velocity as $r \to \infty$ (this solution is, of course, the one found by Jeffery), we consider the equations

$$\mu \nabla^2 \mathbf{u} - \nabla p = \rho \frac{D\mathbf{u}^{(1)}}{Dt}, \qquad \operatorname{div} \mathbf{u} = 0, \tag{5'}$$

and try to find a solution which satisfies the boundary conditions $\mathbf{u} = \boldsymbol{\Omega} \wedge \mathbf{r}$ on the spheroid and $\mathbf{u} - \mathbf{u}^{(1)} \to 0$ as $r \to \infty$.

A most serious difficulty now arises since it can be shown that no solution of (5′) can be constructed which satisfies the boundary condition at infinity: this is sometimes known as Whitehead's paradox and was first encountered by Whitehead (1893) when considering the uniform translation of a sphere. However, there are reasons for believing that this difficulty can be overcome in the following way: there is evidence that if a suitable boundary condition at infinity is chosen for $\mathbf{u}$, then the solution of (5′) that satisfies this boundary condition will represent accurately in the neighbourhood of the particle the second approximation to the solution of (5). This boundary condition at infinity is deduced from the solution of the Oseen-type equations for the problem, but in the present problem these equations are difficult and have so far not yet been solved. However, by analogy with simpler cases, it appears that the requisite boundary condition is $|\mathbf{u} - \mathbf{u}^{(1)} - \lambda R \mathbf{u}^{(1)}| = o(r)$ as $r \to \infty$, where λ is a numerical constant (possibly zero) of order one. Equations (5′) can then be solved, the second approximation to the couple on the particle can be calculated in terms of Ω, κ and λ, and the orbit of the particle can be determined. It is clear that the effect of λ is equivalent to a small change in the magnitude of the undisturbed shear and so, to the order considered, λ will not enter the expression for dk/dt and its actual value is not needed for the purpose of this paper. It must be emphasized, however, that this boundary condition may well be wrong and this doubt is to be kept in mind whilst interpreting the results obtained below.*

Result of the calculation

Although it seems possible, in principle, to carry out the iteration for a spheroid of arbitrary shape, the analysis that appears to be required is such that no practical method could be found. The analysis was therefore confined to the comparatively simple case of a nearly spherical spheroid, so that powers of ϵ higher than the first could be neglected. The solution was then obtained by expanding the velocity and pressure in series of solid harmonics multiplied by powers of r. Since the algebra is tedious and

* I am deeply indebted to Dr I. Proudman for information and advice concerning the validity of iterated solutions of the Navier–Stokes equations and about the boundary condition to be satisfied at infinity. It is regretted that a description of the reasons for suggesting the above boundary condition would be quite lengthy and out of place in the present context.

involved, it would serve no useful purpose to reproduce it here and only the final result will be given.

It was found that when the acceleration terms are taken account of in the above manner,

$$\frac{1}{k}\frac{dk}{dt} \doteqdot 0{\cdot}24\frac{a^2\kappa^2\epsilon}{\nu}. \tag{7}$$

This result is equivalent to $g(k/a)$ having the value $0{\cdot}24 + O(\epsilon)$.

For a prolate spheroid, $\epsilon > 0$ and so $dk/dt > 0$, i.e. the long axis tends to set itself in the direction of the vortex lines; for an oblate spheroid, $\epsilon < 0$ and so $dk/dt > 0$, i.e. the short axis tends to set itself perpendicular to the vortex lines. Thus, the effect of the inertia of the liquid is in accordance with Jeffery's hypothesis and provides theoretical support for this hypothesis.

Comparison with experiment

Let us now compare the observed rates of orientation with those predicted by equations (6) or (7). The relevant experiments are those of Taylor (1923) (these experiments were repeated by myself and similar results obtained). It is true that ϵ is not sufficiently small for (7) to be accurate, and that Coriolis forces of the same order of magnitude as the acceleration terms should be taken into account, but (7) should give the order of magnitude of the effect of the inertia of the liquid without serious error. (The ratio of Coriolis to acceleration terms is Ω'/κ or $(\Omega'/\kappa)^2$, according as to which is the larger, where Ω' is the angular velocity of the particle around the axis of the cylinders; this ratio is either of order one or zero in the experiments described in this paper.) On putting the data given by Taylor into equation (7), or using equation (6) with the plausible assumption that $g(k/a)$ is of order one, we find that $(1/k)(dk/dt)$ is at most $10^{-5}\,\mathrm{sec}^{-1}$. Now a change in the orbit should be observable when k changes by a factor e, and the time for this to happen is not less than 10^5 seconds $\doteqdot$ 28 hours! Since the observed times were not greater than 20 minutes, there can be little doubt that the effects of the inertia of the fluid are too small to produce the observed phenomena.

When the aspect ratio of the particles is large, equation (7) is likely to be in serious error, and a direct comparison with the experimental observations on cylindrical rods cannot be made. However, a general examination of the equations for the case of large aspect ratio shows that $(1/k)(dk/dt)$ is then probably proportional to $b^2\kappa^2(\log a/b)^2/\nu$. If this be so, it is easily shown that the times needed for a change of orbit to be clearly observable are orders of magnitude larger than those observed by Binder (1939), and are also long compared with the duration of the other experiments on cylindrical rods quoted previously.

The motion of small particles in a tube

Of further interest is another phenomenon predicted by Jeffery. It can easily be shown that small particles suspended in the liquid flowing

through a capillary tube will, according to equation (1), remain at a fixed distance from the axis of the tube; however, it is a consequence of Jeffery's hypothesis of minimum energy dissipation that they should move slowly towards the axis since the shear there is least, so the extra energy dissipation owing to the presence of the particles is then reduced. (This phenomenon appears to be quite well known, and is observed, for example, by physiologists studying the motion of blood corpuscles in the capillaries of the body. I am not aware, however, of any accurate quantitative measurements that have been published.)

The effect of the inertia of the fluid on the motion of a small sphere of radius a in a flow with a parabolic velocity profile $u = \alpha z + \beta z^2$ was worked out by iteration as before and it was found that the inertia terms give rise to a sideways velocity w, perpendicular to the directions of the flow and the vortex lines, given by

$$w \doteqdot -0{\cdot}43\,\frac{\alpha\beta a^4}{\nu}. \tag{8}$$

This velocity moves the sphere to a region where the magnitude of the shear is least, and so the effect of the inertia of the fluid is again in accordance with Jeffery's hypothesis. Dr M. J. Taylor has, however, communicated to me some rough experimental data of his own, from which it appears that the velocities predicted by (8) are too small by a factor of order 10.

To sum up, if the inertia of the liquid is the dominant non-linear effect, then there is theoretical support for Jeffery's hypothesis. It appears, however, that in the experiments described in this paper, the inertia terms are too small to account for the observations, and we shall now go on to discuss the possible effects of non-Newtonian properties of the liquid.

5. Non-Newtonian properties of the liquid

It is assumed in the derivation of the Navier–Stokes equations (5) that the stress tensor p_{ij} is linearly related to the rate-of-strain tensor

$$e_{ij} = \left(\frac{\partial u_i}{\partial x_j} + \frac{\partial u_j}{\partial x_i}\right)$$

by the equation

$$p_{ij} = -p\delta_{ij} + \mu e_{ij}. \tag{9}$$

A liquid for which (9) does not hold is said to be non-Newtonian, and this definition obviously covers a wide range of liquids with various properties. However, we are concerned here with incompressible liquids which are almost Newtonian, that is, liquids in which anomalous effects caused by deviations from equation (9) are small. For such liquids, we may take the stress-strain relation as

$$p_{ij} = -p\delta_{ij} + \mu e_{ij} + \sigma Q_{ij}, \tag{10}$$

in which μ is constant and σQ_{ij}, where σ is a constant with the dimensions of viscosity divided by time which is some measure of the non-Newtonian properties of the liquid, is a quadratic functional of the rate-of-strain tensor which may involve both the values of e_{ij} at earlier times and higher spatial

derivatives of e_{ij}. It is also supposed that the motion is sufficiently slow for powers of e_{ij} higher than the second to be neglected.

The nature of the quadratic term in (10) is by no means clear. If it be supposed that the liquid is isotropic when at rest, that the stress depends only on the instantaneous rate-of-strain, and that the stress-strain relation is analytic, then it can be shown that σQ_{ij} may be taken as $\mu' e_{ik} e_{kj} + \mu'' e_{kl}^2 \delta_{ij}$, where μ' and μ'' are constants (for a full review of the subject, see Truesdell (1952)). But in the present problem, where the motion is not steady, this form of the quadratic term may well not be valid. Apart from some evidence that μ' is positive if this form of the quadratic term is valid, there appears to be no non-Newtonian liquid for which the form or magnitude of the quadratic term has been established.

The equations of motion of the liquid are $\partial p_{ij}/\partial x_j = 0$, since the inertia of the liquid may be neglected. Because the non-Newtonian terms are supposed to be small, a solution of these equations could be attempted by iteration, provided that a suitable form for Q_{ij} were postulated. (It is to be noted that the difficulty at infinity which arose when the acceleration terms were taken into account by iteration would not arise here.) It can be seen that, after solving the equations of motion and equating the couple on the particle to zero, we should finally obtain

$$\frac{1}{k}\frac{dk}{dt} = \frac{\kappa^2 \sigma}{\mu} h(k/a), \tag{11}$$

where $h(k/a)$ depends on the shape of the particle and on the form of Q_{ij}. The right-hand side of (11) might be identically zero, but there is no *a priori* reason why this should be so and it seems most unlikely that this should be the case.

The rate of orientation of the particle is known when $h(k/a)$ is known but no attempt was made to determine $h(k/a)$ because the form of Q_{ij} is not known beyond reasonable doubt. Even if σQ_{ij} were known or postulated with a reasonable degree of certainty, there appears to be no practical way of solving the equations for a spheroid of arbitrary shape, and to carry out the analysis for a nearly spherical spheroid would require very heavy algebra and would probably not be of much use since σQ_{ij} would probably contain sufficient unknown constants for agreement with experiment to be reached without difficulty. However, it follows from (11) that the rate of orientation of a particle of given shape in a given liquid is independent of its size; whereas the rate of orientation due to the inertia of the liquid is, for a given shape, proportional to the surface area of the particle. The following simple experiment was therefore carried out in order to see whether the rate of orientation is independent of the size; it was verified roughly that this is indeed the case.

Experimental procedure

The apparatus consisted of two concentric cylinders: the diameter of the outer one was 8·4 cm and that of the inner one was 2·8 cm. Prolate and

oblate spheroids, similar in shape but of different sizes were made on a lathe from aluminium wire. The longest and shortest axes of the smallest prolate spheroid were 0·25 cm and 0·10 cm respectively, and of the smallest oblate spheroid 0·17 cm and 0·10 cm. The other spheroids were twice and three times as large. The outer cylinder rotated one revolution in 4·3 seconds and the inner one was kept at rest. The particles were placed midway between the cylinders so that κ was about 0·82 $\sec^{-1}$. Two liquids were used: a highly viscous form of ammonium polymethyl acrilate, and water-glass. The densities of these liquids were measured in the usual way and the viscosities by timing the rate of fall of a small lead sphere of known size. The density of the ammonium polymethyl acrilate was close to that of water, that of the water-glass was about 1·5 times that of water; the kinematic viscosities were, as it happened, approximately the same, being about 1000 $\mathrm{cm}^2\,\sec^{-1}$.

A common property of a non-Newtonian liquid is that, when confined between rotating cylinders, it will climb up the inner cylinder, provided the upper surface is free (see, for example, Weissenberg 1947). It was noticed that the ammonium polymethyl acrilate climbed up the inner cylinder by as much as one centimetre, whilst the water-glass did not climb up at all. This indicated that the non-Newtonian properties of the water glass were small compared with those of the other liquid.

The experimental results for the ammonium polymethyl acrilate were as follows. The prolate spheroids were placed with their long axis horizontal, and after about five minutes the long axis was vertical. The oblate spheroids were placed with their short axis vertical, and after about six minutes the short axis was horizontal. As far as I could tell from these crude observations, the rate of orientation was independent of the size of the particles. When water-glass was used, it was found that the orbits of the spheroids remained constant over times up to an hour.

These results are consistent with the suggestion that the explanation of the observed phenomena lies in non-Newtonian properties of the liquid. There is an apparent discrepancy, however, between these results for water-glass and the observations of Taylor (1923). But Sir Geoffrey Taylor has informed me that, in his experiment, the water-glass rose some distance up the inner cylinder, and this was also the case when I repeated Taylor's experiment with a different supply of water-glass and at probably a higher temperature than the experiments described above. Bearing in mind that water-glass is by no means a standard product, and that non-Newtonian properties are often critically dependent upon temperature (although the temperature dependence here is in the opposite direction from what would be intuitively expected), this apparent discrepancy appears to yield further evidence in favour of the above suggestion. Further, Dr S. G. Mason has informed me that the corn syrup used in the experiments in which he participated (where no preferred orbits were observed with single particles) was found to be Newtonian over a wide range of velocity gradients.

There thus seems to be strong evidence that the existence of preferred orbits is related to the effect of non-Newtonian viscosity and that some of

the experimental observations of spheroidal particles suspended in the Couette flow between concentric cylinders will be explained when the action and effect of non-Newtonian properties can be calculated.

Further, σ is a measure of the elastic properties of the liquid, since it is easily shown that the quadratic term in (10) does no work when the liquid is deformed and returned to its original state, so that σ/μ is a measure of the relative magnitudes of the elastic and viscous properties of the liquid.* (σ/μ is probably proportional to μ/γ, where γ is the elastic modulus of rigidity of the liquid.) To account for the experiments described above, σ/μ for ammonium polymethyl acrilate would have to be of order $10^{-3}\,\mathrm{sec}^{-1}$.

An experiment to investigate the possible relationship between the elastic properties of a variety of non-Newtonian liquids and the rate at which preferred orbits are reached would be of great interest in this connection, as would also be an accurate experiment to check that the rate of orientation is proportional to the square of the undisturbed shear.

6. Suspensions of many particles

When considering a suspension of many particles, we are primarily interested in the proportion of particles whose orbital parameters lie in a given range, since this is needed for a calculation of the bulk properties of the suspension and is also the quantity that is actually measured. That is, we wish to determine the values of the function $p(k)$ where $p(k)\,dk$ denotes the proportion of particles with orbital parameters in the range $(k,\ k+dk)$. If we were to follow a definite particle, we would find that its orbit is continually being altered in apparently discontinuous jumps by collisions with other particles (see Manley & Mason 1956) and that there might also be a slow change due to the effects described in the previous sections. In this section, however, we shall not discuss these latter effects but confine ourselves to a discussion of the effect of collisions. (It is worth mentioning, in passing, that a suspension of non-spherical particles is anisotropic and this implies that the bulk properties of the suspension may be to some extent non-Newtonian. This in turn may effect the external motion—for example, a suspension contained between rotating cylinders may climb up the inner cylinder, even though the pure liquid does not—and so affect the motion of an individual particle and give rise to preferred orbits. This effect will not be discussed here.)

It does not necessarily follow, of course, that $p(k)$ is altered by collisions, for example, it may be that the effect of a collision is to interchange the orbital parameters of the particles that collide; however, there is no *a priori* evidence that this is the case and it seems most likely that the effect of collisions is to alter the orbits until a statistically steady state is reached. It might at first be thought that, if the interactions were calculated using equations (1), the linearity of the equations and the consequent reversibility of the motion would imply that $p(k)$ is not altered by collisions, since if

* This was pointed out to me by Dr K. Weissenberg.

$dp(k)/dt$ is not zero, its sign is reversed by reversing the external shear. This is a well-known paradox of Statistical Mechanics, however, and it can in fact be shown that the reversibility of the motion does *not* imply that $dp(k)/dt = 0$; see Tolman (1938) where this problem is discussed in connection with the Boltzmann H-Theorem. In other words, it is sufficient to calculate the collisions using the approximate equations (1).

The possibility exists that the steady state could be calculated without a detailed knowledge of the mechanics of an interaction by means of the ideas of Statistical Mechanics. This can be done if it is known whether there is any general property of the orbits that is conserved during a collision, something which corresponds, for example, to the conservation of energy for collisions between the molecules of a gas. With this idea in mind, the mechanics of an interaction in which d, the minimum distance of separation, is always much greater than a, a typical dimension of the particles, was worked out. Since if there is a quantity that is conserved for a general interaction, it will be conserved for an interaction in which a/d is small, and it is possible to carry out the analysis for this case by neglecting powers of a/d higher than the third.

The result of this lengthy calculation was that the arbitrary parameters that give the relative configuration of the particles before the interaction commences can be so varied that the orbits of the particles can be altered independently by the interaction. Further, it was found that the orbits of the particles are changed by the interaction in such a way that the statistical properties of the suspension are unaltered. Hence, there is no conservation principle, so that the ideas of Statistical Mechanics cannot be applied, and it is necessary to consider the detailed mechanics of a close interaction or collision before information about the effect of collisions can be obtained; unfortunately, there appears to be no way of doing this.

Finally, there are two *intuitive* hypotheses about the effect of collisions that are perhaps worth mentioning. The first of these is that those orbits are favoured for which the energy dissipation is small, and the second is that the orbits favoured are those for which the volume swept out by the particle is small. The first hypothesis is reminiscent of Jeffery's, but the situation here is different from that of § 4 since we are concerned with solutions of equations (1) and not with the effect of terms neglected in these equations. The second one, which was suggested to me by Dr J. W. Glen, is based on the intuitive idea that the smaller the volume swept out by a particle, the smaller the frequency of collisions made by the particle, with the result that the particle stays in its orbit longer. It follows from the first hypothesis that there is a tendency for particles to align themselves with the long axis along the direction of the vortex lines, so that $p(k)$ is large for large k if the particles are prolate and for small k if they are oblate; and it follows from the second hypothesis that the tendency is for the axis of symmetry to lie along the direction of the vortex lines, so that $p(k)$ is large for large k for both prolate and oblate particles. Thus, for prolate particles, the predictions are the same and in accordance with the observations of Manley & Mason

(1956), but the predictions for oblate particles are in disagreement. An experiment using oblate particles would be of some interest in this connection.

I wish to thank Sir Geoffrey Taylor for suggesting this problem to me, and I am grateful to both him and Dr G. K. Batchelor for the kind interest that they have shown in this work. I also wish to thank Dr K. Weissenberg for the supply of some ammonium polymethyl acrilate.

References

BINDER, A. 1939 *J. Appl. Phys.* **10,** 711.

JEFFERY, G. B. 1922 *Proc. Roy. Soc.* A, **102,** 161.

LORENTZ, H. A. 1907 *Abhandlungen uber Theoretische Physik*, p. 23. Leipzig.

MANLEY, R. ST. J., ARLOV, A. P. & MASON, S. G. 1955 *Nature, Lond.* **175,** 682.

MANLEY, R. ST. J. & MASON, S. G. 1956 To be published.

TAYLOR, G. I. 1923 *Proc. Roy. Soc.* A, **103,** 58.

TOLMAN, R. C. 1938 *The Principles of Statistical Mechanics.* Oxford University Press.

TREVELYAN, B. J. & MASON, S. G. 1951 *J. Coll. Sci.* **6,** 354.

TRUESDELL, C. 1952 *J. Rat. Mech. Anal.* **1,** 125.

WEISSENBERG, K. 1947 *Nature, Lond.* **159,** 310.

WHITEHEAD, A. N. 1893 *Quart. J. Math.* **23,** 143.

REVIEWS

The Structure of Turbulent Shear Flow, by A. A. TOWNSEND. Cambridge University Press, 1956. 315 pp. 40*s*. or $7.50.

Any steady flow of a fluid is unstable when the Reynolds number (product of a typical flow velocity with a typical length scale, divided by the kinematic viscosity) is great enough, although the required magnitude varies extremely widely with the type of flow and the size of such disturbances as are present. At Reynolds numbers just large enough to produce instability, the disturbed flow may settle into a regular eddy pattern (such as the Kármán trail or Bénard cells), but at higher values an irregular, 'turbulent' flow is produced, in which the velocity at any point varies in a statistically random manner. Fourier analysis shows that fluctuations in a range of frequencies are present, the width of the range increasing with Reynolds number.

The study of turbulent flow is a part of science not founded on the 'principle of uniformity' as expounded by students of scientific method. The velocity record at a fixed point obtained by a hot-wire anemometer recording on to an oscilloscope is quite different every time a given flow (under fixed conditions) takes place. The aim, throughout the seventy years since Reynolds initiated the study of turbulence, has been to recover some partial degree of uniformity by statistical studies, that is, studies of averages of various quantities. In theory, a fluid flow which is known precisely at one instant can have its later development predicted uniquely. Hence, if a complete statistical knowledge of the flows generated in a certain way were available for one instant of time, such knowledge could in theory be deduced for later instants. However, it is of the essence of the problem that the statistical distribution of the initial random disturbances that lead to turbulence is not known in practice. Hence, no definite results can be expected unless there is a tendency for the development with time to obliterate special effects of this initial distribution. Actually, some such tendency is observed, but it is only partial.

Other branches of statistical physics have been more successful than turbulence theory. The obliteration tendency appears most strongly in the kinetic theory of gases, but the 'molecular chaos', which implies a statistical independence of velocity distributions at different places however close, makes any analogy with turbulence tenuous indeed. The existence of spatial correlation brings turbulence closer to that other rather unsuccessful subject, the kinetic theory of liquids.

Again, there is an obvious difference from linear problems where response is frequency-conserving. A better analogy is provided by forced mechanical vibrations whose amplitude is governed by non-linear forces which transfer energy between modes, such as could be observed in the film of the Tacoma Bridge disaster. However, turbulence at high Reynolds number is different in that it possesses a far greater range of wave-numbers, due to weaker internal damping.

This presence of modes of fluctuation with a wide range of wave-numbers, transferring energy among themselves as a result of the non-linear character of the inertial forces, is the basis of the Kolmogoroff–Onsager theory of the 'small eddies', that is, of the components of flow which in a spatial Fourier analysis have large wave-number. This theory is based on the idea that transfer of energy takes place in the direction of increasing wave-number, and in fairly short steps (in terms of the ratio of wave-number of a larger eddy to that of the smaller eddy which draws off some of its energy). Our knowledge of the basic instability of the steady flow already indicates that energy passes from that minimum-wave-number motion most readily to a motion with wave-number greater by half to one order of magnitude, and if this is true right up the wave-number scale the idea follows that the small eddies may have been reached by a statistical combination of many elementary processes which could obliterate the pecularities of the original large-scale disturbances. Hence they may be in an equilibrium which depends only on the viscosity which dissipates their energy and on the total rate at which energy is passed down to them, or (in the case of flows where this rate is changing with time) in a moving equilibrium which may depend also on the rate of change of that rate.

This theory has given a fairly satisfactory statistical picture of the small eddies, close to isotropy and equilibrium, which is useful in many applications. However, because of the increase in rate of energy loss to smaller eddies and in rate of dissipation as wave-number increases, the actual energy in the small eddies at any instant is a small fraction of the whole. The processes, if any, that govern the character of the 'energy-containing eddies' (those larger ones which contain the bulk of the turbulent energy) have remained a mystery, except that some progress has been made in the case of homogeneous turbulence (with a uniform mean flow), which was reviewed in 1953 by Dr G. K. Batchelor in the Cambridge series of Monographs on Mechanics and Applied Mathematics (this book contains also a good account of the small eddies).

Now at last, in the same series, a book has come out which, largely eschewing the small eddies as in the main already understood, takes as its principal subject the problem of how, in general turbulent flows, the character of the energy-containing eddies is controlled. It is called *The Structure of Turbulent Shear Flow*, presumably to disavow any restriction to the cases with uniform mean flow already described by Dr Batchelor, and perhaps also to exclude turbulent flows due to thermal convection, but it might have been called simply *Turbulence*. Its author, Dr Alan Townsend, has a combination of experimental and theoretical ability which no-one entering the subject has possessed since Sir Geoffrey Taylor (in whose Cambridge laboratory he works, and whose encouragement he acknowledges in a preface), and which were almost certainly essential requisites for his task. He has been developing his ideas in a number of exciting articles over the last nine years, but it has not been easy to follow from these what the conclusions would be, as in many cases the views

expressed in one article were retracted in a succeeding one, and the author was plainly feeling his way. But now we have an opportunity to take in as a whole the theory and the experimental evidence on which it is based, both being very plainly set out in the book under review.

A number of basic ideas dominate Dr Townsend's account of an extensive range of different flows. The first three are simple general ideas which have been adopted fairly widely before, although not always, as Dr Townsend points out, with a full understanding of which results follow from them and which from more specialized assumptions about structure. They say that at sufficiently high Reynolds number the energy-containing eddies (and, generally, all except the smallest-scale features of the flow) (i) are independent of Reynolds number (because the viscosity affects only the small eddies) and in time reach a state in which (ii) their velocity and length-scales may be changing but other quantities of the same dimensions change in proportion, and which (iii) is independent of the details of such boundary conditions as are basically responsible for the turbulence, depending only on an overall resultant of them. The last principle is close to that of St Venant in elasticity, and as in that subject it is the resultant force (together with, sometimes, a length scale) which matters. Thus, turbulence in a jet depends on its net thrust, in a wake on the drag of the body producing it, and in pipe flow on the wall resistance. The independence of Reynolds number (principle (i)) and of details of geometry is postulated only for given values of these forces, which on the other hand for a given geometry may vary with Reynolds number owing to the kinematic boundary condition of no slip being applied in the 'viscous layer' near the wall where the variation of mean velocity has a very small length-scale.

Dr Townsend begins his book with two chapters in which he sets forth the principal experimental and mathematical tools which are available for the study of turbulence; here, he departs from previous practice principally by stressing the idea of an eddy as something finite in extent (and even showing a preference for it being round, as indeed so many eddies observed in nature are!) rather than as being simply a Fourier component. In chapter 3 he sets out the evidence for the three principles just outlined in the case of turbulence with uniform mean flow, for which particularly detailed evidence is available. If the principles were completely false the subject of the book could hardly be said to exist, in that practically no uniformity could be imposed on the data. In fact they are broadly true, although only to a rough approximation.

He then develops a number of further principles, and devotes the rest of the book to showing how they illuminate the main features of turbulent flow in wakes, jets, mixing zones, pipes, channels, boundary layers, and between rotating cylinders, and to showing how well the various principles are borne out by experimental observation.

One principle that could be expressed better than in the book itself is that when turbulence is subject to a constant mean rate of strain the anisotropy of its energy tensor tends to a limiting form. If

$$S_{ij} = \tfrac{1}{2}(\partial U_i/\partial x_j + \partial U_j/\partial x_i)$$

represents the mean rate of strain and $\overline{u_i u_j}$ the turbulent energy tensor, this anisotropy is represented by the behaviour of $\overline{u_i u_j}/\overline{q^2}$ (where $\overline{q^2} = \overline{u_i u_i}$). This must depend on S_{ij} in a manner invariant under change of axes, and hence it can only be of the form

$$A\delta_{ij} + BS_{ij} + CS_{ik}S_{kj}, \tag{1}$$

where A, B, C are functions of the invariants $S_{kl}S_{kl}$ and Δ (the determinant of S_{ij}). A form which fits the experimental observations cited by Dr Townsend is

$$\frac{\overline{u_i u_j}}{\overline{q^2}} = \tfrac{1}{3}\delta_{ij} - \frac{0{\cdot}2S_{ij}}{(S_{kl}S_{kl})^{1/2}}. \tag{2}$$

This seems more satisfactory than Dr Townsend's form, which is not invariant. The reason why C in (1) is put equal to zero is that in plane strain (in the $x_1 = 0$ plane) the value of Dr Townsend's $K_2 = 3\overline{u_1^2}/\overline{q^2} - 1$ is observed to vanish. The best-known case of equation (2) is the tendency of the 'shear coefficient' $(-\overline{uv}/\overline{u^2})$ to be about 0·4 in simple shearing flow with $dU/dy > 0$.

The physical explanation of the principle just described is based on the one hand on the known tendency for strain in one direction to increase vorticity in that direction and hence to favour velocity components in the direction at right angles (at the expense of components in that direction). To balance this tendency we no longer have the once-credited 'general tendency to isotropy' of the energy-containing eddies, which this book (together with a number of other contemporary investigations) finally explodes. If, in fact, the mean rate-of-strain is removed, the anisotropy is found to remain practically unchanged (until some new mean rate-of-strain is applied). In place of this, we have the suggestion that eddies too much stretched in the direction of mean strain decay more rapidly than less elongated ones.

A second important principle inferred by Dr Townsend from the data takes its simplest form in free turbulence. This consists of a region of 'uniformly turbulent' fluid (containing all the vorticity and practically all the turbulent energy, uniformly distributed, but with anisotropy as governed by the former principle) with a bounding surface of extremely irregular shape, different at different instants. The uniformity of the turbulent fluid is explained as due to diffusion. The spread of the turbulent region is explained as due to contortion of the bounding surface by 'large eddies' and, on a smaller scale, by all the eddies, which taken together produce an extremely large boundary area over which viscous forces can diffuse vorticity. That this process operates very effectively at high Reynolds numbers is clear from the fact that the observed rate of growth does not decrease as the Reynolds number increases (that is, as the time scale for operation of viscous forces increases relative to the basic kinematic time scales).

The 'large' eddies (larger even that those which contain the bulk of the turbulent energy control the ultimate speed of spread of the turbulence.

They derive energy from the primary instability of the mean flow and pass energy down to the energy-containing eddies. Here Dr Townsend assumes (with some experimental support) that one of the simplest kinds of eddy capable of extracting energy from the mean flow predominates in this range of sizes. This ends up as a round eddy (with axis in the direction of flow) which just fills up the region of substantial mean rate-of-strain of any one sign. Before the eddy is sheared into this form it is bent back at an angle and during this shearing process it gains energy (as the area of its closed streamlines decreases).

Dr Townsend derives the energy of the main turbulence by applying a condition that it extracts energy from a 'large eddy' of this form at the same rate at which the large eddy extracts energy from the mean flow. Thus, he is applying arguments similar to the 'equilibrium' arguments of Kolmogoroff at the small-wave-number end of the scale. The rate of dissipation of energy of the large eddy by turbulence is computed by the use of an 'eddy viscosity', and it is the magnitude of this eddy viscosity (determined empirically in the older theories) which emerges from the Townsend theory as a predicted quantity in satisfactory agreement with experiment.

The mere existence of an effective eddy viscosity is not, however, taken as an *a priori* assumption. Dr Townsend shows how it follows from his theory of the effect of mean rate-of-strain on anisotropy. One of his 'large eddies' effectively re-orients the local rate-of-strain environment of the turbulence, and this alters the local anisotropy of the energy-containing eddies and so produces an addition to the Reynolds stresses. The derivation is simpler from equation (2) above that from Townsend's form, and so may as well be given. A change δS_{ij} in the mean rate of strain produces a change

$$\delta(-\overline{u_i u_j}) = 0{\cdot}2\overline{q^2}\left\{\frac{\delta S_{ij}}{(S_{kl}S_{kl})^{1/2}} - \frac{S_{ij}S_{kl}\delta S_{kl}}{(S_{kl}S_{kl})^{3/2}}\right\} \tag{3}$$

in the Reynolds stresses. In the case of a plane shearing motion only the term $S_{12} = S_{21} = \frac{1}{2}dU/dy$ is present in S_{ij}, and then (3) becomes

$$\frac{0{\cdot}2\overline{q^2}\sqrt{2}}{dU/dy}\begin{vmatrix} \delta S_{11} & 0 & \delta S_{13} \\ 0 & \delta S_{22} & \delta S_{23} \\ \delta S_{13} & \delta S_{23} & \delta S_{33} \end{vmatrix}, \tag{4}$$

which, for an eddy without an especially large δS_{12} component of rate-of-strain, represents closely a viscous resistance by an effective viscosity equal to

$$-\frac{0{\cdot}2\overline{q^2}}{(\sqrt{2})dU/dy} = -\frac{0{\cdot}4\overline{u^2}}{dU/dy} = -\frac{\overline{uv}}{dU/dy}, \tag{5}$$

which is the ordinary 'eddy viscosity' of the old theories.

Throughout the book Dr Townsend walks a very thin tight-rope in his attitude to eddy viscosity. He expects the reader to believe that it is

'accidental' (p. 161) that the assumption of an eddy viscosity in the ordinary sense, which at any cross-section of the turbulent layer is constant within the 'turbulent fluid' and zero outside it, gives dead-on agreement with the observed mean velocity for all free turbulent flows. Earlier (p. 44), he admits the success with which Heisenberg and his followers applied the eddy viscosity idea to predict the whole spectrum of the energy-containing eddies in isotropic turbulence, but presumably he regards this as accidental, too! The reviewer would agree that Dr Townsend's data show that there is no simple single reason why eddy viscosity seems to work, but rather a number of conspiring circumstances—for example, there is Dr Townsend's point that where dU/dy is nearly zero, the eddies consist partly of those which have been positively sheared and partly of those which have been negatively sheared, and hence $\overline{uv}$ also will be nearly zero. However, the rather sweeping and undeveloped arguments on which the older ideas are rejected in this book (for example, on p. 94) do not greatly reinforce the simple objection (p. 128) that they contain undetermined constants.

Chapters 4 to 8 are devoted to the development of the principles described above and their application to flow in wakes and jets. In these applications, it is clear that something has been sacrificed by the decision to study only flows which have reached the self-preserving state (principle (ii)), because the time taken by turbulence to change from one type to another is in fact long. In particular, the strong 'mixing-region' turbulence takes a long time to settle down into the relatively weaker wake turbulence or jet turbulence. On the other hand, the success of this book in throwing light on turbulence completely vindicates Dr Townsend's decision to confine his observations at this stage to the regions of self-preserving flow, far downstream, where this settling-down has taken place, and where there was more hope of uncovering the mechanics of the motion.

In chapter 9, on flow in pipes and channels, the complications due to the presence of a wall are first introduced. Correlation and other measurements in the region of early constant stress near the wall are shown to be consistent with the idea that cylindrical eddies like the 'large eddies' of free turbulent flow sit on the wall and extract energy from the mean flow at the same rate as they pass energy down to not-so-large eddies. This leads to the right ratio of eddy viscosity to distance from the wall.

In chapters 10 and 11 the ideas appropriate to free turbulent flow and to flow near a wall are combined in a discussion of the turbulent boundary layer. The theory of equilibrium of the large eddies is still remarkably effective and the evidence from correlation measurements for their presence and general character is good. In chapter 11 the ideas of the book (including, it must be noted, an eddy viscosity!) are used effectively on the interesting self-preserving flows with adverse pressure gradient recently discovered by Dr Clauser. In both chapters a discussion of three-dimensional effects including secondary flows is given. Finally, in chapter 12, the flows between rotating cylinders are fitted to some extent into the general framework of the book.

A large measure of sound understanding, with some notable gaps, was already present in the world literature on turbulent shear flow, so far as the behaviour of the mean flow and the small eddies was concerned. Dr Townsend's book, while not omitting this material, will always be remembered principally for having first made a reasonably convincing bridge between these extreme features of the flow and given us a pattern for the intermediate parts of the spectrum and a way of thinking quantitatively about the larger eddies that is sufficiently consistent with both the theoretical and the experimental evidence.

M. J. LIGHTHILL

NIV
OF
FE